TEXTILE RESEARCH JOURNAL

VOL. XXII, No. 4 April, 1952

Forced Vibrations of Polyamide Monofils*

Henry Eyring,† Marilyn G. Alder,‡ Stephen A. Rossmassler, and Carl J. Christensen††**

Contribution from the Department of Chemistry and the School of Mines and Mineral Industries, University of Utah, Salt Lake City, Utah

Introduction

In a study of the mechanical properties of high polymers, the rheological behavior exhibited under conditions of dynamic testing is of great interest and value.

Such behavior governs the performance of solid materials when they are subjected to repeated stresses or strains. Strength, internal temperature, fatigue, and failure limits are determined by the intrinsic response of a given molecular aggregate to a repeated mechanical deformation. Thus, a correlation of dynamic rheological behavior with internal molecular structure provides not only basic concepts for the scientist, but also practical information for the engineer and industrialist.

The application of a sinusoidally varying stress to many natural and synthetic high polymers results in a net cyclical expenditure of energy by the driving mechanism. Thus, the magnitude of the net energy absorbed by a test sample during a cycle is a measure of the degree of its departure from ideal Hookean behavior.

This paper represents a theoretical and experimental study of the net cyclical energy absorption characteristic of certain polyamide monofils subjected to sinusoidal loading. The effects of frequency of vibration, cycle number, and ambient temperature are investigated. The results are discussed in terms of the known internal structure of high polymers.

Theory of Plastic Flow as Applied to Forced Vibrations

General Theory

When a fiber is subjected to a given applied force, the stress distributes itself in some fashion over all of the structural elements. The resulting strain is, then, a composite result of (*1*) the straightening out of coiled or otherwise randomly oriented chains, (*2*) the slippage of spatially oriented chains past one another, and (*3*) the breakage of primary bonds. Under the effect of stresses which are smaller than those necessary to rupture the fiber, the first two processes predominate. In the present work, small stresses were applied so that the extent of strain

* This work was supported by Research Contract N7-onr-45101, Project No. NR-032-168, and comprises Technical Reports XV and XXI.

† Dean of the Graduate School and Professor of Chemistry and Metallurgy, University of Utah.

‡ Present address: Dept. of Chemistry, Florida State University, Tallahassee, Florida.

** Present address: E. I. du Pont de Nemours and Co., Wilmington, Del.

†† Dean of the School of Mines and Mineral Industries, University of Utah.

contribution from process (*3*) is considered to be far less than that resulting from (*1*) and (*2*).

Kauzmann and Eyring [7] have shown that with increasing polymer chain length, the unit of flow under stress becomes a decreasing proportion of the chain and approaches 25–30 carbon atoms in length as a limit. Thus, under an applied stress, the motion of the long chain molecules may be described as being a stress-biased thermal diffusion process of molecular segments.

The general treatment of flow as a rate process is patterned after the work of Eyring [5]. The basic concept underlying this approach to the problem of stress response in high polymers is that in order for a segment to move from one probable configuration to another, it must pass through an intermediate state which is characterized by a low probability of occurrence. In an equilibrium state defined in terms of a given constant temperature and zero applied stress, the net distortion of the whole fiber, due to the motion of individual molecular segments from one equilibrium position to another, will be zero. Hence, the fiber maintains constant length and internal energy.

The above situation is shown schematically in Figure 1 (top). In the absence of an applied force, the activation energy, $\Delta F\ddagger$, necessary to move from state I to state II is equal to that required in going from state II to state I (solid line). Hence, the net transfer equals zero.

An applied stress on a deformable material acts to bias the segment motion in a manner to relieve the stress. In a configuration space defined by the transition coordinate, this stress results in a distortion of the potential barrier, as shown in Figure 1 (top) (broken line).

In the presence of an applied force per unit area, F, the rate of passage, k_1', from state I to state II becomes

$$k_1' = \kappa_1 \frac{kT}{h} e^{-\frac{\Delta F_1\ddagger}{kT}} = \kappa_1 \frac{kT}{h} e^{-\frac{(\Delta F\ddagger - FV')}{kT}},$$

where $V' = \lambda\lambda_2\lambda_3/2$, κ_1 = the probability that the segment will continue over into state II once it has reached the top of the potential barrier, k = Boltzmann's constant, and h = Planck's constant. The corresponding rate of passage from state II to state I is given by

$$k_2' = \kappa_2 \frac{kT}{h} e^{-\frac{\Delta F_2\ddagger}{kT}} = \kappa_2 \frac{kT}{h} e^{-\frac{(\Delta F\ddagger + FV')}{kT}},$$

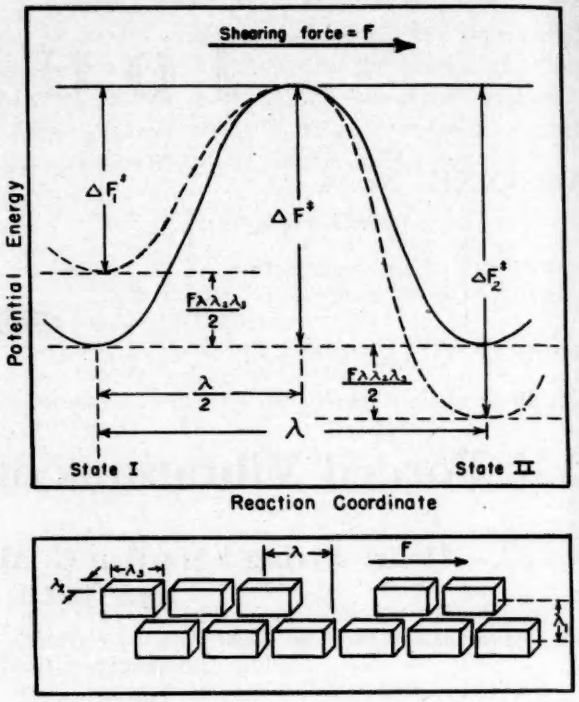

FIG. 1. Top—*Potential energy surface profile for segment motion between state I and state II.* Bottom—*Schematic diagram of the mobile segment units which constitute a high-polymer molecule.*

where κ_2 represents the probability that a segment reaching the top of the potential barrier will continue over into state I. Thus, the net rate of passage from state I to state II becomes

$$k_{net} = k_1' - k_2' = \kappa \frac{kT}{h} e^{-\frac{\Delta F\ddagger}{kT}} \left(e^{\frac{FV'}{kT}} - e^{-\frac{FV'}{kT}}\right)$$

or

$$k_{net} = 2\kappa \frac{kT}{h} e^{-\frac{\Delta F\ddagger}{kT}} \left(\sinh \frac{FV'}{kT}\right),$$

where $\kappa_1 \equiv \kappa_2 \equiv \kappa$.

Now, if λ is the distance between the initial and final states, the velocity of movement of the stress-biased segments will be given by

$$v_{net} = 2\lambda\kappa \frac{kT}{h} e^{-\frac{\Delta F\ddagger}{kT}} \left(\sinh \frac{FV'}{kT}\right). \qquad (1)$$

To correlate equation (1) with the parameters used to define the characteristics of the mechanical model employed, the concept of a viscosity coefficient, η, is used,

$$\eta = \frac{F\lambda_1}{v_{net}}, \qquad (2)$$

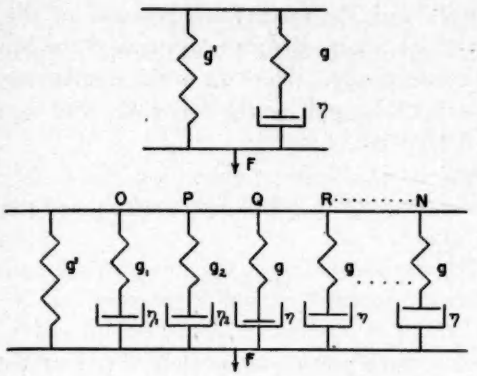

FIG. 2. Top—*Single three-element model characterized by a relaxation time* $= \eta/g$. Bottom—*Model consistent with the observed rheological behavior of three polyamide monofils.*

where F represents a shear force per unit area applied to a material consisting of layers of molecules separated by a distance λ_1. Substituting equation (1) in equation (2) and assuming $\kappa = 1$ gives

$$\eta = \frac{F\lambda_1}{2\lambda \frac{kT}{h} e^{-\frac{\Delta F^{\ddagger}}{kT}} \left(\sinh \frac{FV'}{kT}\right)}.$$

By considering that λ and λ_1 are of the same order of magnitude, one obtains

$$\eta = \frac{Fhe^{\frac{\Delta F^{\ddagger}}{kT}}}{2kT \left(\sinh \frac{FV'}{kT}\right)}. \qquad (3)$$

Now, V' is of the order of molecular dimensions cubed ($\simeq 10^{-24}$ cm.^{3}) so that for small values of F, $kT \ll FV'$, and the expansion of sinh (FV'/kT) will be closely approximated by the first term, FV'/kT. Hence,

$$\eta \approx \frac{Fhe^{\frac{\Delta F^{\ddagger}}{kT}}}{2kT \frac{FV'}{kT}} = \frac{h}{V_h} e^{\frac{\Delta F^{\ddagger}}{kT}}, \qquad (4)$$

where $V_h = \lambda_1\lambda_2\lambda_3$ and a material exhibiting a high viscosity will likewise be characterized by a large free energy of activation.

The independence of viscosity and force is defined as ideal Newtonian behavior. This approximation will be carried over to the problem of forced vibrations.

Forced Vibrations

The experimental method employed here is to place a fiber under a known initial strain bias and then superimpose a sinusoidally varying cyclical strain of constant amplitude. The initial tension assures the attainment of closed loops, as the fiber does not go slack at any point during the cycle.

The area of the stress-strain loop may be taken as a measure of the extent of deviation from fiber equilibrium which occurs during a cycle—that is, the stress and strain are not in phase due to a finite relaxation time necessary for the molecular segments to respond to the applied stress.

Since the viscosity coefficient has been defined in terms of the net rate of flow of the molecular segments, the phase-angle lag should be related to the apparent viscosity. Thus, the area of the stress-strain loop may also be considered to represent the net work done on the viscous (time-dependent) elements of flow.

A molecular segment having a finite relaxation time, τ, may be schematically represented by a single Maxwell unit, where

$$\tau \equiv \frac{\eta}{g}.$$

Here, η represents the viscosity coefficient or the parameter describing the time-dependent phenomena, and g is the elastic constant or the parameter characterizing time-independent effects. A single Maxwell unit with defining parameters is shown in Figure 2 (top).

To obtain a theoretical expression for the net cyclical energy absorption, ΔE, it is convenient to consider first the case of a material whose behavior under stress is defined by a single relaxation time or Maxwell unit. The average tension on the fiber is represented by a pure spring in parallel with the Maxwell unit.

Since the applied stress and strain have very nearly the same wave form but differ by a definite phase angle, a sinusoidal time dependence will be used.

Consider that the motion of a fiber begins at the mid-point of the stroke, so that the displacement with time may be given by

$$s = a \sin \omega t, \qquad (5)$$

where s = relative displacement at time t, a = maximum relative displacement $= \Delta l/l_o$, Δl = amplitude of vibration, l_o = original length of fiber, and $\omega = 2\pi\nu$, where ν = frequency.

Similarly, the expression for the stress may be given as

$$F = b \sin (\omega t + \delta), \tag{6}$$

where δ is the phase-angle difference such that the stress leads the strain, and b is a constant determined by g, η, and ω. Thus, b is a function of the particular characteristics of the test sample.

Classically, the energy per unit volume for a cyclical process is

$$\Delta e = \int_0^\tau F\, ds, \tag{7}$$

where τ = period of vibration. Substitution for F and s gives

$$\Delta e = ab\omega \int_0^\tau \sin (\omega t + \delta) \cos \omega t\, dt, \tag{8}$$

which also may be written as

$$\Delta e = ab\omega \cos \delta \int_0^\tau \sin \omega t \cos \omega t\, dt + ab\omega \sin \delta \int_0^\tau \cos^2 \omega t\, dt.$$

Integration over a complete cycle where $\omega = 2\pi\nu$ gives

$$\Delta e = ab\omega \cos \delta \left(\tfrac{1}{2} \sin^2 \omega t\right)_o^{\frac{2\pi}{\omega}} + ab\omega \sin \delta \left(\frac{1}{2\omega} \sin \omega t \cos \omega t + \frac{t}{2}\right)_o^{\frac{2\pi}{\omega}},$$

which reduces to

$$\Delta e = \pi\, ab \sin \delta. \tag{9}$$

Thus, the density of the net energy absorbed is directly proportional to the phase angle.

Alternatively, equation (9) results when those portions of F and s responsible for energy dissipation are integrated according to

$$\Delta e = \int_0^\tau F_D ds_D,$$

where F_D and S_D are, respectively, the stress and strain characterizing the dashpot at time t.

The characteristic parameters of the mechanical model (Figure 2 (top)) are used in the evaluation of δ and b. Consider that the application of a stress, F, results in a strain such that

$$F = F' + F_D = g's + \eta \dot{s}_D,$$

where F' and F_D are the components of the total stress which act on the pure spring and the Maxwell unit, respectively. Here s_D is the displacement of the dashpot caused by the force F_D, and $\dot{s}_D$ is the time derivative of s_D.

Also,

$$F = g(s - s_D) + g's,$$

such that

$$\dot{s}_D = \frac{(g + g')s - \dot{F}}{g}.$$

Hence, the equation of motion of the mechanical model (Figure 2 (top)) is given by

$$F + \frac{\eta}{g} \dot{F} = g's + \frac{\eta}{g} (g + g')\dot{s}. \tag{10}$$

A substitution of the values of s and F from equations (5) and (6) into equation (10) gives

$$b \sin (\omega t + \delta) + \frac{\eta}{g} b\omega \cos (\omega t + \delta) = g'a \sin \omega t + \frac{\eta}{g} (g + g')a\omega \cos \omega t. \tag{11}$$

Since equation (11) is time dependent in each term, it must be satisfied at $t = 0$ and $t = \pi/2\omega$. An application of these boundary conditions is sufficient to determine the parameters b and δ as

$$b = \frac{\frac{\eta}{g} (g + g')a\omega}{\sin \delta + \frac{\eta\omega}{g} \cos \delta} \tag{12}$$

and

$$\sin \delta = \frac{a\eta g^2 \omega}{bg^2 + b\omega^2\eta^2}. \tag{13}$$

Substitution of equation (13) into equation (9) gives

$$\Delta e = \frac{\pi a^2 g^2 \eta\omega}{\omega^2\eta^2 + g^2} = \frac{\text{ergs}}{\text{cycle cm.}^3}. \tag{14}$$

The total energy absorption, ΔE, for a fiber of volume V is thus

$$\Delta E = \frac{\pi a^2 V g^2 \eta\omega}{\omega^2\eta^2 + g^2}. \tag{15}$$

Hence, equation (15) relates the net cyclical energy absorption to the frequency of vibration and to the parameters of the assumed model.

Frequency Dependence.—Differentiating equation (15) with respect to ω and setting the results equal

to zero so as to locate the frequency at which the net energy absorption is a maximum gives

$$\omega = \frac{g}{\eta} = \omega_m = 2\pi\nu_m, \tag{16}$$

where ν_m is the frequency at which maximum absorption occurs for a unit having a relaxation time of η/g.

Figure 3 shows the calculated frequency dependence of ΔE corresponding to different values of $\nu_m = g/2\pi\eta$ for a monofil of volume = 0.0312 cm.^{3}. Some previous experimental work done on fibers indicates an essentially constant net cyclic energy absorption over certain frequency ranges [4, 8, 9, 10, 12]. This may be interpreted as implying the existence of a distribution of relaxation times which may be represented schematically by a large number of dissipative elements arranged parallel to each other, as shown in Figure 2 (bottom). Thus, the observed net energy absorption, ΔE, may be represented by

$$\Delta E = \pi a^2 V \sum_i \frac{g_i^2 \eta_i \omega}{\omega^2 \eta_i^2 + g_i^2},$$

where each i value is indicative of a value of $\tau_i = \eta_i/g_i$. The results of the present work, which involves a measurement of ΔE over a range of low frequency values, will be discussed in terms of the above approach.

Temperature Dependence.—At constant amplitude of vibration and for a given fiber, the variation of ΔE with temperature may be attributed to the temperature dependence of the molecular parameters η and g.

For the process of flow or slippage of molecular segments past one another, the defining parameter is η. Its temperature dependence (in the Newtonian case) has been shown to be given by

$$\eta = \frac{h}{V_h} e^{\frac{\Delta F^\ddagger}{RT}}, \tag{17}$$

where $R = Nk$, N is Avogadro's number, and $\Delta F^\ddagger$ is the activation free energy necessary for the motion of a mole of a particular type of molecular segment.

The time-independent stress response of a fiber is described by the parameter g. In terms of molecular structure, this parameter may be considered to represent the average elastic stress response which is characteristic of the material under observation. The temperature dependence of this parameter may be treated on the basis of thermodynamics.

By considering a system comprised of a large number of relatively independent molecular segments which are constrained by chemical forces at the ends of the molecules but which are free to assume a number of different configurations due to thermal agitation, Halsey and Eyring [6], giving references to earlier work, obtained the following expression:

$$\Delta A = \frac{N'kT}{2}\left(\alpha^2 + \frac{2}{\alpha} - 3\right). \tag{18}$$

Here, ΔA represents the change in Helmholtz free energy which accompanies a change in length of α = final total length divided by the original length, N' represents the effective number of elastic units

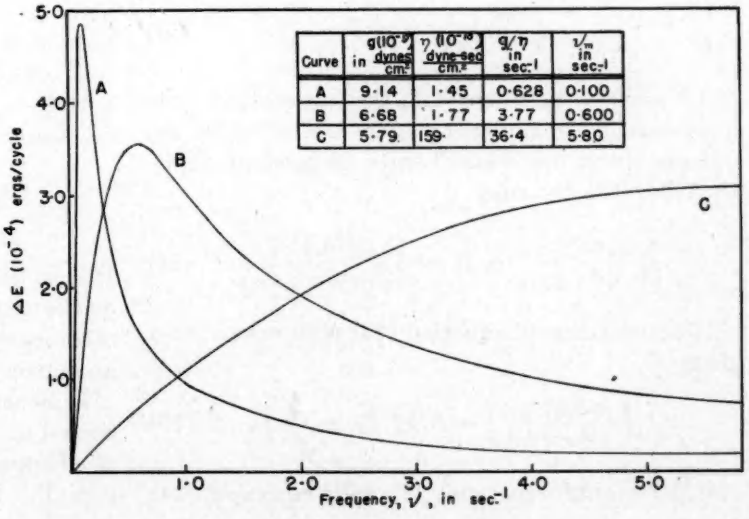

FIG. 3. *Examples of calculated net energy absorption values corresponding to different values of* g/η.

operating at the temperature T, and k is Boltzmann's constant. In the derivation it is assumed that there is no change in potential energy during the elongation process and that the value of α applies to each molecular segment involved.

To obtain an expression relating the elastic constant g to the temperature, it is necessary to relate the applied force per unit area, F, to equation (18).

The combined first and second laws of thermodynamics may be written as

$$TdS = dE + dw, \tag{19}$$

and, by definition,

$$dA = dE - TdS - SdT, \tag{20}$$

where S = entropy, E = internal energy, w = work, and T = absolute temperature. Combining equations (19) and (20) gives

$$dA = -dw - SdT. \tag{21}$$

Now, in stretching a material with rubber-like characteristics, the net work done on it is given by

$$-dw = Fl_o ad\alpha - pdV, \tag{22}$$

where l_o = original length of material, F = the applied force per unit area, a = the cross-sectional area, p = pressure, and V = volume of the system. Hence, equation (22) may be written as

$$dA = Fl_o ad\alpha - pdV - SdT,$$

and, under the conditions of constant temperature and volume,

$$\left(\frac{\partial A}{\partial \alpha}\right)_{T,V} = al_oF. \tag{23}$$

If $\Delta A = A - A_o$, where A_o is the free energy of the unstressed state (independent of α) and A is the free energy of the stressed state (dependent on α), equation (23) becomes

$$\frac{1}{al_o}\left(\frac{\partial A}{\partial \alpha}\right)_{T,V} = F = \frac{1}{al_o}\left(\frac{\partial(\Delta A)}{\partial \alpha}\right)_{T,V}. \tag{24}$$

Differentiation of equation (18) with respect to α gives

$$\left(\frac{\partial(\Delta A)}{\partial \alpha}\right)_{T,V} = N'kT\left(\alpha - \frac{1}{\alpha^2}\right), \tag{25}$$

and combining equation (25) with equation (24) results in

$$N'kT\left(\alpha - \frac{1}{\alpha^2}\right) = al_oF. \tag{26}$$

Hence,

$$F = \frac{N'kT}{al_o}\left(\alpha - \frac{1}{\alpha^2}\right). \tag{27}$$

Here, N'/al_o represents the effective number of molecular segments behaving as elastic units per unit volume at the temperature T.

Writing $s = \alpha - 1$, where s = the relative elongation or the elongation divided by the original length, equation (27) becomes

$$F = \frac{N'kT}{al_o}\left[1 + s - \frac{1}{(1+s)^2}\right], \tag{28}$$

which, upon expansion of the last term, gives

$$F = \frac{N'kT}{al_o}(3s - 3s^2 + \cdots). \tag{29}$$

In the case of the cold-drawn polyamide monofils used in the present work, the maximum s employed will be of the order of 0.1, so that only the first three terms in the expansion of $(1+s)^{-2}$ are considered.

Now, if the apparent elastic constant g be defined as

$$g = \frac{F}{s}, \tag{30}$$

then equation (29) becomes

$$g = \frac{3N'kT}{al_o}(1 - s). \tag{31}$$

Since in practice $s \leq 0.1$, the value of g should remain nearly constant under conditions of constant temperature and constant N'/al_o. Thus, in case of a 10% or less total extension, equation (31) may be closely approximated by

$$g = \frac{3N'kT}{al_o}, \quad \text{or} \quad \frac{al_o}{N'} = \frac{3kT}{g} \equiv \left(\frac{al_o}{N'}\right)_I. \tag{32}$$

It is to be emphasized that this derivation is based on the assumption that the total free energy change accompanying elongation is determined solely by an entropy decrease.

In general, a change in temperature may be expected to influence the value of N'/al_o, the density of effective elastic units which operate at temperature T. Hence, rubber-like substances which ex-

hibit a decrease of elastic modulus with increasing temperature must be characterized by values of N'/al_o that decrease markedly with increasing temperature.

The applicability of this concept of entropy-dependent elasticity to the case of two elastomers, natural rubber tread stock and a vinyl copolymer, is shown in Table I. Values of $(al_o/N')_I$ as calculated according to equation (32) are given. It is to be noted that these values increase rapidly with temperature and approach reasonable values at room temperature. As shown in Table I, an application of the same calculation to brittle and cross-linked polymers—polystyrene, a cast phenolic, and a polymethylmethacrylate resin—results in values of $(al_o/N')_I$ which are almost too small to have any physical significance. These small values may be considered to imply that the elongation process involves both an entropy and a potential energy change.

Thus, a more complete expression for the change of free energy accompanying elongation should include a term which is dependent upon the concomitant potential energy change. In the case of polymer systems which are characterized by a high degree of crystallinity or three-dimensional order (experiments [2] show that the cold-drawn polyamides are 90%–95% crystalline), it is reasonable to assume that an elongation process would involve a marked change in potential energy.

In deriving an approximate expression for the potential energy contribution to the free energy change, it will be assumed that the increase of potential energy on stretching may be attributed to a distortion of the bond angles between the atoms making up the "backbone" of the long chain molecules.

Consider a model (see diagram on p. 230) in which the application of a one-dimensional stress increases the bond angle by $2(\theta - \theta_o)$. Then

$$r = l \sin \theta, \quad \text{and} \quad r_o = l \sin \theta_o. \qquad (33)$$

TABLE I. APPARENT VOLUMES OF ELASTIC UNITS AS CALCULATED ON THE BASIS OF ENTROPY-DEPENDENT ELASTICITY

High polymer	Ambient temperature (°K)	g (10^{-9}) $\left(\frac{\text{dynes}}{\text{cm.}^2}\right)$	$\left(\frac{al_o}{N'}\right)_I$ (10^{24}) $\left(\frac{\text{cm.}^3}{\text{unit}}\right)$
Natural rubber tread stock [3]	215	0.689	129
Natural rubber tread stock [3]	223	0.138	671
Natural rubber tread stock [3]	228	0.0689	1370
Natural rubber tread stock [3]	243	0.0276	3650
Natural rubber tread stock [3]	273	0.0138	8190
Vinyl copolymer [3]	225	6.89	13.5
Vinyl copolymer [3]	231	2.76	34.7
Vinyl copolymer [3]	237	1.38	71.2
Vinyl copolymer [3]	241	0.689	145
Vinyl copolymer [3]	248	0.276	372
Vinyl copolymer [3]	255	0.138	767
Vinyl copolymer [3]	267	0.0689	1580
Vinyl copolymer [3]	278	0.0276	4180
Polystyrene [3]	263	18.6	5.87
Polystyrene [3]	283	17.2	6.83
Polystyrene [3]	303	15.9	7.91
Polystyrene [3]	323	13.8	10.0
Polystyrene [3]	343	10.3	13.8
Polystyrene [3]	363	6.89	21.8
Cast phenolic [3]	213	41.3	2.14
Cast phenolic [3]	233	36.8	2.63
Cast phenolic [3]	253	33.1	3.17
Cast phenolic [3]	283	31.0	3.79
Polymethylmethacrylate resin [3]	242	45.6	2.21
Polymethylmethacrylate resin [3]	353	26.2	5.58

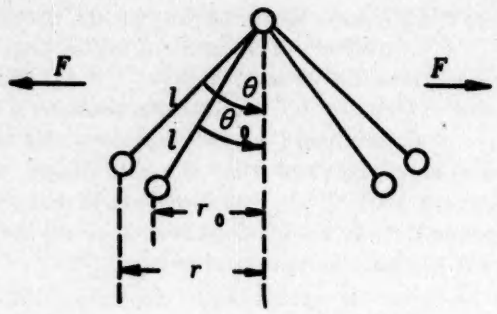

The potential energy, E', for such an idealized system may thus be given by

$$E' = \frac{N'bk_1}{2}(r - r_o)^2, \tag{34}$$

where N' represents the effective number of elastic elements contributing, b is the number of bond angles stretched per elastic unit, and k_1 is an average force constant applicable to the $N'b$ units.

The relative displacement, s, may be defined as

$$s = \frac{r - r_o}{r_o}, \tag{35}$$

and equation (34) becomes

$$E' = \frac{N'bk_1r_o^2}{2}s^2 = \Delta E', \tag{36}$$

since $\Delta E' = E' - E_o'$ and E_o' is independent of s and hence is defined as being equal to zero.

Thus, on including the potential energy change occurring during stretching, the expression for the total change of free energy becomes

$$\Delta A = \frac{N'kT}{2}\left[(1 + s)^2 + \frac{2}{1 + s} - 3\right] + \frac{N'bk_1r_o^2}{2}s^2. \tag{37}$$

Differentiation of equation (37) with respect to s at constant temperature and volume gives

$$\left[\frac{\partial(\Delta A)}{\partial s}\right]_{T,V} = N'kT\left[1 + s - \frac{1}{(1 + s)^2}\right] + N'bk_1r_o^2s, \tag{38}$$

which, upon expansion of $(1 + s)^{-2}$, gives

$$\left[\frac{\partial(\Delta A)}{\partial s}\right]_{T,V} = 3N'kT(s - s^2) + N'bk_1r_o^2s. \tag{39}$$

Now, according to equation (24),

$$\left[\frac{\partial(\Delta A)}{\partial \alpha}\right]_{T,V} = \left[\frac{\partial(\Delta A)}{\partial s}\right]_{T,V} = al_oF, \tag{24}$$

and, equating equations (24) and (39) gives

$$F = \frac{3N'kT}{al_o}(s - s^2) + \frac{N'bk_1r_o^2}{al_o}s. \tag{40}$$

Using the expression for the elastic constant (equation (30)), equation (40) becomes

$$g = \frac{N'}{al_o}[3kT(1 - s) + k_1br_o^2], \tag{41}$$

which, in view of $s \leq 0.1$, may be written as

$$g = \frac{N'}{al_o}(3kT + k_1br_o^2). \tag{42}$$

Here the apparent volume of an effective elastic unit becomes

$$\frac{al_o}{N'} = \frac{3kT + k_1br_o^2}{g} \equiv \left(\frac{al_o}{N'}\right)_{II}, \tag{43}$$

whereas on the basis of purely an entropy change it is given according to equation (32) as

$$\frac{al_o}{N'} = \frac{3kT}{g} \equiv \left(\frac{al_o}{N'}\right)_{I}. \tag{32}$$

Thus, the effect of adding an approximate potential energy contribution to the free energy change accompanying elongation is to increase the apparent volume of the elastic unit.

A discussion of the temperature dependence of g, al_o/N', and η, as derived from measurements on the polyamide monofils used in the present experiment, is given in a later section.

Experimental Method and Results

Apparatus

The apparatus employed was designed to permit a study of the mechanical properties of fibers under conditions of sinusoidal elongation. The following features were incorporated into the design: (1) a vibrator which would perform true sinusoidal motion; (2) a framework sufficiently rigid to eliminate extraneous vibrations over a given frequency range; (3) facilities for making arbitrary adjustments of frequency, amplitude, and initial elongation of the fiber sample (the latter adjustment being employed in order to maintain the fiber under tension throughout each entire cycle); (4) a means of recording

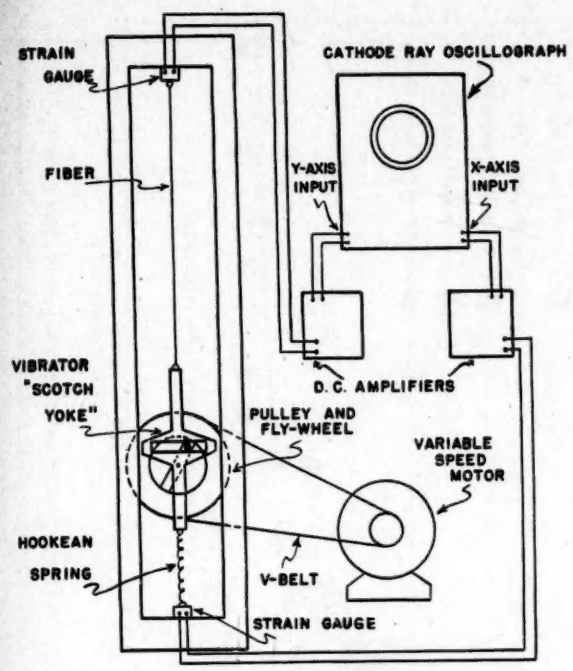

FIG. 4. *Diagram of forced vibrations apparatus.*

accurately the response of the fiber so as to facilitate the calculation of cyclical energy absorption.

Figure 4 is a diagram of the apparatus. The vibrator frame was made of $\frac{1}{4}$-in. steel angle and channel beams, and weighed about 250 lbs. The vibrator was machined from $\frac{1}{2}$-in. Dural plate, with tolerances of less than 0.002 in. at all bearing surfaces.

The oscillograph used was a Du Mont model 304 H, designed for D. C. and low-frequency use. A 5CP-11A oscillograph tube was employed.

The preamplifiers were single-stage D. C. amplifiers, and proved to be linear in the range of frequency and gain in which they were used.

A variable-speed Master "Speed Ranger" motor served as the driving mechanism.

Method

The method employed was the application of simple harmonic motion to a fiber specimen through the medium of the motor-driven eccentric or "Scotch Yoke." As shown in Figure 4, the fiber was mounted in a vertical position, with its upper and lower ends connected directly to a strain gage and to the eccentric, respectively. The eccentric, in turn, was connected through a linear spring to a second strain gage. Thus, the output of the upper transducer was a measure of the instantaneous force exerted on or by the fiber, while the output of the lower transducer gave a measure of the corresponding instantaneous displacement of the fiber.

The instantaneous force on the fiber was recorded on the ordinate, while the corresponding instantaneous displacement appeared on the abscissa. The area of the loop formed during a complete cycle was thus a measure of the net energy absorbed by the fiber.

The data were recorded photographically by using a 35-mm. camera attachment for the oscillograph. After photographing the net energy absorption loop, vertical calibrations on the frame were made by disconnecting the fiber, hanging known weights on the upper transducer, and photographing the resultant light spots. Horizontal calibrations were made by disconnecting the fiber and photographing the horizontal trace representing the motion of the motor-driven eccentric as recorded by the lower tranducer.

Following development of the films, 5 in. by 7 in. prints were made to facilitate measurement of the loop area. The loop area was subsequently measured with a planimeter, and an average of from three to five readings was used for each print. A minimum of two separate exposures was taken at each frequency to insure a check on the net energy absorption values.

By employing a temperature-control unit consisting of an insulating jacket surrounding the fiber sample, measurements were made over a 0° to 65°C range with an accuracy of ± 2°C. At room temperature, values of the net cyclic energy absorption were made over a 100-fold frequency range of 0.058 sec.$^{-1}$ to 5.80 sec.$^{-1}$. While using the temperature-control unit, the frequency range employed was 0.350 sec.$^{-1}$ to 5.80 sec.$^{-1}$.

Three different polyamide monofils were used in the experimental procedure. All were DuPont condensation-type polymers formed from the condensation of six or seven carbon atom diamines with α,ω-dicarboxylic acids. During manufacture the fibers were extruded from the melt, cooled in air, and then cold-drawn to about 600% of their original length. The monofils were thus characterized by a high degree of crystallinity.

In mounting each monofil, a stress bias of 100 g. or its equivalent was used. This was found to decrease to about 75 g. during the attainment of consistent ΔE values. The amplitude of vibration was

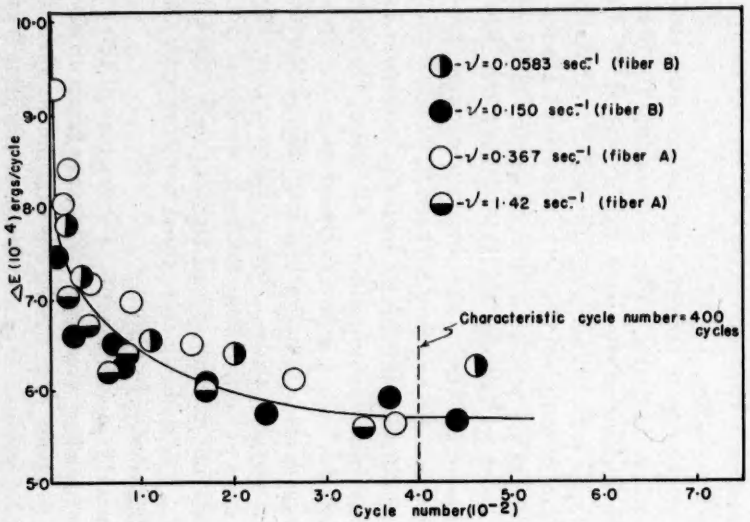

FIG. 5. *Net energy absorption as a function of cycle number for nylon 66. The fibers were allowed to relax to their original lengths before each frequency change. The values listed represent single readings.*

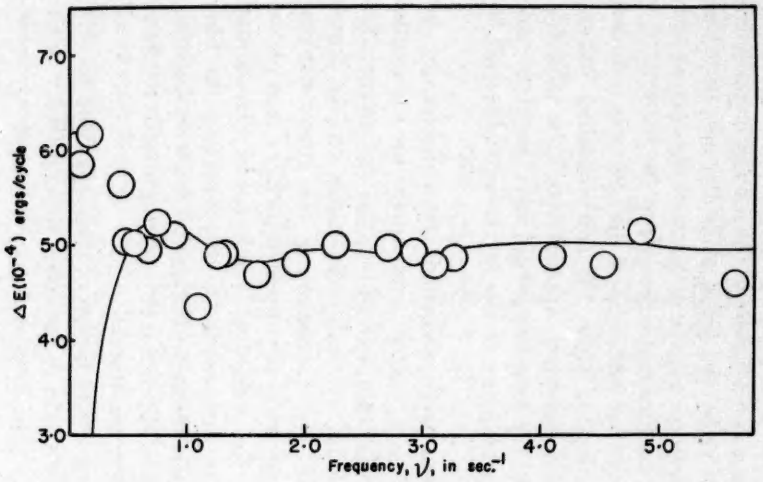

FIG. 6. *Frequency dependence of net energy absorption for nylon 66 at 25°C. The solid line gives theoretical values.*

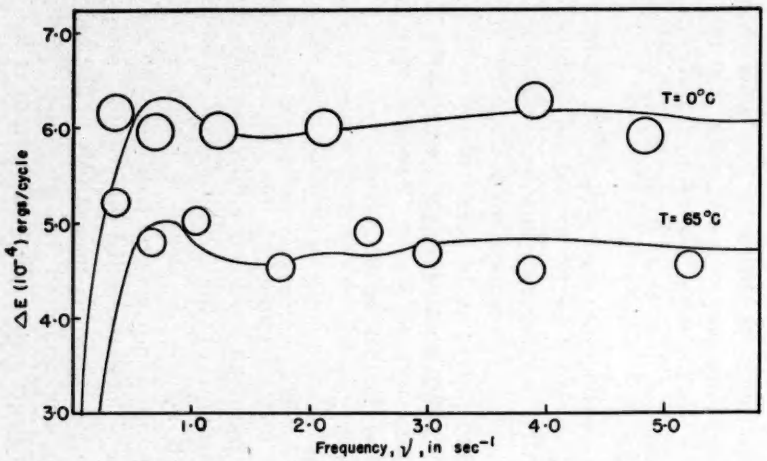

FIG. 7. *Frequency dependence of net energy absorption for nylon 66 at 0°C and 65°C. The solid lines give theoretical values.*

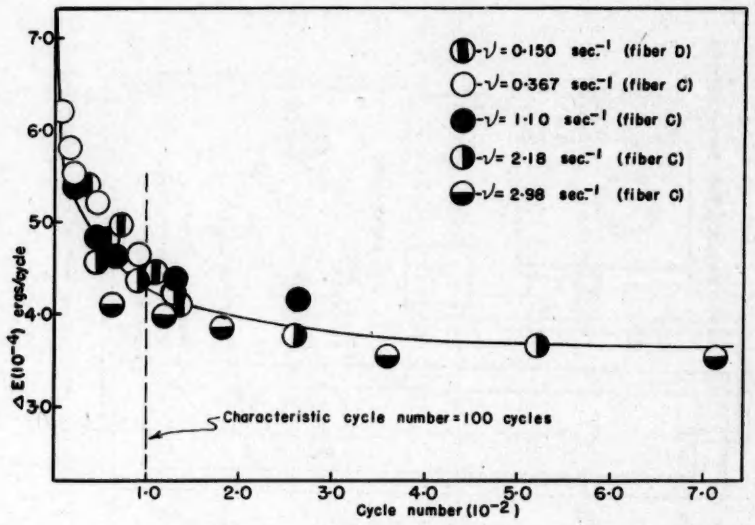

FIG. 8. *Net energy absorption as a function of cycle number for nylon 610. The fibers were allowed to relax to their original lengths before each frequency change. The values listed represent single readings.*

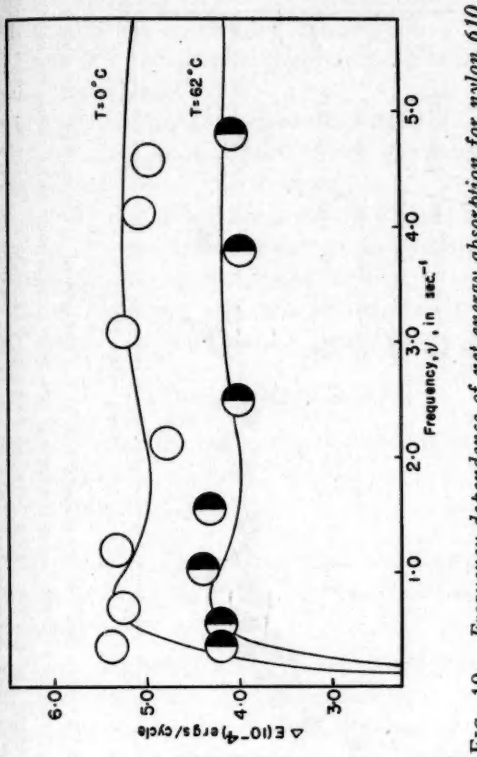

FIG. 10. *Frequency dependence of net energy absorption for nylon 610 at 0°C and 62°C. The solid lines give theoretical values.*

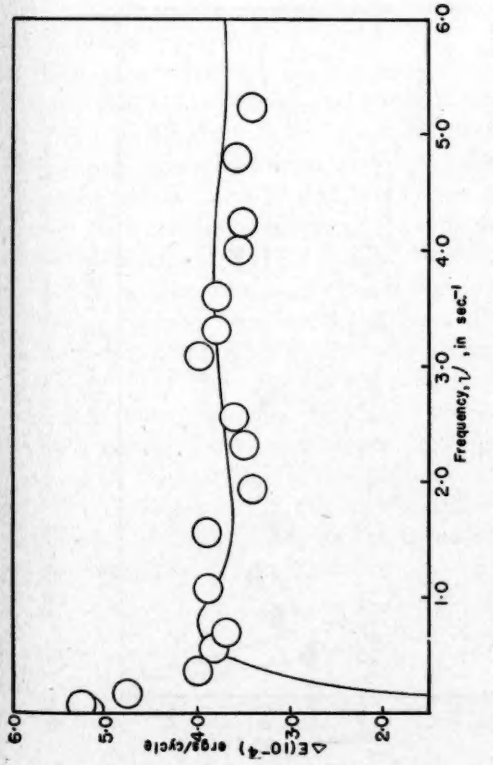

FIG. 9. *Frequency dependence of net energy absorption for nylon 610 at 29°C. The solid line gives theoretical values.*

adjusted so that a total elongation of 2% was employed in all measurements.

For each monofil, the initial datum obtained was the measurement of ΔE, the net cyclical energy absorption, as a function of cycle number at constant frequency values. This procedure was undertaken as it was observed that the measured ΔE reached a relatively constant value only after a certain number of cycles had elapsed. By making the measurement at different frequencies, it was possible to pick an average characteristic cycle number necessary for the attainment of the steady-state energy absorption for each fiber.

After the establishment of the characteristic cycle number, measurements of ΔE as a function of ν were made. All values of ΔE were measured only after the characteristic cycle number had been completed. Thus, all ΔE values were obtained under comparable conditions.

The third type measurement was that of ΔE as a function of ν at different ambient temperatures. To standardize the procedure, the characteristic cycle number was again completed before each of the values was recorded.

Results

The experimental results obtained are discussed below for the specific fibers investigated.

Polyhexamethyleneadipamide or Nylon 66 (340 denier, 0.008 in. diameter).—Figure 5 gives the ΔE *versus* cycle number values at several different frequencies. A characteristic cycle number of 400 was chosen and adhered to in all subsequent work with this polymer.

The frequency dependence of ΔE at room temperature is given in Figure 6. At very low frequencies the net energy absorption is increasing. This is explained by assuming that the number of relaxation times contributing to the total energy absorption increases as the frequency of vibration decreases. Theoretically, a frequency eventually should be reached such that the curve passes through the origin. However, an experimental determination of this might involve an infinite period of vibration.

The frequency dependence of ΔE at 0°C and 65°C is shown in Figure 7.

Polyhexamethylenesebacamide or Nylon 610 (340 denier, 0.008 in. diameter).—Net energy absorption values *versus* cycle number at constant frequencies

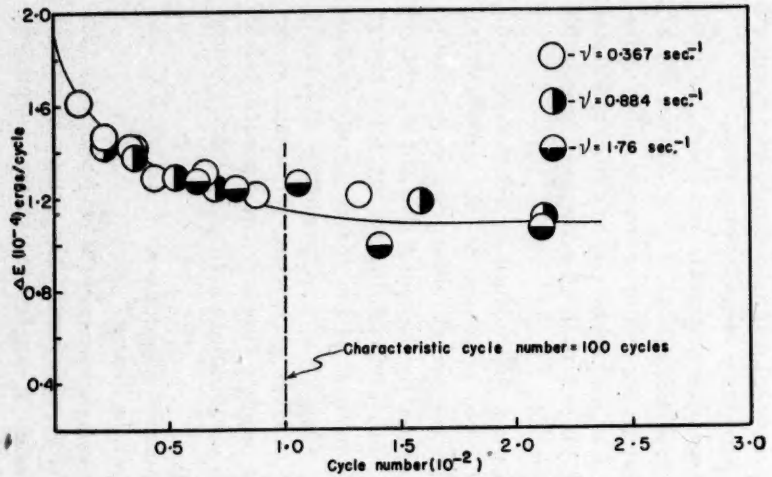

FIG. 11. *Net energy absorption as a function of cycle number for nylon 2-Me-66. The fibers were allowed to relax to their original lengths before each frequency change. The values listed represent single readings.*

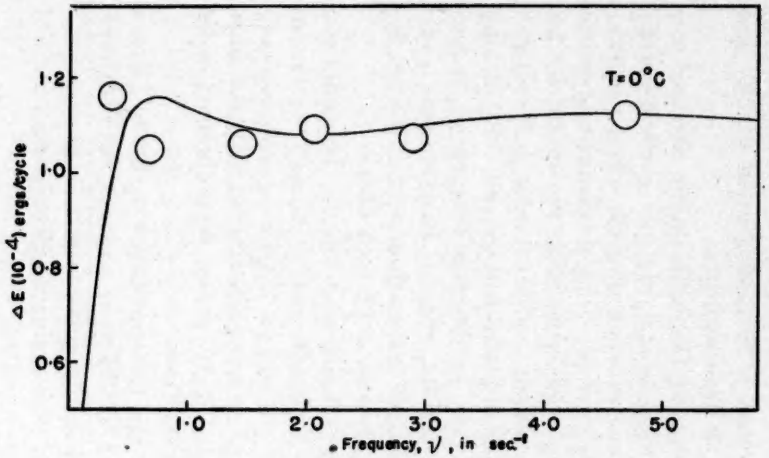

FIG. 12. *Frequency dependence of net energy absorption for nylon 2-Me-66 at 0°C. The solid line gives theoretical values.*

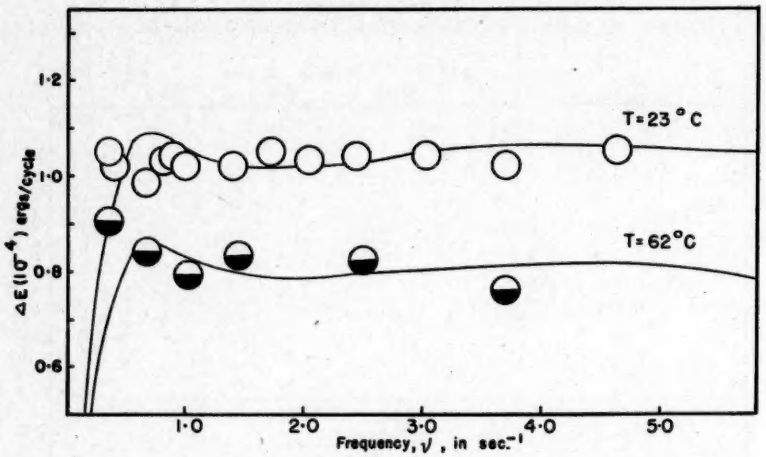

FIG. 13. *Frequency dependence of net energy absorption for nylon 2-Me-66 at 23°C and 62°C. The solid lines give theoretical values.*

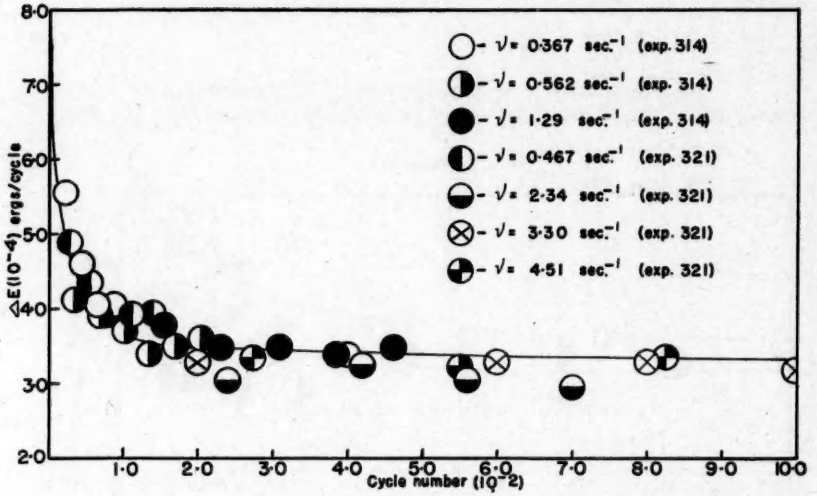
ν = 0·367 sec.⁻¹ (exp. 314)
ν = 0·562 sec.⁻¹ (exp. 314)
ν = 1·29 sec.⁻¹ (exp. 314)
ν = 0·467 sec.⁻¹ (exp. 321)
ν = 2·34 sec.⁻¹ (exp. 321)
ν = 3·30 sec.⁻¹ (exp. 321)
ν = 4·51 sec.⁻¹ (exp. 321)
ΔE (10⁻⁴) ergs/cycle
Cycle number (10⁻²)

FIG. 14. *Net energy absorption as a function of cycle number for nylon 610. Each experiment represents a series of consecutive runs made without allowing the fiber to relax between frequency changes. The same fiber was used in both experiments, with relaxation between experiments.*

are shown in Figure 8. A characteristic cycle number of 100 was chosen for this monofil.

Figures 9 and 10 give the frequency and temperature dependence of ΔE.

Poly-2-Methylhexamethyleneadipamide or Nylon 2-Me-66 (60 denier, 0.0034 in. diameter).—Data leading to the determination of a characteristic cycle number of 100 are given in Figure 11. Here, the energy absorption is clearly independent of frequency during the transient range.

The frequency and temperature dependence of ΔE are shown in Figures 12 and 13.

Discussion of Results

The discussion of results is divided into sections corresponding to the specific set of variables investigated.

Cycle Number Dependence of the Net Energy Absorption at Constant Frequency and Constant Ambient Temperature

Each monofilament tested was found to be characterized by an experimentally determined characteristic cycle number. Thus, in order to obtain a consistent net energy absorption value at a given frequency, it was necessary first to load the fiber through a given number of cycles before making a measurement. This effect is shown in Figures 5, 8, and 11.

The attainment of the steady-state net energy absorption values was found to be independent of the previous history of the fiber. Examples of this effect are shown in Figure 14. The series of tests represented by experiment 314 were run in the order listed, without allowing for relaxation of the fiber between frequency changes. Experiment 321 was run on the same fiber after it had been allowed to relax back to its original length. All of the ΔE values measured as a function of cycle number during tests 314 and 321 fall very close to a single curve. This behavior validates the use of the characteristic cycle number to obtain consistent values of the net energy absorption.

The decrease in ΔE during the transient region corresponds to a decrease in the apparent viscosity, η, according to

$$\Delta E = f(\eta_i), \tag{44}$$

where

$$\eta_i = \frac{h}{V_h} e^{\frac{\Delta F_i^{\ddagger}}{RT}}.$$

Here η_i and $\Delta F_i^{\ddagger}$ characterize the ith flow unit, and $f(\eta_i)$ is a frequency-dependent function of the η_i's.

According to equation (44), the transient decrease of ΔE may be attributed to (*1*) an increase of temperature accompanying the attainment of the steady-state values, (*2*) a thixotropic effect in which $\Delta F^{\ddagger}$ decreases to a limiting value with cycling, or (*3*) a combination of processes (*1*) and (*2*).

To check on the magnitude of the heating effect, the temperature existing within the fiber at the steady-state condition was calculated. Considering a homogeneous fiber of radius a, the rate of energy supply per unit volume is given by

$$c = \frac{\Delta E(\nu)}{V},$$

where ΔE is the steady-state net energy absorption at a frequency ν, and V is the fiber volume. In cylindrical coordinates, the differential equation giving the temperature, T_f, as a function of the fiber radius, r, is

$$K_f \left(\frac{d^2T_f}{dr^2} + \frac{1}{r}\frac{dT_f}{dr} \right) = -c, \tag{45}$$

where K_f is the thermal conductivity of the fiber. Integration of equation (45) gives

$$T_f = c_1 \ln r - \frac{c}{4K_f} r^2 + c_2 \tag{46}$$

for the temperature within a fiber as a function of the distance from its axis.

The surface of the moving fiber will be at a slightly higher temperature than the ambient temperature, and hence the fiber may be considered to be surrounded by a film of air of thickness δ, across which exists a temperature gradient. Since this film serves merely as a conductor of heat, the relationship of T to r is given by

$$\frac{d^2T}{dr^2} + \frac{1}{r}\frac{dT}{dr} = 0, \tag{47}$$

which integrates as

$$T = c_3 \ln r + c_4. \tag{48}$$

The boundary conditions relating equations (46) and (48) are

(*a*) $T_f = T$ at $r = a$

(*b*) $K_f \frac{dT_f}{dr} = K \frac{dT}{dr}$ at $r = a$

TABLE II. SURFACE AND INTERNAL TEMPERATURES AS CALCULATED FOR NYLON 66 MONOFILS AT STEADY-STATE CONDITIONS

Ambient temperature (°K)	Surface temperature (°K)	Temperature ($r = 10^{-3}$ cm.)	Temperature ($r = 10^{-4}$ cm.)	Temperature ($r = 10^{-5}$ cm.)	Temperature ($r = 10^{-6}$ cm.)
273.000	273.053	273.079	273.091	273.103	273.114
298.000	298.043	298.070	298.087	298.104	298.121
338.000	338.044	338.064	338.073	338.082	338.091

(*c*) T = ambient temperature at $r = a + \delta$

(*d*) At the steady state, and for $r = a + \delta$, the heat flux is constant as given by

$$K\frac{dT}{dr} = -\frac{\Delta E(\nu)}{A},$$

where A is the surface area of the fiber.

Application of these boundary conditions is sufficient to determine the parameters c_1, c_2, c_3, and c_4 as

$$c_1 = \frac{K}{K_f}c_3 + \frac{ca^2}{2K_f},$$

$$c_2 = (c_3 - c_1)\ln a + c_4 + \frac{ca^2}{4K_f},$$

$$c_3 = -\frac{\nu(a+\delta)\Delta E}{AK},$$

$$c_4 = T_A - c_3 \ln (a + \delta),$$

where T_A is the ambient temperature. Using $K = 5.4 \times 10^{-5}$ cal./cm. sec. degree, $K_f = 2 \times 10^{-4}$ cal./cm. sec. degree, average values of ΔE as obtained from Figures 6 and 7, and estimating $\delta = 0.005$ cm., the surface and internal temperatures given in Table II were calculated.

The surface and internal temperatures are seen to be only very slightly greater than the corresponding ambient temperatures. This is reasonable in view of (*1*) the relatively small amount of energy expended upon the fiber per cycle, and (*2*) the large ratio of surface area to volume (≈ 200 cm.$^{-1}$), which characterizes the polyamide monofils used and results in a rapid conduction of heat away from the fiber.

Thus, in view of the small temperature effects shown in Table II, the phenomenon of thixotropy is apparently largely responsible for the transient decrease of ΔE with cycle number.

A stress-free fiber at thermal equilibrium with its surroundings will be characterized by a free-energy minimum. The entropy contribution to this minimum will represent the maximum internal disorder that is tenable with the intrinsic structure of the particular fiber.

The cycling process during the transient region may be looked upon as serving to reorient some of the disordered regions. Thus, the flow process is gradually facilitated, and a state is finally reached (at the characteristic cycle number) in which the imposed strain is accommodated by the sample with a minimum amount of difficulty. In other words, the flow units become "oiled up" during the transient region of the net energy absorption. Upon removal of the imposed strain for a period of time (minimum of about 1 min.), the simulated flow units revert back to their original stress-free configurations. The attainment of a convenient flow unit thus implies a decrease of activation energy to a limiting value. These limiting values of $\Delta F^{\ddagger}$ are listed in Table V.

Frequency Dependence of Net Energy Absorption Under Conditions of Constant Cycle Number and Constant Ambient Temperature

It has been shown theoretically that the net energy absorption, ΔE, is related to the frequency of vibration in the following fashion:

$$\Delta E = \frac{\pi a^2 V g^2 \eta \omega}{\omega^2\eta^2 + g^2},$$

where $\omega = 2\pi\nu$. Also, the frequency at which ΔE is a maximum for a given value of the parameters g and η has been shown to be

$$\nu_m = \frac{g}{2\pi\eta} = \frac{1}{2\pi\tau},$$

where τ is the relaxation time characterizing a given dissipative unit.

Examination of a ΔE *versus* ν curve, as measured at a given ambient temperature, indicates an almost constant net energy absorption over the frequency range studied. This frequency independence of the net energy absorption is seen to occur for all three

TABLE III. VALUES OF AVERAGE PARAMETERS USED IN THE DERIVATION OF THEORETICAL EXPRESSIONS FOR ΔE AS A FUNCTION OF FREQUENCY

Fiber type	Ambient temperature (°K)	ν_m (sec.$^{-1}$)	ω_m (sec.$^{-1}$)	$\Delta E_m(10^{-4})$ $\left(\frac{\text{ergs}}{\text{cycle}}\right)$	$g_1(10^{-9})$ $\left(\frac{\text{dynes}}{\text{cm.}^2}\right)$	$\eta_1(10^{-9})$ $\left(\frac{\text{dyne sec.}}{\text{cm.}^2}\right)$	ν_m (sec.$^{-1}$)	ω_m (sec.$^{-1}$)	$\Delta E_m(10^{-4})$ $\left(\frac{\text{ergs}}{\text{cycle}}\right)$	$g_2(10^{-9})$ $\left(\frac{\text{dynes}}{\text{cm.}^2}\right)$	$\eta_2(10^{-8})$ $\left(\frac{\text{dyne sec.}}{\text{cm.}^2}\right)$
66	273	0.60	3.77	5.25	9.45	2.53	5.80	36.4	5.00	9.09	2.50
66	298	0.60	3.77	4.30	7.54	2.00	5.80	36.4	4.10	7.19	1.98
66	338	0.60	3.77	4.10	7.46	1.98	5.80	36.4	3.88	7.05	1.94
2-Me-66	273	0.60	3.77	0.950 (5.42)*	9.95	2.64	5.80	36.4	0.900 (5.13)*	9.43	2.59
2-Me-66	296	0.60	3.77	0.894 (5.10)	9.83	2.61	5.80	36.4	0.853 (4.87)	9.37	2.57
2-Me-66	335	0.60	3.77	0.690 (3.94)	7.23	1.92	5.80	36.4	0.660 (3.76)	6.92	1.90
610	273	0.60	3.77	4.41	8.02	2.12	5.80	36.4	4.21	7.64	2.10
610	302	0.60	3.77	3.22	5.65	1.50	5.80	36.4	3.07	5.38	1.48
610	335	0.60	3.77	3.54	6.44	1.71	5.80	36.4	3.38	6.14	1.69

* Bracketed entries are ΔE_m values for the 0.0034-in. diameter monofil recalculated on the basis of a 0.008-in. diameter monofil.

monofils over the temperature range investigated. The average values of the net energy absorption over the frequency range investigated are thus dependent on the particular fiber being tested and on the value of the ambient temperature.

The observed ΔE *versus* frequency curves may be predicted theoretically by assuming the presence of two separate average relaxation times, τ_1 and τ_2. These values of τ define four average parameters, as follows:

$$\tau_1 = \frac{\eta_1}{g_1}, \quad \tau_2 = \frac{\eta_2}{g_2},$$

and each value of τ is also characterized by a corresponding maximum energy loss—that is, ΔE_{m1} for τ_1 and ΔE_{m2} for τ_2. The mechanical analog of this model is given in Figure 2 (bottom). The units labeled Q, R, $\cdots$ N are considered to act as pure springs because the corresponding values of η are assumed to be too high to contribute over the observed frequency range. The significance of these units is discussed in a later section (p. 242).

By picking appropriate values of ΔE_{m1} and ΔE_{m2} at frequencies defined by ν_1 and ν_2, it is possible to obtain an expression containing the sum of two terms each of the form of equation (15). Values of the average parameters used are listed in Table III, while the theoretical expressions for ΔE as a function of ν and temperature are given in Table IV. The solid curves giving ΔE *versus* ν data (Figures 6, 7, 9, 10, 12, and 13) were calculated from the derived equations listed in Table IV. The same relaxation times, τ_1 and τ_2, are found to describe the behavior of all three fibers over the observed temperature and frequency ranges.

TABLE IV. THEORETICAL EXPRESSIONS FOR NET CYCLIC ENERGY ABSORPTION AS DEPENDENT ON FREQUENCY AND TEMPERATURE

Fiber type	Ambient temperature (°A)	Theoretical expressions for ΔE as a function of frequency
66	273	$\Delta E = \frac{2.79 \times 10^4\,\omega}{0.0709\,\omega^2 + 1} + \frac{2.75 \times 10^3\,\omega}{0.000752\,\omega^2 + 1}$
66	298	$\Delta E = \frac{2.28 \times 10^4\,\omega}{0.0709\,\omega^2 + 1} + \frac{2.25 \times 10^3\,\omega}{0.000752\,\omega^2 + 1}$
66	338	$\Delta E = \frac{2.18 \times 10^4\,\omega}{0.0709\,\omega^2 + 1} + \frac{2.13 \times 10^3\,\omega}{0.000752\,\omega^2 + 1}$
610	273	$\Delta E = \frac{2.33 \times 10^4\,\omega}{0.0709\,\omega^2 + 1} + \frac{2.31 \times 10^3\,\omega}{0.000752\,\omega^2 + 1}$
610	302	$\Delta E = \frac{1.71 \times 10^4\,\omega}{0.0709\,\omega^2 + 1} + \frac{1.69 \times 10^3\,\omega}{0.000752\,\omega^2 + 1}$
610	335	$\Delta E = \frac{1.88 \times 10^4\,\omega}{0.0709\,\omega^2 + 1} + \frac{1.86 \times 10^3\,\omega}{0.000752\,\omega^2 + 1}$
2-Me-66	273	$\Delta E = \frac{5.04 \times 10^3\,\omega}{0.0709\,\omega^2 + 1} + \frac{4.95 \times 10^2\,\omega}{0.000752\,\omega^2 + 1}$
2-Me-66	296	$\Delta E = \frac{4.72 \times 10^3\,\omega}{0.0709\,\omega^2 + 1} + \frac{4.68 \times 10^2\,\omega}{0.000752\,\omega^2 + 1}$
2-Me-66	335	$\Delta E = \frac{3.66 \times 10^3\,\omega}{0.0709\,\omega^2 + 1} + \frac{3.63 \times 10^2\,\omega}{0.000752\,\omega^2 + 1}$

The temperature variation of ΔE thus appears in the values of g_1, η_1, g_2, and η_2, while their respective quotients remain constant, as defined by τ_1 and τ_2. This treatment implies that essentially the same process of temperature-dependent stress-biased seg-

ment diffusion occurs in all of the fibers tested. This is reasonable when it is recalled that all three fibers employed are characterized by a high degree of crystallinity resulting from the cold-drawing process involved.

According to the data listed in Table III, the average parameter values g_1, η_1, g_2 and η_2 have somewhat similar values for nylon 66 and nylon 2-Me-66. Corresponding values for nylon 610 are lower.

A possible explanation of this difference in the parameters used to describe the observed rheological behavior may be made in terms of known x-ray data.

Bunn and Garner [2] described the crystal structure of nylon 66 and nylon 610 as follows:

"Detailed interpretations of the x-ray diffraction patterns of fibers and sheets of the two polyamides indicate that the crystal structures of the two substances are completely analogous.

"Fibers of these two polyamides usually contain two different crystalline forms, α and β, which are different packings of geometrically similar molecules; most fibers consist chiefly of the α form. In the case of the nylon 66 polymer, fibers have been obtained in which there is no detectable proportion of the β form.

"Unit cell dimensions and the indices of reflection for the α form were determined by trial, using normal fiber photographs, and were checked by using doubly oriented sheets set at different angles to the x-ray beam. The unit cell of the α form is triclinic, with $a = 4.9$ Å., $b = 5.4$ Å., c (fiber axis) $= 17.2$ Å., $\alpha = 48\frac{1}{2}°$, $\beta = 77°$, $\gamma = 63\frac{1}{2}°$ for the 66 polymer; $a = 4.95$ Å., $b = 5.4$ Å., c (fiber axis) $= 22.4$ Å., $\alpha = 49°$, $\beta = 76\frac{1}{2}°$, $\gamma = 63\frac{1}{2}°$ for the 610 polymer. One chain molecule passes through the cell in both cases.

"Atomic coordinates in α crystals were determined by interpretation of the relative intensities of the reflexions. The chains are planar or very nearly so; the oxygen atoms appear to lie a little off the plane of the chain. The molecules are linked by hydrogen bonds between

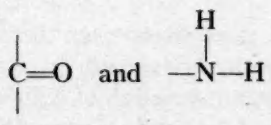

groups to form sheets. A simple packing of these sheets of molecules gives the α arrangement. An alternative packing of the sheets gives a two-molecule triclinic cell, and this is the structure proposed for the β form. Streaks on the layer lines (but not on the equator) of fiber photographs are attributed to an arrangement of molecular sheets in which α and β groupings occur at random."

Thus, the structure of a nylon 66 and a nylon 610 polymer (of the same crystalline form) may be considered to be completely analogous except that the monomer unit in the latter case is four carbon atoms longer than it is in the former case.

Apparently, the two polymers differ mainly in that the density of hydrogen bonds is slightly greater in the 66 than in the 610 polymer. The molecules comprising the former should be more strongly held together by secondary valence forces than those comprising the latter case.

It appears that the addition of a methyl group in the 2 position of the 66 polymer has but little effect upon the values of the average parameters as derived for the 66 polymer. This is further evidence that the density of secondary bonds plays a large part in determining the rheological properties of the polyamides.

Since the melting point of a solid is a good criterion of its internal or cohesive energy, the density of hydrogen bonding should be reflected in the observed melting points of the polyamides. Baker and Fuller [1] list the following values:

Polyamide	Melting point (°C)	Identity period (Å.)
66	265	17.4
106	230	20.0
610	214	21.6
1010	197	25.6
99	175	24.0

Thus, as the identity period increases, the melting point decreases and the density of hydrogen bonds apparently decreases.

The observed differences in the average parameters obtained in the present work may be ascribed to the effect of secondary or hydrogen bonding.

Temperature Dependence of the Viscosity Coefficient, Elastic Constant, and Net Energy Absorption at Constant Cycle Number

Viscosity Coefficient.—A first approach to an elucidation of the temperature dependence of the net cyclical energy absorption is through an examination of the free energy of activation as calcu-

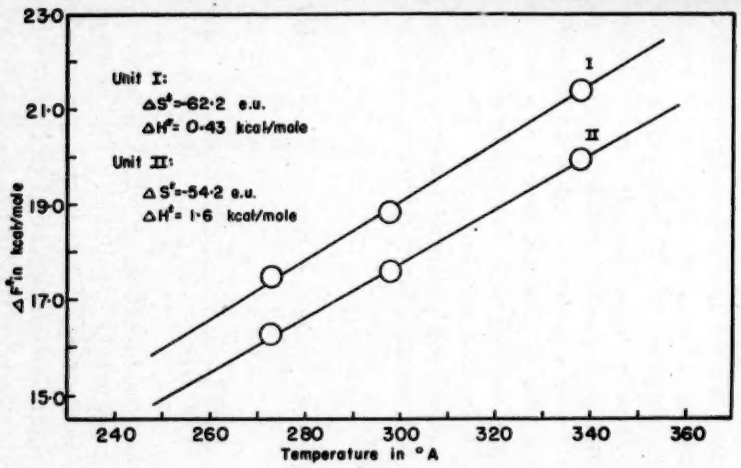

FIG. 15. *Variation of* ΔF‡ *with* T, *showing the values of the activation parameters corresponding to the two average segment-moving processes found to characterize nylon 66.*

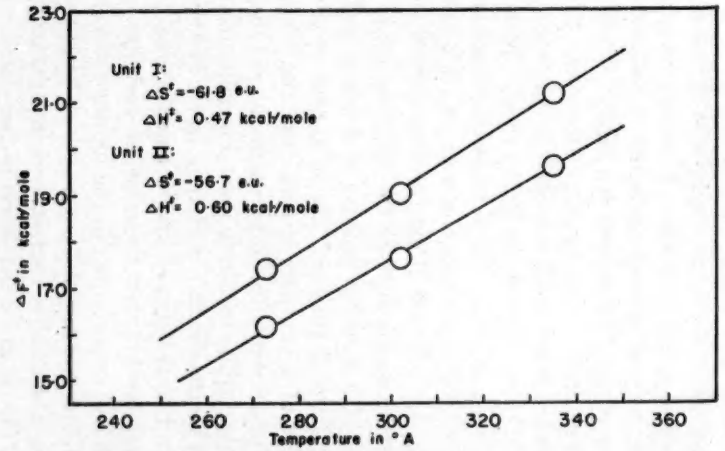

FIG. 16. *Variation of* ΔF‡ *with* T, *showing the values of the activation parameters corresponding to the two average segment-moving processes found to characterize nylon 610.*

TABLE V. ACTIVATION PARAMETERS FOR THE FLOW PROCESS OF THREE POLYAMIDE MONOFILS

Fiber type	Ambient temperature (°K)	η/g (sec.)	$\Delta F‡$ $\left(\frac{\text{kcal.}}{\text{mole}}\right)$	$\Delta S‡$ (e. u.)	$\Delta H‡$ $\left(\frac{\text{kcal.}}{\text{mole}}\right)$
66	273	0.265	17.4		
66	298	0.265	18.9	−62.2	0.430
66	338	0.265	21.4		
66	273	0.0275	16.2		
66	298	0.0275	17.5	−54.2	1.60
66	338	0.0275	19.9		
610	273	0.265	17.3		
610	302	0.265	19.0	−61.8	0.470
610	335	0.265	21.1		
610	273	0.0275	15.9		
610	302	0.0275	17.6	−56.7	0.600
610	335	0.0275	19.6		
2-Me-66	273	0.265	17.4		
2-Me-66	296	0.265	18.9	−60.5	0.870
2-Me-66	335	0.265	21.2		
2-Me-66	273	0.0275	16.2		
2-Me-66	296	0.0275	17.5	−54.6	1.30
2-Me-66	335	0.0275	19.6		

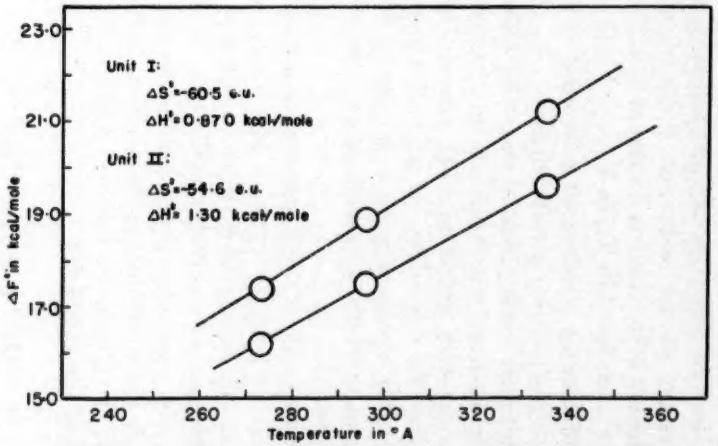

FIG. 17. *Variation of* ΔF‡ *with* T, *showing the values of the activation parameters corresponding to the two average segment-moving processes found to characterize nylon 2-Me-66.*

ated from the apparent average viscosity values characteristic of the relaxation times, τ_1 and τ_2. The values of $\Delta F\ddagger$, based on a value of $V = 2 \times 10^{-22}$ cm.^{3} [11], are listed in Table V.

Before drawing conclusions from these values, it is well to restate their significance.

The cyclical testing used in this work represents a specific method for determining the characteristic fiber parameters g and η. The magnitude of η determines the free energy of activation necessary for flow, and is thus actually a measure of the ease of attainment of the activated state by the molecular segments.

The magnitude of the free energy of activation is the result of both an entropy and a heat effect. The former is associated with the extent of orientation accompanying segment activation, while the latter gives a measure of the net bond energy absorbed or given off during the segment activation process. To obtain the values of $\Delta S\ddagger$ and $\Delta H\ddagger$, use is made of the expression

$$\Delta F\ddagger = \Delta H\ddagger - T\Delta S\ddagger.$$

Figures 15, 16, and 17 are plots of $\Delta F\ddagger$ *versus* T, giving straight lines whose slopes $= -\Delta S\ddagger$ and whose intercepts are $\Delta H\ddagger$. The data so obtained are summarized in Table V.

Judging from the large negative $\Delta S\ddagger$ values, the process of segment activation is largely one of the attainment of an appropriate spatial configuration. Since the crystalline regions are characterized by a high initial degree of order, the attainment of such an activated state must involve the amorphous or randomly oriented regions of the fiber. Hence, it may be that in order for a molecular segment to move, at least part of the chain to which it belongs must first be oriented along the direction of stress.

The main significance of the $\Delta H\ddagger$ values is that they are of a positive nature, and hence indicate an endothermic process. Such a process is undoubtedly of a complex nature, and the observed $\Delta H\ddagger$ values serve only to represent the net over-all energy absorption resulting from a number of stress response mechanisms. A change in the number of hydrogen bonds between chains constituting layers in a crystalline region (increase or decrease of % crystallinity) or a change in the number of van der Waals' bonds between layers may well be involved.

Elastic Constant.—The second temperature-dependent factor to be discussed is the parameter g, the elastic constant. Values of g_1 and g_2 as derived from the values of τ_1 and τ_2 at different temperatures for the three polyamide monofils are listed in Table III. In general, the g values decrease with increasing temperature.

Hence, according to equation (32),

$$g = \frac{3N'kT}{al_o}, \qquad (32)$$

derived on the basis of purely entropy-dependent elasticity, the values of N'/al_o must decrease fairly rapidly with rising temperature. Then, al_o/N', the effective volume of the elastic unit, must increase with increasing temperature. Values of $(al_o/N')_{\mathrm{I}}$ calculated for the three polyamides on the basis of equation (32) are listed in Table VI.

As shown earlier (Table I), the concept of entropy-dependent elasticity best describes the behavior of elastomers which are characterized by a very low degree of internal symmetry. In this case, the change in potential energy on stretching may be considered to be small and the free-energy change thus accredited to the entropy decrease accompanying elongation of the material. Plausible values of $(al_o/N')_{\mathrm{I}}$ for elastomers were obtained using this approach.

Values of $(al_o/N')_{\mathrm{I}}$ listed in Table I for polystyrene, a cast phenolic, and polymethylmethacrylate are seen to be of the same small order of magnitude as those obtained for the polyamides (Table VI). All of these materials possess a much higher degree of three-dimensional symmetry or crystallinity than do the elastomers. Hence, the small values of $(al_o/N')_{\mathrm{I}}$ may be attributed to a lack of consideration of the potential energy change occurring during the process of elongation. The inclusion of an approximate potential energy contribution to the free energy change occurring has been shown to give

$$g = \frac{N'}{al_o}(3kT + k_1br_o^2), \qquad (42)$$

so that

$$\left(\frac{al_o}{N'}\right)_{\mathrm{II}} \equiv \frac{3kT + k_1br_o^2}{g}. \qquad (43)$$

As an indication of its effect on $(al_o/N')_{\mathrm{I}}$, a potential energy term will be calculated. The problem involves an evaluation of $k_1br_o^2$, and, since r_o is known, an approximate calculation of $k_1r_o^2$ can be made. The average force constant, k_1, is assumed

to be applicable to the $N'b$ effective bond angles involved during the elongation process.

Consider the model shown on page 230 to be composed of three carbon atoms comprising part of the "backbone" of a long chain molecule. The known parameters are $l = 1.54$ Å., $\theta_o = 55.5°$, $r_o = 1.27$ Å., and the potential energy, E', is assumed to be equal to the average total amount of work done per cycle on the polyamide monofils over the observed frequency range of the present experiments. Then, as

$$r = l \sin \theta,$$

a change of $\delta\theta$ will cause a corresponding change of δr,

$$\delta r = l \cos \theta \delta\theta, \tag{49}$$

such that for a 2% elongation,

$$\frac{\delta r}{r} = 0.020 = \frac{l \cos \theta \delta\theta}{l \sin \theta} = \cot \theta \delta\theta. \tag{50}$$

Hence, for $\cot \theta = \cot \theta_o$,

$$\delta\theta = 0.029 \text{ radian}, \tag{51}$$

and a 2% elongation of r requires that θ increase by 1.67°.

As defined by equation (34),

$$E' = \frac{N'bk_1}{2}(r - r_o)^2$$

$$= \frac{N'bk_1l^2}{2}[\sin(\theta_o + \delta\theta) - \sin\theta_o]^2, \tag{52}$$

and, using $E' = 3.71 \times 10^5$ ergs, equation (52) becomes

$$k_1 = \frac{1.22 \times 10^{25}}{N'b}. \tag{53}$$

Hence, k_1 is inversely proportional to N', and, as a first approximation, an average N', based on the values of $(al_o/N')_I$ as calculated for the polyamides, is used. The value of $k_1r_o^2$ thus becomes

$$k_1r_o^2 = \frac{1.05 \times 10^{-12} \text{ erg}}{b}.$$

Hence,

$$\left(\frac{al_o}{N'}\right)_{II} \approx \frac{3kT + 1.05 \times 10^{-12}}{g}; \tag{54}$$

the values of $(al_o/N')_{II}$ so calculated are listed in Table VI.

Thus, on the basis of this first approximation to the potential energy contribution, the values of al_o/N' are increased by a factor of 8 to 10. According to the above method of approach, the actual extent of the potential energy contribution is fixed by the values of E' and N' characteristic of a given fiber and experiment.

TABLE VI. APPARENT VOLUMES OF ELASTIC UNITS AS CALCULATED ON THE BASIS OF (I) ENTROPY-DEPENDENT ELASTICITY AND (II) ELASTICITY DEPENDENT ON ENTROPY AND POTENTIAL ENERGY

Fiber type	η/g (sec.)	Ambient temperature (°K)	$g(10^{-9})$ $\left(\frac{\text{dynes}}{\text{cm.}^2}\right)$	$\left(\frac{al_o}{N'}\right)_I (10^{24})$ $\left(\frac{\text{cm.}^3}{\text{unit}}\right)$	$\left(\frac{al_o}{N'}\right)_{II} (10^{24})$ $\left(\frac{\text{cm.}^3}{\text{unit}}\right)$
66	0.265	273	9.45	12.0	123
66	0.265	298	7.54	16.3	156
66	0.265	338	7.46	18.8	160
66	0.0275	273	9.09	12.4	128
66	0.0275	298	7.19	17.2	163
66	0.0275	338	7.05	19.8	169
2-Me-66	0.265	273	9.95	11.4	117
2-Me-66	0.265	296	9.83	12.5	119
2-Me-66	0.265	335	7.23	18.2	164
2-Me-66	0.0275	273	9.43	12.0	123
2-Me-66	0.0275	296	9.37	13.1	125
2-Me-66	0.0275	335	6.92	20.0	171
610	0.265	273	8.02	14.1	145
610	0.265	302	5.65	22.1	208
610	0.265	335	6.44	21.5	185
610	0.0275	273	7.64	14.8	152
610	0.0275	302	5.38	23.2	218
610	0.0275	335	6.14	22.6	194

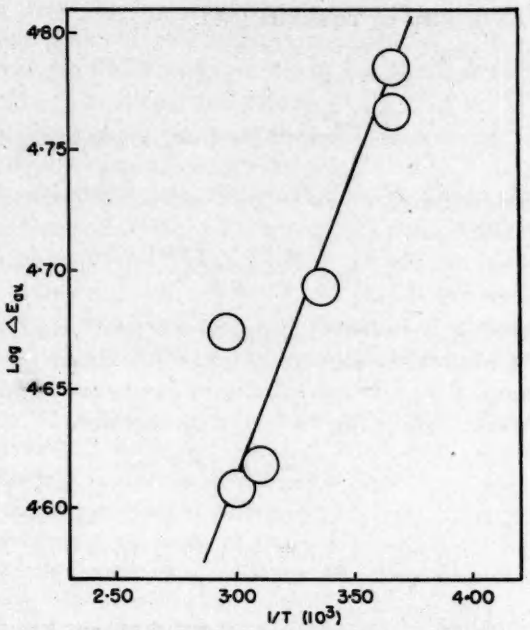

FIG. 18. *Ambient temperature dependence of the average net cyclical energy absorption for nylon 66.*

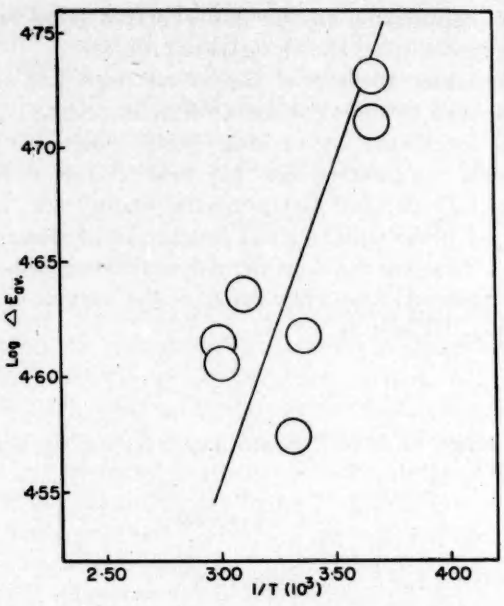

FIG. 19. *Ambient temperature dependence of the average net cyclical energy absorption for nylon 610.*

In the case of the highly crystalline polyamides, N' would be expected to be smaller than the values obtained by considering entropy elasticity alone. Hence, the actual values of al_o/N' would presumably be larger than those listed as $(al_o/N')_{II}$.

Net Energy Absorption.—The values of ΔE_{av} (average values of ΔE over the observed frequency range for a given fiber at a given ambient temperature) are experimentally found to decrease almost exponentially with increasing temperature. This is consistent with the concept that the magnitude of ΔE is a measure of the extent of nonequilibrium existing during the cycling process. Hence, the observed temperature dependence of ΔE should be of the same form as that (equation (4)) derived for the time-dependent parameter η (g considered to be independent of time)—that is,

$$\Delta E_{av} \propto e^{\frac{B}{T}},$$

where B should be a constant for a given fiber. Figures 18, 19, and 20 give the observed temperature dependence of the average net energy absorption values. The plots of $\log \Delta E_{av}$ *versus* $1/T$ are approximately linear with slopes = $B/2.30$.

Nonlinear Spring Characteristic of the Net Energy Absorption Loops

Without exception, all of the stress-strain loops representing net energy absorption were characterized by a nonlinear bisectrix or spring line. Figure 21 is an example of the observed loop shape. Also, the loop shape is essentially independent of fiber, frequency, and ambient temperature. Theoretically, for a system characterized by a linear spring, the loops should comprise a symmetrical hysteresis area located on both sides of a linear spring line.

The nonlinearity of the spring line is indicative of the possible existence of at least two phenomena: (*1*) different viscous units come into play at different points during a cycle, and (*2*) different springs come into play at different points during a cycle. The former possibility may be ruled out because the loop shown in Figure 21 has very nearly a plane of symmetry through the line AB. If there had been a marked sporadic movement of viscous elements during a given cycle, this symmetry would completely disappear.

The second approach is used to treat the problem of the nonlinear spring line.

Consider that the shape of the apparent nonlinear spring line is given by the bisectrix of the stress-strain loop of Figure 21. A model predicting the observed results is shown in Figure 2 (bottom). Here, the Maxwell units O and P are characterized by the parameters obtained from fitting the frequency-dependent curves. Consider that the remaining Maxwell units, Q, R, ··· N, have very

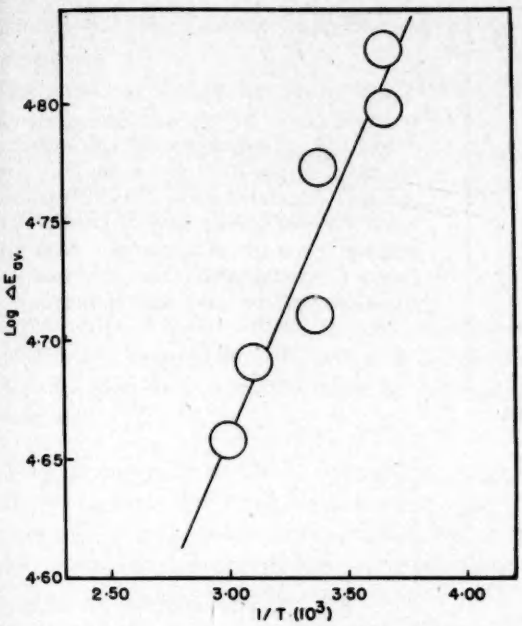

FIG. 20. *Ambient temperature dependence of the average net cyclical energy absorption for nylon 2-Me-66.*

high values of η so that they behave as pure springs, each with an elastic constant g over the frequency range investigated. The dashpots of the units Q, R, $\cdots$ N are considered to be elongated initially to different extents so that the springs come into play at different values of s.

Then, let the slope at any point on the bisectrix or nonlinear spring line be given by g_a. Thus, g_a is assumed to be a continuously varying function of the imposed strain. If n is the number of springs operating at a given elongation, then $g_a = ng$.

As the fiber is elongated through a distance ds, assume that

$$\frac{dn}{ds} = a,$$

where a is a constant dependent upon the degree of polymerization and the extent of crystallinity existing in the polymer structure. Integration gives

$$\int_{n_o}^{n} dn = a \int_{o}^{s} ds,$$

so that

$$n = n_o + as, \tag{55}$$

where n_o = number of springs under tension due to the initial stress bias, F_o. Justification for this assumption of linearity appears through the correlation attained with the observed data.

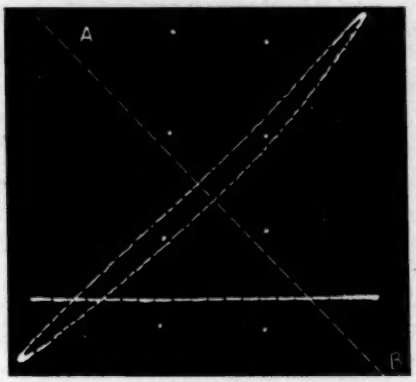

FIG. 21. *Typical net energy absorption loop.*

Now, if F is the applied force per unit area, and s is again the resultant relative displacement, we have

$$dF = g_a ds = ngds, \tag{56}$$

and, from equation (55),

$$dF = (n_o + as)gds. \tag{57}$$

Integration over the appropriate limits gives

$$\int_{F_o}^{F} dF = \int_{o}^{s} (n_o g + ags)ds, \tag{58}$$

or

$$F = F_o + n_o gs + \frac{ag}{2} s^2. \tag{59}$$

Equation (59) thus describes the apparent over-all stress-strain relationship of a large number of separate spring units that come into play at different values of s. This equation, which describes the observed behavior of the polyamide monofils, differs somewhat in form from equation (40), due presumably to the approximations involved in arriving at the potential energy contribution to equation (40).

From the actual slopes of the observed nonlinear spring lines, the values of the constants $n_o g$ and $ag/2$ have been derived for nylon 66 and nylon 610. The resultant equations are

$$F = F_o + 112\, s + 12.1\, s^2$$

and

$$F = F_o + 106\, s + 10.0\, s^2,$$

respectively. It is to be noted that the conditions of testing to which these equations apply are

$$\frac{ds}{dt} = a\omega \cos \omega t$$

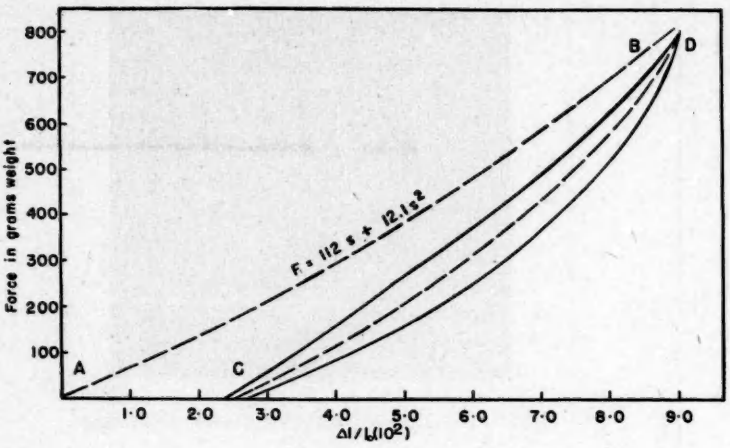

FIG. 22. *Comparison of calculated and observed spring lines for nylon 66. Curve AB was calculated using the expression derived for the spring line of a loop representing cyclical net energy absorption. Curve CD is the spring line observed under conditions of constant rate of loading.*

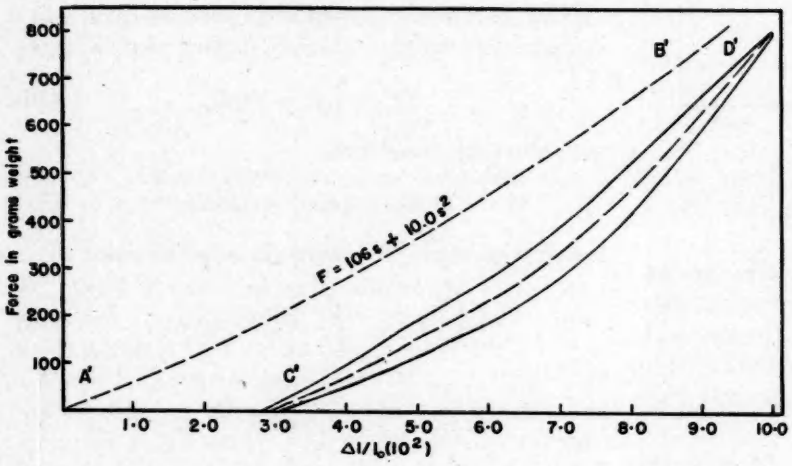

FIG. 23. *Comparison of calculated and observed spring lines for nylon 610. Curve A'B' was calculated using the expression derived for the spring line of a loop representing cyclical net energy absorption. Curve C'D' is the spring line observed under conditions of constant rate of loading.*

and

$$\frac{dF}{dt} = f(t) = b\omega \cos(\omega t + \delta).$$

The criterion of worth of such a derivation as is given above lies in its applicability to data obtained under diverse conditions of testing.

Figures 22 and 23 represent the sixth consecutive stress-strain loops as obtained under conditions of a constant rate of loading and unloading. For a fiber of cross section m, and at a rate of $\frac{1.67}{m}\frac{\text{g.}}{\text{sec.}}$, the fiber was loaded to a maximum stress value of $\frac{800}{m}$ g. This upper stress limit was set because it was found that at this rate of loading, rupture of the fiber occurred between $\frac{900}{m}$ and $\frac{1000}{m}$ g. The conditions of this test are thus described by

$$\frac{ds}{dt} = f_1(t)$$

and

$$\frac{dF}{dt} = \frac{1.67}{m}\frac{\text{g.}}{\text{sec.}}.$$

As was done in the case of the sixth consecutive loops obtained under conditions of sinusoidal loading, the sixth consecutive stress-strain loops of Figures 22 and 23 have been bisected to yield spring lines CD and C'D'. Again, they are of a nonlinear form.

The correlation of these very different tests is obtained by reading abscissa values from the constant rate of loading nonlinear spring line and calculating the corresponding ordinate values using the derived expressions for the cyclical loading tests. Curves AB and A'B' are obtained in this fashion. Thus, the calculated curves are practically parallel to the observed curves up to about 7% elongation. The deviation at values greater than this may be attributed to an increase of crystallinity which occurs as the rupture point is approached, as

shown in the case of the constant rate of loading experiments.

The good agreement between the calculated and observed nonlinear spring lines, in view of the very different conditions of testing involved, is evidence in favor of the assumed linear distribution of spring-like units according to equation (55).

Summary

The results of this theoretical and experimental approach to the problem of certain dynamic properties of polyamide monofils may be summarized as follows:

(1) The application of a sinusoidally varying strain to highly crystalline monofilaments of polyhexamethyleneadipamide, polyhexamethylenesebacamide and poly-2-methylhexamethyleneadipamide results in a net cyclical energy absorption. Using a 2% average strain bias, with a superimposed sinusoidal strain having an amplitude of 1%, the values of the net cyclical energy absorption are found to vary from 0.8×10^4 ergs per cycle to 9.0×10^4 ergs per cycle.

(2) A theory based on the absolute reaction-rate treatment of viscous flow is developed which relates the net cyclical energy absorption to the frequency of vibration. The model used in an evaluation of the parameters g and η includes both elastic (time-independent and nondissipative) elements and viscous (time-dependent and dissipative) elements.

(3) Each monofilament is found to exhibit a characteristic cycle number. This constant represents the number of cycles through which a fiber must be worked in order to attain a steady-state net energy absorption. The constant is found to be essentially independent of frequency.

The phenomenon of the transient net energy absorption is attributed to a thixotropic change involving the simulation of a most convenient flow unit under the given conditions of testing. Calculations of the internal temperature at the steady state indicate that the increase of temperature over the ambient temperature during the transient period is very small.

(4) At the steady state, the observed values of the net energy absorption are found to be practically independent of frequency over a 20-fold frequency range, 0.350 sec.$^{-1}$ to 5.80 sec.$^{-1}$, and a temperature range of 0°C to 65°C. Measurements made at room temperature on samples of polyhexamethyleneadipamide and polyhexamethylenesebacamide over a 100-fold frequency range, 0.058 sec.$^{-1}$ to 5.80 sec.$^{-1}$, indicate a frequency independence except in the very low frequency region.

(5) By considering two average relaxation times, τ_1 and τ_2, it is shown to be possible to reproduce the observed net energy absorption *versus* frequency curves for the three fibers at the various temperatures. The values of $\tau_1 = \eta_1/g_1$ and $\tau_2 = \eta_2/g_2$ fix values of g_1, g_2, η_1, and η_2. The consistent usage of the relaxation times τ_1 and τ_2 implies that the stress response of all three fibers is similar. This is justifiable in light of the high degree of crystallinity common to the three fibers.

An advantage of the cyclical method of testing is emphasized in the isolation of the parameters describing two average flow units. An extension of the experiments to a larger frequency range should result in an isolation of parameters corresponding to a large number of average flow units.

(6) From the values of η_1 and η_2 at different temperatures, free energies of activation are calculated. For the average flow unit characterized by a relaxation time τ_1, the values of $\Delta F^{\ddagger}$ vary from 17.3 to 21.4 kcal./mole. For the relaxation time τ_2, $\Delta F^{\ddagger}$ varies from 15.9 to 19.9 kcal./mole. The increase of activation energy with increasing temperature is characteristic of processes involving large negative entropies of activation. The magnitude of these activation energies is typical of processes which occur during a convenient time scale of measurement.

(7) The average values of the net absorbed energy as measured for each type of fiber over the observed frequency range appear to be roughly exponential functions of the reciprocal absolute temperature.

(8) The temperature dependence of the apparent elastic constant, g, is discussed in terms of both pure entropy elasticity and elasticity involving a change of potential energy as well as of entropy. Theoretical expressions are derived and actual data are cited to support the fact that the potential energy contribution is of great importance in determining the elastic constants of the polyamides and other polymers characterized by a high degree of three-dimensional symmetry.

(9) The observed nonlinear spring characteristics of the net energy absorption loops as determined under conditions of (*a*) sinusoidal loading and (*b*) constant rate of loading are theoretically treated and correlated.

Acknowledgment

The authors wish to thank Dr. Taikyue Ree for his helpful criticisms and suggestions. Thanks are also due to E. I. du Pont de Nemours and Co. for providing the polyamide samples used in this work.

Literature Cited

1. Baker, W. O., and Fuller, C. S., *J. Am. Chem. Soc.* **64**, 2399 (1942); *ibid.* **65**, 1120 (1943).
2. Bunn, C. W., and Garner, E. V., *Proc. Roy. Soc. (London)* **A189**, 39 (1947).
3. Carswell, T. S., and Nason, H. K., *A. S. T. M. Symposium on Plastics*, p. 66 (Feb. 1944).
4. Dillon, J. H., Prettyman, I. B., and Hall, G. L., *J. Applied Phys.* **15**, 396 (1944).
5. Glasstone, S., Laidler, K. J., and Eyring, H., "The Theory of Rate Processes," New York, McGraw-Hill Book Co., Inc., 1941.
6. Halsey, G., and Eyring, H., TEXTILE RESEARCH JOURNAL **15**, 451 (1945).
7. Kauzmann, W., and Eyring, H., *J. Am. Chem. Soc.* **62**, 3113 (1940).
8. Lyons, W. J., TEXTILE RESEARCH JOURNAL **19**, 123 (1949).
9. Lyons, W. J., and Prettyman, I. B., *J. Applied Phys.* **19**, 473 (1948).
10. Rinehart, J. S., *J. Applied Phys.* **12**, 811 (1941).
11. Rossmassler, S. A., Ph. D. Thesis, University of Utah, Salt Lake City, Utah, 1950.
12. Stambough, R. B., *Ind. Eng. Chem.* **34**, 1358 (1942).

(Manuscript received July 23, 1951.)

Some Observations on the Wetting of Greige Cotton

R. E. Wolfrom and A. C. Nuessle

Textile Research Laboratory, Rohm & Haas Company, Philadelphia, Pennsylvania

Introduction

Because of the large volume of cellulose fabrics subjected to wet processing, it is not unusual that most practical methods for measuring the efficiency of wetting assistants employ cotton as the test substrate. Since regenerated cellulose or boiled-off cotton is readily wetted, only natural, unboiled cotton containing relatively high percentages of hydrophobic impurities has found use in such tests. Cotton yarns and fabrics are generally employed because tests with single fibers require specialized techniques for handling. Thus, the Draves-Clarkson test [3], floating-patch method [2], submerged-patch method [10], hydrometer method [6], and Shapiro tape method [11] all rely upon natural, unboiled cotton yarns or fabrics to provide a hydrophobic substrate.

Of all these methods, the Draves test has had the most widespread popularity due to its simplicity and rapidity of operation. Its value is further enhanced by the ease with which cotton skeins having essentially the same wetting characteristics may be prepared or purchased.

The present work, which stems from some observations made during routine use of the Draves test, concerns (*1*) the influence of temperature on the observed wetting time, and (*2*) the relationship between wet pickup and observed wetting time. It is not our intention to question the validity of data obtained through the use of this or other tests employing greige cotton; rather, we are presenting the results of our experiments in the hope that they will aid in the interpretation of such data, and also serve as a basis for further research.

Experimental Methods and Materials

The equipment required and the procedure for the Draves test are fully described elsewhere [1]. In brief, the test is run as follows: A 5-g. skein of greige cotton yarn is attached to a 3-g. metal hook which is fastened by a short length of thread to a 40-g. lead anchor. This assembly is dropped into a 500-ml. graduated cylinder containing the test solution, and a stop watch is started. When the thread slackens and the skein definitely starts to sink, the watch is stopped; the elapsed time is recorded in seconds as wetting-out time (*WOT*). Four replicate determinations are usually made.

The official procedure also recommends that, since temperature often markedly affects wetting, tests be made at temperatures of 77°F (25°C), 122°F (50°C), 158°F (70°C), and 194°F (90°C) to include the complete commercially useful range.

The skeins employed in the present tests were from a single shipment having a coefficient of variation of 9.9% at 25 sec. *WOT*; this is completely representative of the usual material.

All solutions of surfactants were prepared with distilled water of near neutral pH. Concentrations are on an active-solids basis.

Effect of Temperature on Wetting of Submerged Skeins

In employing the Draves test over a wide range of temperatures, we were puzzled by the fact that the curve for wetting-out time *vs.* temperature almost invariably has the form shown in Figure 1. Other investigators have noted the phenomenon; the sharp peak was reported by Lucas and Brown [8], and the pronounced decrease in *WOT* between 190°F and the boil was very early observed by Farrow and Neale [4].

This peculiar change in wetting efficiency with temperature first came to our attention in 1947 in the course of some routine evluations of commercial wetting agents at typical use concentrations. From the data shown in Table I it is apparent that ten of the twelve surfactants investigated showed higher wetting-out times at 180°F than at either 150°F or 210°F.

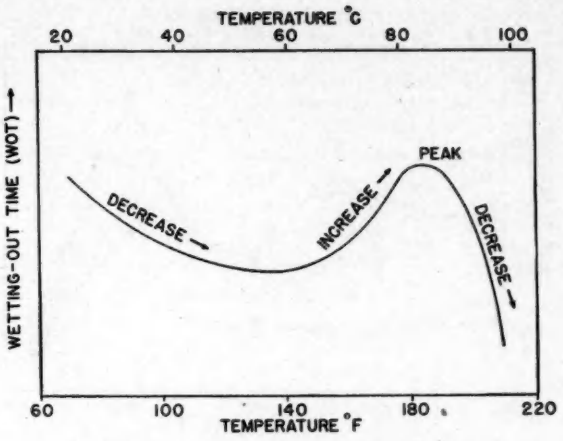

FIG. 1. *Characteristic wetting-out time* vs. *temperature curve for the Draves test.*

Subsequent studies made over narrower temperature intervals confirmed the decrease in *WOT* up to 140°F, the increase to a peak at 180°F to 190°F, and the sharp decrease in *WOT* as the wetting solution appeared to become more efficient approaching the boil. Representative data are listed in Table II and plotted in Figure 2. Even though no attempt was made to smooth out the curves and make them continuous, it is obvious that each set of points would fit rather closely a curve such as is shown in Figure 1.

Variations in concentration do not alter the form of the curve; typical data are shown in Table III and Figure 3.

We attempted to explain the temperature effect as follows: At the end-point of the Draves test, the skein

TABLE I. DRAVES WETTING-OUT TIME AS A FUNCTION OF TEMPERATURE FOR VARIOUS SURFACTANTS

% Solids concentration	Proximate composition	*WOT* (sec.) at the following temperatures: 70°F	120°F	150°F	180°F	210°F
0.16	sulfated fatty acid ester	14	9	8	10	6
0.12	dialkyl aryl sulfonate	12	8	7	11	5
0.12	alkyl aryl sulfonate	21	11	10	13	5
0.08	polyethanolamine fatty acid condensate	27	21	21	21	9
0.08	highly sulfated fatty ester	32	18	16	20	8
0.06	alkyl aryl polyether alcohol	19	14	14	29	11
0.06	alkyl aryl polyether sodium sulfate	35	29	25	44	18
0.05	2-ethyl hexanol-1 sodium sulfate	14	10	7	14	6
0.04	tri *n*-hexyl carballylate sodium sulfonate	10	10	8	15	9
0.04	3,9-diethyl tridecanol-6 sodium sulfate	12	9	7	28	9
0.04	sodium salt of *N*-methyl tauride	100	33	27	25	9
0.03	alkyl ester of sulfosuccinic acid	12	9	10	19	11

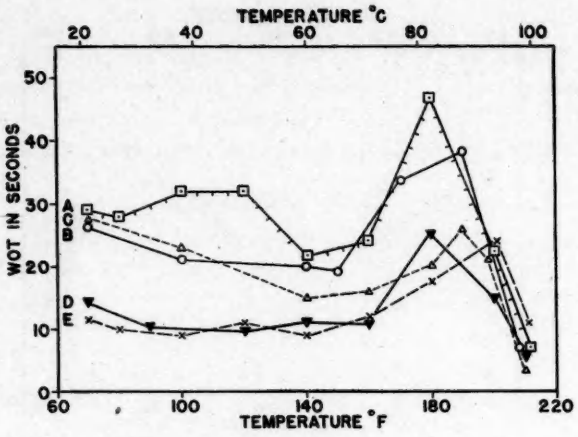

FIG. 2. *Effect of surfactant type on the shape of the* WOT-*temperature curve.*

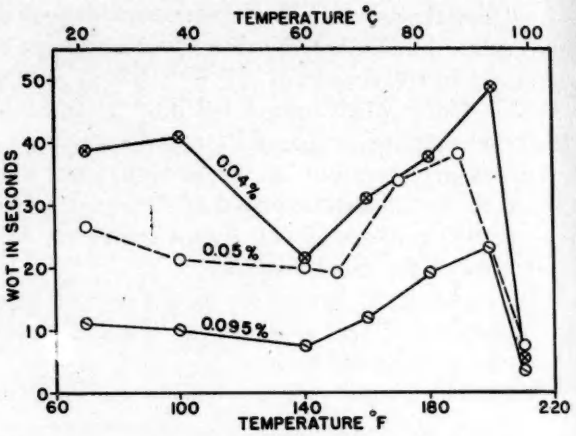

FIG. 3. *Effect of concentration on the shape of the* WOT-*temperature curve for nonionic B.*

TABLE II. MORE DETAILED STUDY OF THE *WOT*–TEMPERATURE EFFECT

Temperature (°F)	Draves wetting-out time (sec.) Nonionic A* 0.042%	Nonionic B* 0.05%	Nonionic C* 0.075%	Anionic D* 0.028%	Anionic E* 0.10%
70	29	26	28	11	14
80	28	—	—	10	—
100	32	21	23	9	10
120	32	—	—	11	10
140	21	20	15	9	11
150	—	19	—	—	—
160	24	—	16	12	11
170	—	34	—	—	—
180	47	—	20	18	25
190	—	38	26	—	—
200	22	—	21	24	15
210	7	7	4	11	6

* Nonionics A, B, and C are various alkyl aryl polyether alcohols (cloud points, respectively, 100°, 154°, and 186°F). Anionic D is an alkyl ester of sulfosuccinic acid. Anionic E is decyl benzene sodium sulfonate.

TABLE III. EFFECT OF CONCENTRATION ON THE *WOT*–TEMPERATURE CURVE

Temperature (°F)	Draves *WOT* (sec.) for the following concentrations of nonionic B: 0.04%	0.05%	0.095%
70	39	26	11
100	41	21	10
140	21	20	8
150	—	19	—
160	31	—	12
170	—	34	—
180	38	—	19
190	—	38	—
200	49	—	23
210	5	7	5

sinks, but is by no means completely wet. Gruntfest [6], using the hydrometer method on skeins and strips of canvas, and Shapiro [11], employing tapes, showed unambiguously that the "wet-out" skein or fabric retains a considerable quantity of occluded air which is only slowly released. When Draves tests are made at increasing temperature increments, the buoyancy of the occluded air increases with temperature, and since the skeins will not sink until part of this air has been liberated, higher sinking times result. This effect is offset, to a greater or lesser extent, by the enhanced surface activity of the solution with increasing temperature, which accounts for the initial decrease in *WOT*. When the added buoyancy of the trapped air eventually supersedes this enhanced activity (as occurs with all but a few surfactants), the sinking times increase sharply up to a peak at about 185°F (85°C).

However, we had no ready explanation for the sharp reversal in the neighborhood of 180°–190°F (82°–88°C). There was no particular reason why the wetting agent should cause this, since a wide variety of surfactants with unquestioned stability and solubility follow the pattern. Farrow and Neale [4] offered the explanation that near the boil the interstices of the yarn are filled with almost pure water vapor, and the fluctuations in the volume of this, due to small local changes in temperature, permit the liquid to advance. Powney [7], investigating the penetration of detergent solutions into fabrics, generally concurred that such a thermo-mechanical action, either on air or on water vapor, could cause the observed effect. Lucas and Brown [8] merely

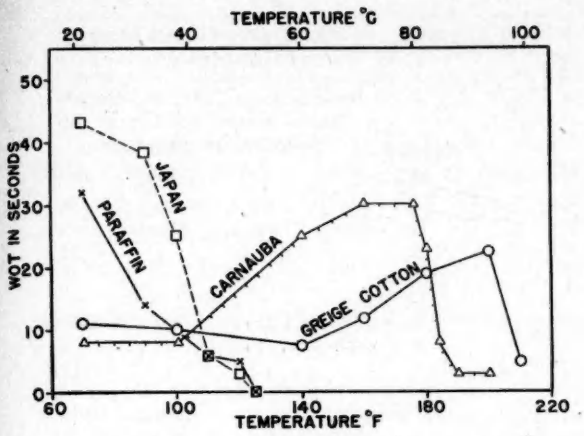

FIG. 4. *Comparative sinking times of waxed skeins.*

stated that near the boiling point all surfactants appear to recover and become excellent wetting agents, but that this seems to be a property of water rather than of the surfactant.

It occurred to us, however, that it might be more than a coincidence that the melting point of cotton wax, which gives the skein its hydrophobicity, is about 186°F (86°C). We suspected, therefore, that the melting or softening of the cotton wax was in some way responsible for the drop in *WOT* (or increase in wetting efficiency) beyond 180°–190°F.

This cotton wax is a mixture of fatty acids and alcohols, and is closely analogous to carnauba wax in physical and chemical properties. It fuses at 186°F (86°C) and solidifies at 180°F (82°C) [9]. The weight of the wax plus impurities, such as pectic acid, coloring matter, cotton oil, and albuminous matter, totals 4% to 5% of the weight of the skeins.

In order to study the effects of this wax coating on a systematic basis, regular Draves skeins were treated in the following manner:

The skeins were boiled for 1 hr. in a dilute solution containing 1.5% sodium hydroxide, 0.25% tetrasodium pyrophosphate, and 0.1% of a nonionic detergent, and were then rinsed thoroughly for an additional hour and dried. These skeins showed a 4.4% weight loss due to scouring.

Some of the dewaxed skeins were then immersed in a 4.4% solution of carnauba wax (No. 1 yellow, congealing point 179°F (82°C)) in aliphatic solvent naphtha. The wet skeins were centrifuged to a wet pickup of 100%, dried in air, and then baked at 300°F (149°C) for 5 min. to smooth out the wax sheath. Other skeins were similarly treated with 4.4% paraffin wax (congealing point 126°F (52°C)) or 4.4% refined Japan wax (congealing point 105°F (41°C)).

TABLE IV. SINKING TIMES OF "SYNTHETIC" GREIGE SKEINS IN 0.095% NONIONIC B

Temperature (°F)	Sinking times (sec.) of skeins waxed with the following: Japan wax	Atlantic No. 131	Carnauba wax
70	43	34	9
90	38	14	—
100	25	10	9
110	6	6	—
120	3	5	—
125	0	0	—
140	—	—	25
160	—	—	30
176	—	—	30
180	0	0	23
184	—	—	8
190	—	—	3
200	0	0	3
Congealing point of wax (°F)	105	126	179

These "synthetic" greige skeins were then used in Draves tests over the temperature range previously employed for the natural skeins, using a 0.095% solution of nonionic B. The results listed in Table IV and plotted in Figure 4 show the influence of the melting point of the wax on the form of the curve.

The carnauba skeins closely resembled the natural cotton in performance, except that the inflections in the curve for the latter came somewhat earlier. The paraffin and Japan wax skeins had much higher wetting times at room temperature than did the others; but as the test temperature was increased, the curves fell off rapidly so that by the time the waxes had completely melted, wetting times were almost instantaneous.

The failure of the latter skeins to show a peak cannot at present be explained; perhaps these waxes contain a number of fractions having different melting points. In any event, however, it is obvious that a waxed skein will wet-out more quickly once the wax has melted (and possibly emulsified). It may be concluded, therefore, that the rapid decrease in wetting-out time of a greige cotton skein beyond 180°–190°F (82°–88°C) is a property of the greige cotton itself, and not of the surfactant solution.

Work by Fischer and Gans [5] has already shown the interrelation between Draves wetting time, surface tension of the solution, and contact angle of the

wetting solution against paraffin wax, all at room temperature. It might be worth-while to extend such studies to carnauba, Japan, and natural cotton wax at a variety of temperatures.

Soap as a Wetting Agent

It was noted earlier (Table I) that two surfactants failed to give a peak, but leveled off between 120°F and 180°F before showing a final drop in wetting time near the boil. These were the polyethanolamine fatty acid condensate and the sodium salt of *N*-methyl tauride. We have since observed that ordinary soap gives a similar curve. Sodium stearate having a solids concentration of 0.10% gave the following *WOT* values at the temperatures indicated: 70°F, 300 + sec.; 120°F, 31 sec.; 150°F, 30 sec.; 180°F, 31 sec.; 210°F, 7 sec.

We suggest that such materials fail to show a peak because of the pronounced increase in solubility and decrease in micelle formation with temperature, which so enhances their surface activity that the added buoyancy of the occluded air is overbalanced throughout the entire temperature range. Further study may show most materials of this type to be moderately polar compounds having long straight chains, and characterized as good high-foam detergents, but only mediocre wetting agents. At the opposite end of the scale, the short-branched-chain, highly polar materials, which do not readily form micelles and which make better penetrants than detergents, may be found to give a curve having little or no initial decrease, but a pronounced peak.

In connection with the relationship between solubility and wetting efficiency, it should be noted, however, that in the case of the nonionics (Table II) the reduced solubility at the cloud point has little adverse effect on the wetting times and produces no change in the location of the peak. Although generally considered to be out of solution beyond the cloud point, the individual molecules appear to retain considerable mobility and can readily replenish the solution as other molecules concentrate at the interface.

Alkalies and Water as Wetting Agents

Cotton greige goods can be freed of wax by boiling in 1.5% sodium hydroxide, 0.25% tetrasodium pyrophosphate (*TSPP*), and as little as 0.01% of a suitable surfactant. These alkalies are known to be poor wetting agents at room temperature; but since the cotton wax would be melted at the boil, and therefore removable by saponification or emulsification, the alkalies could conceivably be fairly good wetting agents at 210°F (99°C). In confirming this, Draves tests were made on solutions of the alkaline materials and on water alone over a range of temperatures. In Table V are listed the sinking times of successive skeins in each test solution. Note that at 180°F (82°C) or below, none of the skeins sank within 300 sec. At 210°F (99°C) in 1.5% NaOH, the first skein sank in 80 sec., while succeeding skeins averaged only 40 sec. At 210°F in *TSPP*, the first skein failed to sink, while succeeding skeins sank in about 109 sec. At 210°F in water, the first skein generally failed to sink, but the second wet-out rapidly.

TABLE V. ALKALIES AND WATER ALONE AS WETTING AGENTS

Solution	Skein No.	Sinking times (sec.) of successive skeins in same solution at the following temperatures: 70°F	130°F	180°F	210°F
1.5% NaOH	1	300+	300+	300+	80
	2	300+	300+	300+	45
	3				35
	4				39
0.25% *TSPP*	1	300+	300+	300+	300+
	2	300+	300+	300+	106
	3				111
Water only	1	300+	300+	300+	300+
	2	300+	300+	300+	11
	3				15

We suggest that the melted cotton wax (or some fraction thereof) from the first skein in each set acts as a surface-active agent in causing the succeeding skeins to sink; but this explanation is admittedly incomplete.

Removal of Wax by the Wetting Agent

It should also be possible to remove much of the wax by treatment with a suitable surfactant alone at 210°F (99°C). To show this, the following series of tests was run:

(*1*) A skein was wet-out in 0.1% nonionic B at 70°F (21°C) and then dried. Sinking time in distilled water was 177 sec., due to the rewetting effect of the retained detergent.

(*2*) A skein treated as above and then rinsed thoroughly to remove the detergent and dried regained

TABLE VI. Relationship Between Draves *WOT* of Solution and Wet Pickup of Fabric at 80°F

Cotton fabric	Preparation of fabric	Pad solution: Concentration	Draves *WOT*	% Wet pickup after the following number of dips and nips: 1	2	3
No. 6 duck	natural (nonabsorbent)	distilled water	300+	3	9	14
		.04% nonionic B	40	10	17	23
		.095% nonionic B	10	11	18	24
		.015% anionic D	50	10	17	23
		.028% anionic D	10	12	19	24
2.60-yd. twill (108 × 56)	partially desized (non-absorbent)	distilled water	300+	23	43	53
		.04% nonionic B	40	37	57	58
		.095% nonionic B	10	42	57	61
1.61-yd. twill (107 × 56)	partially desized (non-absorbent)	distilled water	300+	14	28	38
		.04% nonionic B	40	25	44	52
		.095% nonionic B	10	27	52	52
2.41-yd. twill (118 × 58)	desized, boiled off and bleached (absorbent)	distilled water	300+	58	64	66
		.04% nonionic B	40	59	61	62
		.095% nonionic B	10	58	64	65
80 × 80 sheeting	desized, boiled off and bleached (absorbent)	distilled water	300+	74	76	79
		.04% nonionic B	40	73	76	79

its normal 300 + sinking time in distilled water. The treatment with detergent at room temperature had obviously removed little or no wax.

(*3*) A skein immersed in 0.1% of the nonionic for a few seconds at 210°F (99°C) and then rinsed to remove the detergent and dried was found to sink in 34 sec. in distilled water at room temperature. This increased absorbency is due primarily to removal of cotton wax, which appears to occur rapidly at the elevated temperature without mechanical action.

By contrast, similar treatment with water alone at either 70°F or 210°F for as long as 5 min. did not remove sufficient wax to bring the sinking time below 300 sec.

Wet Pickup *vs.* Surfactant Concentration

One of the chief reasons for adding a wetting agent to a dyeing or finishing bath is to increase the penetration of the liquor into the less absorbent areas, with resulting increase in wet pickup, and therefore greater over-all uniformity. Even in padding operations, where the heavy pressure at the nip is commonly believed to "drive the liquor into the fabric," a penetrant can be of use; actually, the pressure can only force out much of the air and bring the liquor into close contact with the fibers, and, unless the solution can thoroughly wet the fibers, most of it will be squeezed out of the fabric and back into the pad box. Thus, a wetting agent is helpful when padding fabrics having limited absorbency, either throughout or in scattered areas.

We have noted, however, that when solutions of wetting agents are padded onto cotton fabrics, the wet pickup remains rather constant in spite of the fact that the concentration of surfactant is varied over the customary range of Draves wetting times. For example, a variety of fabrics were padded at room temperature through water solutions of nonionic B and anionic D at concentrations corresponding to 10 sec. and 40–50 sec. Draves *WOT*. Wet pickup measurements were made with 4 in. × 36 in. strips of weighed, conditioned fabric using a constant-set motor-driven laboratory padder at speed of 5.14 in./sec. (approximately 8.5 yds./min.). The portion of the fabric in the pad box was 4.6 in., with a total immersion of 0.90 sec. After leaving the pad box, the fabric travelled 13.0 in. to the nip in an elapsed time of 2.54 sec. This would be roughly equivalent to 67 yds./min. on a full-scale padder with a 1-yd. dip and a 2.8-yd. travel to the nip (the latter figure is somewhat higher than usually encountered in practice).

The data shown in Table VI indicate that a wetting agent does not appreciably alter the wet pickup of an already absorbent fabric. This is probably due to the fact that in water alone the fabric just about reaches its maximum obtainable pickup, as leveled-off by the

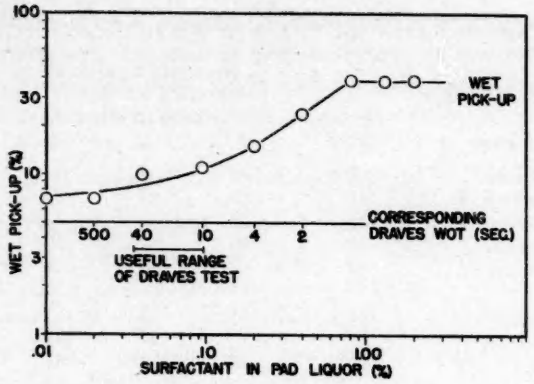

FIG. 5. *Effect of increased concentration of surfactant on wet pickup and Draves wetting time.*

pad pressure. The effect is evident on the 80 × 80 cotton sheeting and the 2.41-yd. twill.

With partially desized and unbleached fabric, the wetting agent definitely enhances the pickup; 2.60-yd. and 1.61-yd. cotton twill illustrate this point. In a like manner, the greige duck shows improved pick-up due to the surfactant. The results are typical of those obtainable with a variety of surface-active agents in addition to those illustrated here.

However, the effect of increased concentration of wetting agent is more obscure. Close examination of the data reveals that the difference in wetting-agent concentration (0.04% to 0.095%, with a four-fold difference in Draves *WOT*) does not appreciably change the wet pickup. In fact, in the case of the duck, the twofold increase in concentration increases the pickup by only 1% or 2%. Draves wetting times between 10 and 50 sec. are those usually selected for comparisons of wetting agents because the log log plot of concentration *vs.* time is a straight line between these limits; it would appear that this range has little significance in padding operations.

In order to further study the effect of concentration, greige duck was padded through 0.005% to 2.0% solutions of a nonionic surfactant (*WOT* in the range 30,000 to 1 sec.) The data in Table VII and Figure 5 show that the wet pickup increases up to the point at which the pad pressure levels it out at approximately 40%.

Although no measurement of completeness of wetting was made (as, for example, by the hydrometer test [6, 11]), it is obvious that multiple padding is just as effective a way of obtaining high pickup as is increased concentration of wetting agent. For example, three paddings at 0.095% are as effective as one padding at 0.4%, and three at 0.2% are as effective as one at 0.8%.

TABLE VII. WET PICKUP WITH VARIOUS CONCENTRATIONS OF NONIONIC B ON NO. 6 COTTON DUCK AT 80°F

% Nonionic solids	Approximate Draves *WOT* (sec.)	% Wet pickup after the following number of dips and nips: 1	2	3
0	—	4	10	14
.005	30,000	7	14	17
.01	3,500	7	15	18
.02	500	7	15	20
.04	40	10	17	23
.095	10	11	18	24
.20	4	15	24	38
.40	2	24	32	36
.80	2	39	41	41
1.50	1	38	38	38
2.00	1	39	40	40
0.04 at 210°F (99°C)	5	17	26	29

Further, it is again evident that the practical range of the Draves test covers only a small portion of the pickup *vs.* wetting curve, in a range which is far below the usual desired add-on or pickup of pad liquor. This is an intrinsic drawback of a wetting test which is dependent upon partial displacement of air without complete wetting.

Effect of Increased Immersion Time

In order to test the effect of increased immersion time in the pad box, another brief experiment was conducted. Here, the lag between dip and nip was varied, while the immersion time in the pad box was held constant. Another test with the reverse condition was also made. (See Table VIII.)

The data show that the wet pickup increases slowly with wetting-agent concentration when immersion and lag times are short. Merely lengthening the lag

TABLE VIII. EFFECT OF VARIATION IN IMMERSION TIME AND LAG BETWEEN PAD BOX AND NIP ON WET PICKUP OF NO. 6 COTTON DUCK

Solution	Wet pickup at constant 0.9 sec. dip and the following lags: 2.5 sec.	5.1 sec.	7.6 sec.	15.2 sec.	Wet pickup at constant 0.6 sec. lag and the following dips: 0.9 sec.	2.3 sec.	3.7 sec.	7.4 sec.
Water	4	—	—	4	—	—	—	—
.095% nonionic B	12	15	15	25	—	—	—	—
.38% nonionic B	19	28	29	31	19	19	23	35

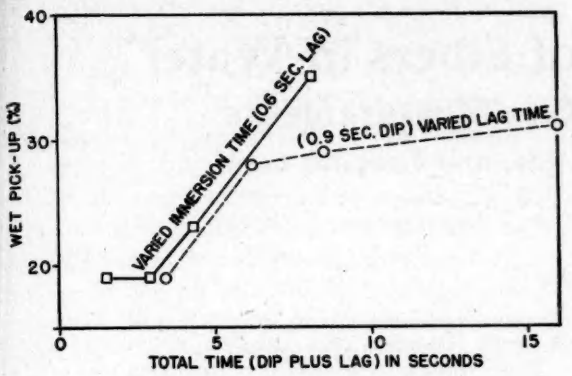

FIG. 6. *Effect of immersion and lag time on wet pickup.*

time appreciably raises the pickup, provided some wetting agent is present. Increased dipping times produce greater pickup than corresponding increases in lag time, as shown in Figure 6.

We would therefore recommend for improved pickup the use of the normal amounts of wetting agent with increased immersion time. Considering the effect of multiple dips (*cf.* Tables VI and VII), we would also suggest a 3-bowl padder, with a dip before each nip. If this is not practical in the mill, the only solution to increased pickup is increased concentration of wetting agent, perhaps to levels heretofore considered excessive. The normal range of concentration for this particular wetting agent, as employed in padding, is about 0.02% to 0.10% solids; in the present case (*cf.* Table VII) the benefit derived from additional wetting agent was apparent up to 0.8% solids. These speculations are based on a constant pad setting; obviously a lighter nip will increase the pickup, but the wetting will be superficial rather than thorough.

Summary

In a study of the effect of temperature on Draves wetting time, it has been shown that most wetting agents follow a typical curve characterized by decreased wetting time up to about 140°F (60°C), an increase to a peak near 185°F (85°C), followed by a sharp drop as the solution approaches the boil. With soap and a few other surfactants the curve levels off after the initial decrease so that there is no peak; but here, too, there is a marked drop beyond 185°F. The peak occurs at approximately the melting point of the cotton wax; it would appear that once the wax is completely melted, the skein will sink very rapidly in any surfactant solution. Thus, the reversal at 185°F is a property of the skein itself, and not of the wetting agent.

A study of wet pickup by cotton fabrics padded through solutions of a wetting agent has revealed that: (*1*) pickup of absorbent fabrics is not enhanced by the use of a wetting agent; (*2*) pickup of non-absorbent fabrics, such as greige cotton, increases with amount of wetting agent, leveling off only at concentrations considerably in excess of normal use and far above the range of the Draves test; (*3*) pickup can be effectively increased at normal concentrations of wetting agent (0.02% to 0.1%) by means of multiple padding, or by increasing either the immersion time or the lag time between dip and nip.

Acknowledgment

Grateful acknowledgment is made to Mrs. Mary Flanagan for her assistance in obtaining the data. Appreciation is also extended to the Rohm & Haas Company for permission to publish the information contained herein.

Literature Cited

1. American Association of Textile Chemists and Colorists, "Technical Manual and Yearbook," Vol. XXVI, New York, Howes Publishing Co., Inc., 1951, pp. 139–41.
2. Draves, *Am. Dyestuff Reptr.* **28**, 421 (1939).
3. Draves and Clarkson, *Am. Dyestuff Reptr.* **20**, 201 (1931).
4. Farrow and Neale, *J. Textile Inst.* **16**, 209 (1925).
5. Fischer and Gans, *Ann. N. Y. Acad. Sci.* **46**, 389 (1946).
6. Gruntfest, Hager, and Walker, *Am. Dyestuff Reptr.* **36**, 225 (1947).
7. International Society of Leather Trades Chemists (British), "Wetting and Detergency," New York, Chemical Publishing Company, 1937, p. 188.
8. Lucas and Brown, "Food Technology," Vol. IV, 1950, p. 121.
9. Matthews, "Textile Fibers," 4th Ed., New York, John Wiley & Sons, 1923, p. 469.
10. Seyforth and Morgan, *Am. Dyestuff Reptr.* **27**, 525 (1938).
11. Shapiro, *Am. Dyestuff Reptr.* **39**, 38 (1950).

(Manuscript received February 6, 1952.)

Swelling Capacities of Fibers in Water*

Part I: Desiccation Rate Measurements

Lars A. Welo,† Hilda M. Ziifle, and Leopold Loeb

Southern Regional Research Laboratory,‡ New Orleans, Louisiana

Abstract

Swelling in water is one of the important fundamental properties of cellulosic fibers, and is also a factor in determining the proper fiber for a specific utilization. An example of this is the selection of cottons for self-sealing fabrics. Since existing techniques for measuring swelling capacities, as they have been used, are tedious and time-consuming, it was desired to find a rapid method which would be sensitive enough to establish, with certainty, small differences in swelling capacity due to variety, conditions of growth, and state of maturity such as might be decisive in the choice of a cotton for an application dependent upon swelling. In Part I of this study a method is discussed for determining swelling capacities of cotton and other fibers. It is based on the measurement of the rate of loss of moisture from a moisture-saturated sample. Experimentally, this method is exceedingly simple—the fiber samples, fully swollen and containing excess water, are dried very slowly and weighed periodically. It is shown that for a time the moisture is lost at a nearly constant rate. Eventually, however, the drying rate changes and thereafter steadily diminishes. It is believed that this change occurs only after all nonswelling water external to the fiber has evaporated. The moisture regain at this point of transition in the desiccation rate is considered to be indicative of the maximum water-holding capacity of the cellulose—*i.e.*, the swelling capacity. The moisture regain values determined are in general agreement with the regain values estimated from adsorption isotherms at 100% relative humidity. The maximum regain values from the desiccation rate technique, when expressed in terms of volume increases, agree with the swelling capacities as determined by microscopic measurements.

Although the experimental method is simple and direct and more rapid than microscopic methods, the long drying periods required make it suitable mainly for use in research when time is not an important consideration.

THESE STUDIES on the measurement of the swelling capacities of textile fibers were carried out with two principal objectives: to contribute to the knowledge of the fundamental properties of cotton, and to contribute to the development of water-resistant fabrics of the type which resist water penetration by self-sealing following wetting. To meet the first objective requires a method that is precise enough and sensitive enough to detect the small differences in swelling capacity that may be due to variety, growth conditions, maturity, etc. To meet the second objective requires a simple and rapid technique for selecting the most suitable cotton in advance of the spinning and weaving operations, since self-sealing has been shown to be materially dependent upon swelling capacity [8].

A method is discussed herein for ascertaining swelling capacities which is based on the measurement of the rate of loss of moisture by the fiber sample. Experimentally this method, called the "desiccation rate" technique, is exceedingly simple—the fiber samples are dried very slowly and weighed from time to time. Under controlled conditions the loss of moisture proceeds at a constant rate at first, as nearly as can be determined. However, eventually the rate of loss changes to a steadily diminishing one. It is considered that this change of rate is indicative of a transition from surface evaporation to evaporation of water that initially was not at the surface—*i.e.*, water which reaches the surface by migration. The moisture regain at this moment is considered to be indicative of the maximum water-holding capacity within the cellulose—*i.e.*, the "swelling capacity." This regain corresponds in magnitude to the regain values estimated from adsorption isotherms at 100% relative humidity. Furthermore, when these regains are expressed in terms of volume increases, general agree-

* Presented in part before a meeting of The Fiber Society, April 27, 1950, Fontana Village, N. C.

† Retired June 23, 1950.

‡ One of the laboratories of the Bureau of Agricultural and Industrial Chemistry, Agricultural Research Administration, U. S. Department of Agriculture.

ment is found with the swelling capacities as measured by cross-sectional area increases.

The technique is simple and direct. However, while it appears to be considerably more rapid than the method involving microscopic measurements of cross sections, it is still not very suitable for routine use when the time to secure a determination is an important consideration. There are three reasons for describing it here and reporting the results: it is believed to be new; it provides an additional criterion by which to judge the results from the centrifuge studies discussed in Part II (page 261); and it provides a means of fixing the ordinates of the adsorption isotherm at 100% relative humidity. Because of the very large slope of the adsorption isotherm in the region of 95%–100% relative humidity, the ordinate at saturation cannot be accurately fixed, but can only be estimated from isotherm data alone.

The Desiccation Rate Technique

The fiber samples were swollen by submerging them in boiling distilled water for 5 min. They were allowed to cool and to remain in the water overnight at room temperature.

After swelling, the samples were placed in weighing bottles and were allowed to dry slowly in a desiccator over calcium chloride as the drying agent. The bottles with their samples were weighed four times daily in the earlier experiments, and seven times daily in later experiments. To minimize interruption of the drying while weighing, a separate desiccator was used for each sample. Also, a systematic procedure was followed so that the bottle, which was capped while weighing, was out of the desiccator and on the balance pan only during the time required for the milligram and fractional milligram adjustment.

Depending upon sample structure—cord, yarn, or lint—the total drying periods varied from 2 days to 2 weeks. Once started, the drying would best be uninterrupted. The practice was followed, however, of capping the bottles and leaving them in a desiccator without drying agent overnight or over the week end. At the beginning of the drying period the overnight losses in weight of the wet material were of the order of 2 to 3 mg. Over a week end the losses were from 6 to 8 mg. Towards the end of the drying period small gains in weight sometimes occurred. These losses were added to the observed weights of the succeeding day. It was kept in mind that they were cumulative over a succession of days.

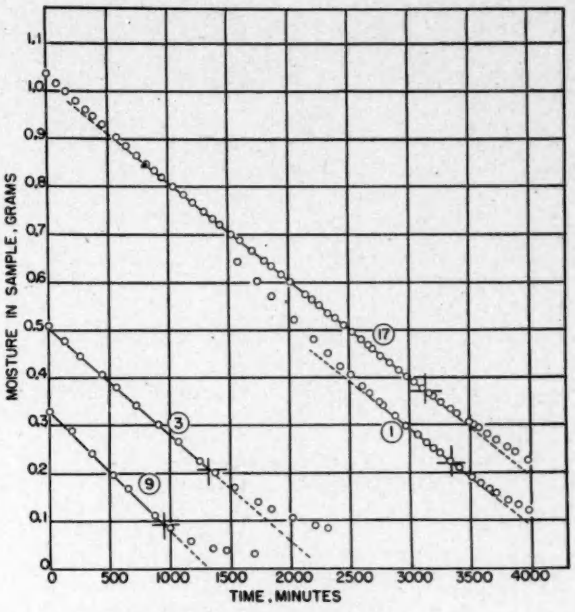

FIG. 1. *Typical desiccation rate curves. Curve 9 is for a ½-g. sample. Other samples weighed about 1.2 g.*

Figure 1 shows the results obtained when the corrected weight less the weight of the bottle and of the oven-dry sample was plotted against elapsed time. Four typical plots are shown. These were chosen from the 58 plots available because they could be fitted into a composite plot without overlapping or intersecting and at the same time show that (*1*) the first portion of a plot (preceding the trailing curve representing steadily decreasing drying rate) may or may not be a single straight line throughout the whole drying period it represents, and (*2*) the straight-line segment immediately preceding the trailing curve is sometimes very long and sometimes very short.

The crosses mark the points of tangency of the trailing curves to the preceding straight-line segments, as estimated by inspection. The ordinates of the tangent points are the moisture contents at maximum swelling capacity, on the assumption that under controlled conditions departure from linearity marks the cessation of loss of free, external moisture and the beginning of loss of water that had a part in the swelling. These ordinate values, after division by the oven-dry weight of the sample and multiplication by 100, give the maximum moisture regains. These maximum regain values are given in Table I. The four curves of Figure 1 are identified by item numbers, which are also given in Table I.

In order to express the results as swelling capacities, it is necessary to calculate the volume change

TABLE I. GENERAL SUMMARY OF SWELLING CAPACITY MEASUREMENTS, DESICCATION RATES, AND FIBER CROSS-SECTIONAL AREA INCREASES

Item No.	Material description	Moisture regain (% of oven-dry weight) Desiccation rate technique at estimated tangent point*	Swelling capacity (%) Computed from previous column	Swelling capacity (%) Fiber cross-sectional measurements†
	Cotton			
1	Tire cord; 23/4/3; variety, Wilds	21.1±0.7	28.8	—
2	Yarn; 17.5/1; variety, Wilds	19.4±0.5	26.2	—
3	Yarn; 12/1; variety, Empire	17.0±0.3	22.5	26.3‡
4	Yarn; 34/2; variety, Acala (Bollies)	20.6±0.4	28.1	32.1‡
5	Yarn; 34/2; varitey, Acala (Well Grown)	20.9±0.5	28.5	27.7‡
6	Yarn; mature	23.6±1.0	32.7	—
7	Yarn; immature	28.0±0.3	39.0	—
8	Lint; mature; variety, Empire	17.8±0.3	23.7	31.7
9	Lint; immature; variety, Empire	19.4±0.1	25.9	20.8
10	Lint; mature; variety, Sea Island Special	16.4±0.1	21.6	33.3
11	Lint; immature; variety, Sea Island Special	19.6±0.4	26.2	29.3
	Rayon			
12	Tire cord; 1100/2; Cordura	39.1±0.7	52.5	—
13	Yarn; 1100/480; Cordura	42.2±1.5	57.1	—
14	Yarn; 240/120; Fiber G	39.1±0.5	52.5	—
15	Avisco	—	—	66.2
	Miscellaneous			
16	Yarn; flax	40.1±0.5	58.1	64.9
17	Yarn; 1100/1440; 2.5Z; Fortisan	30.4±0.3	39.3	19.9
18	Yarn; 210/69; 1Z; nylon	7.5±0.2	7.3	−1.9
19	Yarn; 40/13; 2Z; nylon	7.2±0.1	6.9	—

* Mean of from two to four determinations.

† Structure descriptions in the second column do not apply to this column. The cottons were swollen in 0.5% Aerosol solution.

‡ Unweighted means of separate determinations on mature and immature fibers.

brought about by a given moisture regain. According to Hermans [6], the fiber volume measured in organic liquids may be considered as the actual volume of the very substance of the fiber wall. Hence, the initial volume of the various materials, prior to swelling, may be taken as the reciprocal of the density measured in a nonswelling liquid. Thus:

$$V_i = 1/d_B, \tag{1}$$

where V_i is the volume of 1 g. of the dry fiber, and d_B is the density of the bone-dry fiber as measured in benzene (values taken from the literature). According to Hermans (p. 79 of [6]), the volume, V_f, of the originally dry sample after swelling in water is given by the following:

$$V_f = \varphi_w + a, \tag{2}$$

where φ_w is the reciprocal of the apparent density of the fiber sample as measured when immersed in an excess of liquid water—*i.e.*, it is the volume which is displaced by 1 g. of the dry fiber when immersed in excess of water. The quantity a is the moisture regain divided by 100. It is obvious that the final volume can be given by the sum of two terms only in the region of high regain—that is, regain values above that at which the apparent contraction of the water ceases. The simple two-term equation for the final volume should apply to cotton at regains above approximately 12% and to rayons at regains above approximately 25%. Since we are interested in the volume at maximum moisture regain (for cottons, approximately 22%; and for rayons, approximately 40%) the equation may be applied.

The percentage volume change of the wall substance from equations (1) and (2) will be:

$$\frac{V_f - V_i}{V_i} \times 100$$

or

$$\frac{(\varphi_w + a) - 1/d_B}{1/d_B} \times 100$$

or, simplifying,

$$[d_B(\varphi_w + a) - 1] \times 100. \quad (3)$$

In Table II are listed the densities of the dry materials together with the literature sources for these values. The φ_w values for the materials concerned were determined by weighing the samples under their own swelling water.

Swelling capacities derived according to equation (3) from the maximum moisture regain values and the density data given in Table II are listed in Table I.

The long and irrelevant early periods of drying could have been and in many cases were avoided by preliminary partial drying with a centrifuge or by mopping with towels. Curves 9 and 3 in Figure 1 are examples of the effect of gentle and brief preliminary centrifuging. It was generally preferred not to risk having linear segments in the moisture-time curves which were too short to reveal the linear segment. When the approximate maximum moisture regain was known, a safe working procedure was to add 30 or 40 to this percentage and compute the corresponding bottle plus wet-sample weight. Regular, frequent, and precise weighings were first started when the computed weight was approached. Curve 1 in Figure 1 illustrates this procedure.

A daily periodicity was found in the curves, arising from overnight or week-end interruption of the drying. The effect is nearly of the second order. The catenary-like segments, one for each day, become noticeable when the plotting scales are made five times as large as they are in Figure 1. No daily periodicity can be detected in Figure 1 nor in any of the other 54 plots when plotted to comparable scales.

The rates of moisture loss are determined mainly by the neck areas of the weighing bottles, although there are undetermined factors present that cause considerable variations for a given neck area. Of the 58 desiccation rate runs, 39 were made with weighing bottles having necks 2.2 cm. in diameter, 10 with 2.4 cm., 8 with 4.0 cm., and one with 4.5 cm. The neck areas, respectively, were: 3.8, 4.5, 12.5, and 15.9 cm.^{2}. The mean moisture loss rates computed from the slopes of the straight lines, such as those of Figure 1, and their standard errors, respectively, were: 0.25 ± 0.01, 0.27 ± 0.02, 0.53 ± 0.05, and 0.74 mg./min. In these computations all rates for a given neck diameter were grouped together, without regard to the materials that were being studied and without regard to mean temperature differences within the range 25.4°–27.1°C.

TABLE II. DENSITY DATA FOR CALCULATING THE SWELLING CAPACITIES

Material	d_B	Literature source	φ_W
Cotton (mature)	1.541*	[14]	0.625
Cotton (immature)	1.537	[14]	0.625
Rayon	1.511	[14]	0.618
Fortisan	1.506†	[5]	0.621
Nylon	1.145	[1]	0.862
Flax	1.541‡		0.625

* Average value for the four mature cottons discussed in [14].

† Density measured in carbon tetrachloride as the immersion medium.

‡ No density value for flax measured in a nonswelling liquid was found in the literature. The value taken is that for mature cottons.

An essential feature of the desiccation rate technique is to have the samples in containers, such as weighing bottles, in order to maintain near equilibrium and ensure slow drying. During the early stages of the drying, when there is still much water in the fiber-to-fiber contacts, the whole space occupied by the sample remains saturated so that there are no moisture gradients within the sample. The full water vapor pressure corresponding to the prevailing temperature exists between a region immediately above the sample and the neck of the weighing bottle, and above the neck a low vapor pressure is maintained by the drying agent. Loss of water by diffusion through the neck is steadily replaced by evaporation from the sample at a rate controlled by the area of the weighing-bottle neck. Ideally, the rate of loss should be the same as that of the bottle containing water of a depth equal to the vertical dimension of the sample. Eventually, but before the moisture content corresponding to the swelling capacity has been reached, the residual nonswelling water will consist of small accumulations in the fiber contacts or aggregates dispersed over the surface of the fibers, both of which have meniscuses of sufficiently strong curvature to lower the vapor pressure. We see in this at least one reason why the curves in Figure 1 are not linear all of the way from the beginning of drying to the tangent points marked by the crosses. One might not expect constant vapor pressure and constant drying rate during this "second" stage in the drying. But the experimental fact remains that

a linear segment in the drying curve just before the trailing part of the curve corresponding to diminishing drying rate has been found in every desiccation rate experiment. The linear segment is sometimes very long, as in curve 17 of Figure 1; sometimes a single linear segment is found, as in curve 9; and sometimes the linear segment is too short for accurate interpretation, as in curve 1.

As soon as the drying sample reaches the moisture content corresponding to the swelling capacity, the vapor pressure begins to fall continuously. The vapor pressure follows the regain-relative humidity curve of the adsorption isotherm. The vapor pressure corresponds to, and is, in fact, controlled by the existing regain [3]. The regain and consequently also the vapor pressure gradient diminish continually, giving rise to the trailing curves shown at the end of each plot in Figure 1.

It is this circumstance which gives a restrictive condition for a clear choice of the point on a moisture-time curve that corresponds to the swelling capacity. Since the vapor pressure diminishes continually after the point in question has been passed, the drying rate also diminishes continually and the moisture-time curve cannot thereafter have a linear segment. Any prior change in slope, either tangency or discontinuity, which is followed by a linear segment is therefore ruled out as representative of the moisture content corresponding to the swelling capacity. This restrictive condition is also a minimum-value condition. Among the points on a moisture-time curve marking changes in slope, the point to be chosen for computation of the swelling capacity is that which gives a minimum value. Also, it is only when this restrictive condition is observed that the computed swelling capacities for a given material are invariant from sample to sample, within the limits of error of estimation of the tangent points or discontinuities. The degree of invariance attained is indicated by the standard errors for the moisture regain values given in Table I. In some of the later runs this uncertainty was diminished by weighing the samples seven times instead of four times daily.

It was noticed that water frequently condensed on the inner walls of the capped bottles while they were stored overnight in a closed vessel without the desiccant. This condensation of moisture disappeared on resumption of drying and did not noticeably affect the subsequent drying rate unless it was, in part, responsible for the near second-order daily periodicity discussed above.

Jolly Balance Experiments

The "protective" function of the weighing bottle was brought out in variations of the desiccation rate technique that were tried. Fully exposed samples suspended from a Jolly balance spring were dried either in a slow stream of dry air flowing in a vertical glass tube or within a desiccator with calcium chloride. Periodic height observations with a cathetometer provided data for the equivalent of a moisture content-time curve. Straight lines followed by smooth curvilinear portions were always obtained, but the tangent points were never as well defined as they are in the curves of Figure 1. The moisture contents corresponding to the estimated tangent points were far from invariant for a given material, scattering badly from sample to sample. Also, the computed swelling capacities were always larger than those recorded in Table I, showing that the departure from a constant drying rate occurred too early. The more accessible exteriors of the samples passed below the maximum swelling moisture stage while the sample interior still had free, nonswelling moisture. Undoubtedly, free liquid water did flow from the more moist to the drier parts of the samples, but not rapidly enough to maintain approximately uniform moisture distribution. For this to occur, all water exterior to the fibers must disappear in the vapor phase, as has already been pointed out.

A dependence upon the geometrical arrangement of the sample was also noted in the Jolly balance experiments. The computed swelling capacities depended upon whether the small skeins, made by winding on a cylinder 1¼ in. in diameter, were simply hung from the balance spring, or whether they were arranged as rings in a horizontal plane. The latter arrangement served to partially eliminate the gravity moisture gradients.

The principal reason for attempting the Jolly balance-cathetometer modification of the technique was to avoid interruption of the drying while weighing. There is no reason why a light bucket cannot be used to contain the sample. But, unless continued, uninterrupted observations can be arranged for, the sample must be removed overnight and replaced on resuming the observations. In doing so, care must be taken that discontinuities in the series of cathetometer height readings are not introduced.

The primary essential—long drying periods—cannot be avoided. The desiccation rate technique cannot be rapid, nor very suitable for routine swelling

capacity measurements. However, this disadvantage is partially offset by the number of determinations that can be made simultaneously. Concurrent runs with a dozen samples keep the observer occupied at the balance about half of the working day if each sample is weighed seven times. It is thus possible for one observer to handle easily twenty samples at a time.

General Agreement with Adsorption Isotherm Data

Broadly speaking, considering the difficulties inherent in estimating moisture regains from adsorption isotherms, the maximum regains tabulated in Table I match them very well as to general range. Estimates of the regains at 100% relative humidity from a few of the published isotherms are: cotton [11, 12], 21%; rayon [10], 42%; nylon [1, 9], 8%; and Fortisan [2], 33%. The first three of these estimates follow from straightforward inspection of the curves and tabulated data. The Fortisan isotherm referred to above ends at 87% relative humidity with 19% regain, so that a long-range extrapolation was carried out as follows. At 87% and 100% relative humidity, respectively, the regains in cotton were taken to be 12% and 21%. The Urquhart-Williams rule [13] was then applied. This rule states that the ratio of the moisture contents of two different materials at the same humidity is appreciably independent of humidity. As these authors state it, the rule is intended to apply particularly to mercerized cotton and the original soda-boiled cotton. According to the rule, at 100% humidity the regain in Fortisan would be $19/12 \times 21 = 33\%$, which is in satisfactory agreement with the 30.4% for item 17 in Table I. Adsorption isotherms for flax were unavailable for comparison.

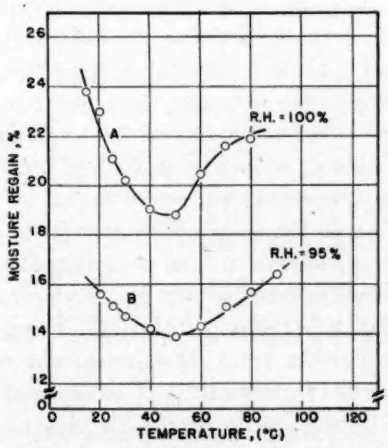

FIG. 2. *Effect of temperature on moisture regain.*

The general averages of the maximum moisture regains given in Table I for each kind of material are: cotton, 20.4%; rayon, 40.0%; nylon, 7.4%; and Fortisan, 30.4%. These all seem low as compared with the published adsorption isotherms cited in the preceding paragraph; they should be lower. Most, although not all, isotherm work has been done at 20°C. The laboratory room temperatures in New Orleans generally are considerably higher. The desiccation rate observations leading to the moisture regain data in Table I were made within three periods, during which the means of all temperature readings were as follows: July–August, 1948, 27.1°C; September–October, 1948, 25.4°C; and February, 1949, 25.4°C. It is pertinent to inquire how much higher the maximum moisture regains in Table I would have been if the temperature had been 20°C. This inquiry can be answered for cotton with the Urquhart and Williams data [12] for adsorption as a function of temperature and with Davidson's [4] swelling capacities at various temperatures, as calculated from the Urquhart-Williams data. Figure 2, curve B, reproduces the Urquhart-Williams curve for 95% relative humidity (Figure 8 in [12]). Curve A is plotted from Davidson's data (Table VI, column 4 against column 1, in [4]). In curve A the moisture content-temperature function is very steep in the interval 20°–25°C, and the mositure difference is at least 1.5%. Accordingly, all moisture regain values in Table I for cotton should be increased by 1.5 units before comparing with maximum moisture regains estimated from adsorption isotherms. The temperature effects are probably in proportion to the moisture regains themselves, so that the values for rayon should be increased by about 3 units, for nylon by less than 1 unit, and for Fortisan by more than 2 units.

Among the cottons, the moisture regains given in Table I differ considerably among themselves. The ease and naturalness with which moisture regains follow directly from the experimental curves support the belief that these differences are real and not spurious. The only leeway for the exercise of judgment is in the estimation of the tangent points. In the latter part of the work, when the weighings were done more frequently, this leeway was reduced, but the differences persisted. That the swelling capacities of immature cottons are larger than those of

mature cottons is also indicated by the centrifuge studies, as is shown in Part II (page 261). The relative swelling capacities of mature and immature cottons are discussed in the following section.

Comparison of Results with Cross-Sectional Area Increases

In the evaluation of swelling capacity by microscopically comparing the cross-sectional area of the same fibers in the wet and dry condition [7], the swelling capacity is given as the percentage change in area of the fiber as compared to the area of the dry fiber. An examination of the swelling capacity data in Table I indicates that the values obtained from the desiccation rate technique and from cross-sectional area measurements agree as to general magnitude for the cottons, the rayons, and the flax.

In regard to the major discrepancies between the data obtained by the two methods, that for Fortisan, item 17, has already been disposed of in the discussion of its adsorption isotherm. The measured maximum moisture regain is 30.4%. The corresponding swelling capacity is 39.3%. Since, as experiments showed, the longitudinal swelling is negligible, this volume increase must appear as a cross-sectional area increase. The value given in the last column, 19.9%, must be far too small.

The second major discrepancy is the apparent contraction of 1.9% shown for nylon by the cross-sectional technique. As has already been stated, the adsorption isotherms indicate a maximum regain of about 8%. The longitudinal swelling in nylon is not negligible, as it was assumed or proved to be in all other fibers studied. After the initial contraction that occurred in nylon on the first wetting, the changes in length in repeated wet-dry cycles were 2.9% of the dry length. This accounts for 3.7% of the mean water retention, 7.4%, for items 18 and 19 in Table I. The remainder, $7.4 - 3.7 = 3.7\%$, corresponding to a volume increase of 2.9%, must appear as a cross-sectional area increase. The apparent contraction of 1.9% cannot be accepted as real.

The third major discrepancy relates to the relative swelling capacities of mature and immature cottons. By the desiccation rate technique they are, in all cases, larger for the immature cottons: compare item 6 with item 7, 8 with 9, and 10 with 11 in Table I. By the cross-sectional technique the relative swellings are the reverse: compare item 8 with item 9, 10 with 11, and, possibly, 4 with 5 in Table I. This reversal in relative swelling is due to the inclusion of the lumen areas as part of the total microscopically measured fiber cross section. When fiber lumen areas are excluded, the ratios of the wet to dry cross-sectional areas are always larger than when lumen areas are included. In immature fibers these ratios are sufficiently larger than in the mature to reverse the relative swellings. The resulting relative swellings correspond to the desiccation rate data rather than to the cross-sectional data.

The effect of excluding the lumen areas from the cross-sectional areas of the fibers can be illustrated by remeasurements of the cross sections of some of the wet-dry pairs of photomicrographs of Sea Island Special cotton, both mature and immature (items 10 and 11, Table I). Of the available 500 pairs of mature sections, 114 were measured again. Likewise, 77 of the available 500 pairs of immature sections were remeasured. The increases in cross-sectional area, which are also the equivalent swelling capacities, were: mature (lumen included), 32.8%; mature (lumen excluded), 35.0%; immature (lumen included), 30.7%; immature (lumen excluded), 37.8%.

Having accounted for the main apparent discrepancies, and having considered the lack of precision involved in swelling capacities obtained from either adsorption isotherms or cross-sectional measurements, it is seen that the desiccation rate technique yields swelling capacities in agreement with both as to general levels.

Summary and Conclusions

As part of a study on the fundamental properties of cotton and on its use in self-sealing fabrics, a simple and rapid means of measuring swelling capacity was needed. It was thought that swelling might depend upon variety, growth conditions, maturity, etc. In this paper a desiccation rate technique has been described for the measurement of the swelling capacity of textile fibers. What are considered to be nearly correct swelling capacities were obtained by this technique, in which the moisture remaining in a sample is given as a function of time of desiccation. It was observed that the trailing part of a drying rate curve, representing a steadily decreasing drying rate, is always preceded by a straight-line segment, representing a constant drying rate. It is believed that the departure from linearity marks the cessation of loss of external or "free" water and the beginning of dif-

fusion from fiber interiors. It was shown that the maximum moisture regain values so determined were in agreement with the data from adsorption isotherms at 100% relative humidity. It was also shown that when these regain values are expressed as swelling capacities, general agreement is obtained with swelling values from fiber cross-sectional area measurements.

An essential requirement of this method seems to be that the rate of moisture loss be very slow in order that the distribution of moisture throughout the sample be nearly uniform during the drying period. Although it is somewhat more rapid than the microscopic cross-sectional method, the method is probably not sufficiently rapid for routine work, but seems acceptable for certain research purposes.

Acknowledgment

We gratefully acknowledge the suggestions offered and the aid given by Dr. C. M. Conrad, who had general supervision over these studies. We are indebted to Miss Mary L. Rollins for the useful information given by her photomicrographs of fiber cross sections.

Literature Cited

1. Abbott, N. J., and Goodings, A. C., *J. Textile Inst.* **40**, T232 (1949).
2. Barry, J. K., *Textile Mfr.* **72**, 428 (1946).
3. Cassie, A. B. D., *J. Textile Inst.* **37**, P154 (1946).
4. Davidson, G. F., *J. Textile Inst.* **18**, T175 (1927).
5. Fortess, F., Textile Research Journal **19**, 23 (1949).
6. Hermans, P. H., "Contributions to the Physics of Cellulose Fibers," New York, Elsevier, 1946.
7. Moore, A. T., Scott, L. W., deGruy, I. V., and Rollins, M. L., Textile Research Journal **20**, 620 (1950).
8. Smith, H. O., Murphy, A. L., and Goldthwait, C. F., Textile Research Journal **18**, 124 (1948).
9. Speakman, J. B., and Saville, A. K., *J. Textile Inst.* **37**, P271 (1946).
10. Urquhart, A. R., and Eckersall, N., *J. Textile Inst.* **23**, T163 (1932).
11. Urquhart, A. R., and Williams, A. M., *J. Textile Inst.* **15**, T138 (1924); *ibid.* **17**, T38 (1926).
12. Urquhart, A. R., and Williams, A. M., *J. Textile Inst.* **15**, T559 (1924).
13. Urquhart, A. R., and Williams, A. M., *J. Textile Inst.* **16**, T155 (1925).
14. Wakeham, H., Textile Research Journal **19**, 595 (1949).

(*Manuscript received August 31, 1951.*)

Part II: Centrifuge Studies

Lars A. Welo, Hilda M. Ziifle, and Allan W. McDonald

Abstract

In an effort to develop a simple and rapid means of measuring swelling capacities in water of cotton and other fibers in mass, the centrifuge technique has been subjected to a rather extensive study. In this technique the swelling capacity appears as a function of the moisture retention after swelling and centrifuging.

Many previous workers have employed the centrifuge empirically for the removal of external, nonswelling water from fibers, but under conditions which have varied greatly as to time and intensity of centrifuging. In the present work, the complication of dealing with the two variables of time and speed of centrifuging simultaneously has been circumvented by noting that straight lines (to a high degree of approximation) were obtained when the moisture regains of the sample were plotted against the squares of the rotational speeds. The intercept of these straight lines on the moisture regain axis was characteristic for a given fiber in a given physical form. The intercept values were shown to be the same and reproducible for any selected centrifuging time of 20 min. or more, provided the minimum acceleration was above 3,200 g.

It was found that the zero-speed intercepts on the moisture regain axis, while highly reproducible, did not represent true swelling capacities. That the intercept values were too large was shown by the sizable intercepts obtained with glass fibers, which obviously are incapable of swelling.

It was found that the excess moisture retentions could be reduced considerably in samples "oriented" so that the axis of the yarns or cords lay parallel to the direction of centrifugal force. Still further reductions occurred on cutting such "oriented" samples after centrifuging and determining the moisture regains of the cut lengths nearest the centrifuge axis.

Although it was not found possible to obtain true swelling capacities with the centrifuge, it appears that the technique could be very useful for detecting and measuring differences in water-holding capacity brought about by chemical treatment.

A quantitative theory of the behavior of the fiber-water system in the centrifuge was developed, based on simple capillary considerations.

THE DEVELOPMENT of water-resistant fabrics has been under study for several years at this laboratory. Of especial interest was that type of fabric which resists water penetration due to self-sealing after wetting. In line with the objectives of this work, the need was apparent for a simple and rapid technique for the determination of the swelling capacities of fibers in water. At the outset, the centrifuge technique seemed to meet the requirements well. In this technique the swelling capacity appears as a function of the moisture retention after swelling and centrifuging. This method is well known as a means of partial drying in technical operations, and many attempts have been made, frequently with success from an empirical point of view, to use it is an index of swelling [5]. With a given material and closely controlled speeds and times of centrifuging, the observed moisture retentions—*i.e.,* regains—have been satisfactorily reproducible. On the other hand, the general magnitudes of the moisture regains reported have varied greatly from observer to observer, far more than could be due to any probable difference in a given kind of fiber. The moisture regains after centrifuging, as recorded in the literature, appear to be too large. The moisture regain values obtained with the centrifuge have always exceeded the regain values estimated from the adsorption isotherms at 100% relative humidity. Also, the regain values, when expressed in terms of volume increases, exceed the swelling capacities as determined by microscopic measurements. It seems certain, therefore, that the centrifuge never completely removes all water external to the fibers, the presence of which cannot have any part in the swelling.

In the centrifuge studies described here, the measured quantity was the moisture regain of the sample after centrifuging. These regain values, when expressed in terms of the equivalent volume increases, give abnormally large values for the swelling capacity. Therefore, most of the results presented herein are the regain values themselves. Any of these observed regains can be converted to the equivalent volume effect according to the calculations given in Part I (page 254).

In the previous use of the centrifuge technique for similar studies the accelerations have been relatively small, 1,000 times gravity or even less ($G \leqq 1{,}000$ g). Seldom have they been as high as $G = 2{,}000$ g, and only once, as far as we know, has the acceleration reached $G = 5{,}000$ g. The times of running have also been short, usually 15 min. or less. The plan in the present study was to use much higher accelerations and longer centrifuging times. A centrifuge capable of $G = 18{,}000$ g was available. It was hoped that the moisture regain would vary in a different manner with acceleration when the centrifuging time was long, or that the variation with time would be different at the higher accelerations. Either of these changes should occur if the regain corresponding to the swelling capacity is ever actually reached. Neither hope was realized. The curves, moisture regain plotted against either acceleration or time, showed no discontinuities; nor was there any tendency for the moisture regain values to assume strictly constant values independent of one variable or the other. There was always the initial steep decline in the curves, followed by slow decreases to smaller and smaller regain values. No regain value was found which was characteristic of a given kind of fiber and at the same time independent of either of the two working variables.

But a quantity, derivable from the retentions, was found which is characteristic of a given kind of fiber in a given physical form and which does not depend upon time. This quantity is the intercept on the moisture regain axis of the extrapolated straight line which closely approximates a long segment of the curve obtained when moisture regain values are plotted against the squares of the centrifuge speeds. These intercepts proved to be the same for various selected centrifuging times. However, the swelling capacities cannot be derived from these intercept values since they are too high. Sizable intercepts were obtained for glass fibers, which obviously have zero swelling capacities. That they are too large for fibers in general was demonstrated with oriented samples—samples supported in such a way that the axes of the cords or yarns lie along the direction of

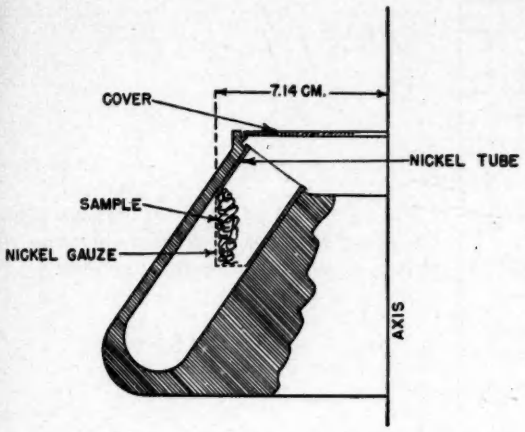

FIG. 1. *Partial median section through the rotor of a high-speed centrifuge, with sample holder.*

the centrifugal force while being centrifuged. The regain values for samples thus arranged were not only smaller, but they were attained with much lower accelerations.

Still lower regain values were obtained by cutting the oriented samples after centrifuging and determining the regains of the cut lengths nearest the centrifuge axis.

The Centrifuges

For the main part of the work an angle centrifuge having a maximum speed of about 15,000 r.p.m. was used. Part of a median section through the rotor is shown in Figure 1. The sample holder is shown in place; it is a thin nickel tube, flared for a shoulder at the top, cut in two perpendicular planes at the bottom. The horizontal cut avoids a wedge-shaped pocket when the lower end of the tube is closed with the shaped piece of 40-mesh nickel gauze. The plane of the vertical cut is 7.14 cm. from the rotor axis. The gauze actually bulges outward, but the centers of mass of the samples are, very approximately, at this distance from the axis. In the preliminary work the centrifuge was run up to its maximum speed, giving the acceleration $G = 18{,}000$ g. In all of the work reported here the maximum speeds were of the order 10,000 r.p.m., giving $G = 8{,}000$ g. There were eight wells in the rotor, so that up to eight samples could be centrifuged simultaneously.

In the later work with oriented samples an ordinary laboratory centrifuge was used, since alignment of materials in the direction of the centrifugal force could not be realized in the angle centrifuge. The arrangement of the oriented sample in the standard

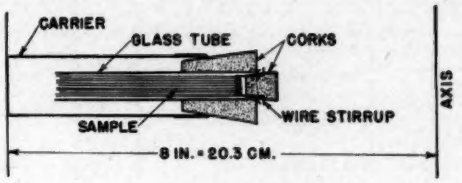

FIG. 2. *Arrangement for support of oriented samples in low-speed centrifuge.*

$3\frac{3}{4}$-in. × 1-in. centrifuge carrier is shown in Figure 2 to scale. The flared $\frac{1}{2}$-in. glass tube is 4 in. long. The large cork is oversized to prevent slipping into the carrier. The wire stirrup which supports the half-skein samples must be quite stiff. The small cork merely closes the system. The maximum speed attainable with this centrifuge was 3,100 r.p.m., and the mid-sections of the oriented samples were 13.8 cm. from the rotor axis. The maximum mean acceleration was therefore $G = 1{,}480$ g. As before, eight samples could be centrifuged simultaneously.

The Standard Swelling Procedure

The procedure used in swelling consisted of dropping the samples into boiling distilled water and boiling for 5 min. The samples were left in the water overnight at room temperature. In the work with a wetting agent, consisting of 0.5% or 0.2% Aerosol solutions, the samples were not boiled, but remained in the solutions overnight. Unoriented sample weights were about 1 g., oriented samples about 2 g. The oven-dry weights of the samples were determined after drying overnight at 105°–107°C.

Elimination of Centrifuging Time as a Variable

The derivation of the regain axis intercept was described above and its invariance with respect to time was noted. The very useful property of eliminating time as a working variable justified a thorough test. The intercept also has the characteristic of being a constant for a given material. It is reproducible, provided the selected times of centrifuging and the accelerations exceed the minimum values given below. The test was made with a cotton tire cord and a cotton yarn. The data are plotted in Figure 3, and the intercepts, with their standard errors, for the four different times are shown in Table I. Each point in Figure 3 is the mean from four different samples. The lines are the least-squares solutions.

It will be noted in Figure 3 that the very nearly

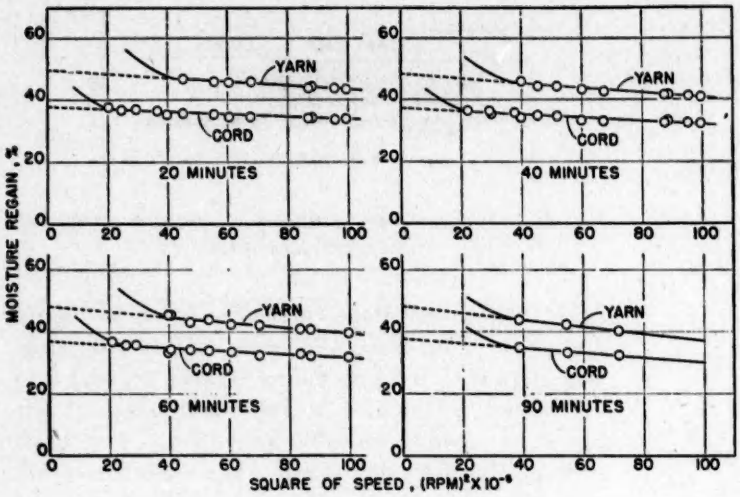

FIG. 3. *Plot of moisture regain against square of speed of centrifuge, showing constancy of moisture regain intercepts.*

TABLE I. INTERCEPTS AND SLOPES OF THE S^2-R CURVES

Centrifuging time (min.)	Intercept Moisture regain (%)		Slope (%/(r.p.m.²×10⁻⁶))	
	Cord	Yarn	Cord	Yarn
20	37.8	49.6	−0.044	−0.062
40	37.1	48.2	−0.049	−0.074
60	36.9	48.3	−0.054	−0.088
90	37.8	48.2	−0.077	−0.112
Average	37.4±0.2	48.6±0.3	—	—

linear relationship of regain to speed squared * appears only after the initial rapid fall in retention as the speed is increased. It is to be noted that as the S^2 value is increased, the S^2-R linear relationship is approached, first by the cord and then at a somewhat higher S^2 value by the yarn. It would be expected that the linear relationship would be reached at still higher values of S^2 for looser structures such as slivers and rovings. In these and subsequent experiments, the S^2-R linear relationship could be depended upon for all fiber structures for S^2 values of 40×10^6 and beyond and for centrifuging times of 20 min. or more. With the rotor and sample holder arrangement shown in Figure 1, $S^2 = 40 \times 10^6$ corresponds to an acceleration of $G = 3{,}200$ g.

It should be emphasized that the linear S^2-R relationship is a close approximation only. Slight concavity upwards is noticeable in the curves of Figure 3 and in nearly all those of Figures 4, 5, and 6. This is in keeping with the difficulty, already discussed, of

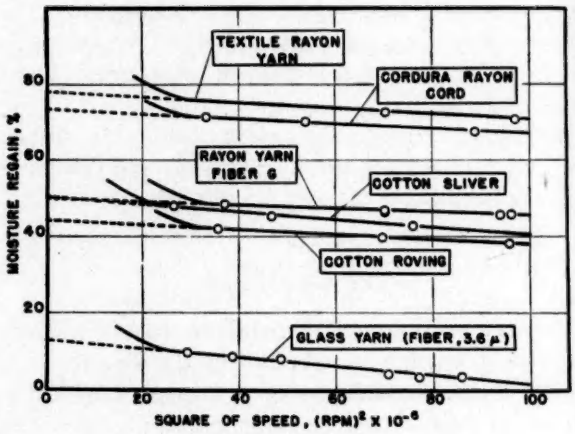

FIG. 4. *Some typical* S²-R *curves.*

removing all water in excess of the true regain corresponding to swelling. Progressive increase of the centrifuge speed is less and less effective in reducing the regain values.

There were originally two reasons for plotting the regains against the squares of the speeds, rather than against the speeds themselves. One was that the abscissas would then be proportional to an appropriate physical quantity, the acceleration. Thus, closer approximations to straight lines are obtained. The second reason was that this manner of plotting shortens the extrapolation range. Consider, for example, a series of abscissas within the range of 6 to 10 units. On a direct plot the extrapolation would be from 6 to zero on a scale of 10. When the abscissas are squared, the extrapolation range extends only from 36 to zero on a scale of 100.

* The expressions "speed squared" and "speed squared-regain" will hereafter be referred to as "S^2" and "S^2-R," respectively.

TABLE II. General Summary of Moisture Retention Measurements—Centrifuge Studies

Item No.	Material description	Moisture regain (%) Intercepts, unoriented samples*	Oriented whole samples†‡	Oriented nearest fourths of cut samples‡	By desiccation rate technique
	Cotton				
1	Cloth; mature	32.5			
2	Cloth; immature	43.5			
3	Tire cord; 17.5/4/3; variety, Wilds	46.2			
4	Tire cord; 23/4/3; variety, Wilds	37.4±0.2	31.7±0.4	28.0±0.1	21.1±0.7
5	Yarn; 17.5/1; variety, Wilds	48.6±0.3	43.3±1.7	34.0±1.7	19.4±0.5
6	Yarn; 12/1; variety, Empire		41.8±0.8**		17.0±0.3
7	Yarn; 34/2; variety, Acala (Bollies)		63.1±0.2**		20.6±0.4
8	Yarn; 34/2; variety, Acala (Well Grown)		43.0±0.5**		20.9±0.5
9	Yarn; mature	39.2	29.3±0.1		23.6±1.0
10	Yarn; immature	55.1	43.6±0.4		28.0±0.3
11	Roving; variety, S × P	44.5	41.6±0.1		
12	Card sliver; variety, Wilds 1943	50.3			
	Rayon				
13	Tire cord; 1100/2; Cordura	73.8	63.5±0.2		
14	Tire cord; 1100/2; Cordura		64.9±0.5	58.7±1.0	39.1±0.7
15	Yarn; 1100/480; Cordura	73.0	67.8±0.1		42.2±1.5
16	Yarn; 150/60; textile	78.2	71.4±0.6		
17	Yarn; 240/120; Fiber G	48.4	44.7±0.1		39.1±0.5
18	Yarn; 240/120; Fiber G‡		41.5±1.0	40.5±0.4††	
	Miscellaneous				
19	Yarn; flax		65.2±0.3**		40.1±0.5
20	Yarn; 210/69; 1Z; nylon		7.7±0.4	6.9±0.0††	7.5±0.2
21	Glass yarn; 450–4/5; $d = 3.6\mu$	12.8	1.1±0.1		
22	Glass; bonded mat No. 6; $d = 7.6\mu$	9.0			
23	Glass; type N wool; $d = 17.9\mu$	7.7			
24	Glass; Fiber A; $d = 2.2\mu$	3.5			

* Single determination from least-squares line, except items 4 and 5, which are means of four. (See Figure 3.)
† Means from two highest centrifuge speeds. (See typical curves, Figure 6.)
‡ In simultaneous centrifuge runs.
** Swollen in 0.5% Aerosol solution. Others were swollen in boiling distilled water.
†† Nearest third of oriented sample.

Survey of Various Fibers—Centrifuging, with Intercept Procedure

The moisture regains at the intercepts for a variety of fibers in various structural forms are shown in Table II. Some typical S^2-R curves from which intercepts were derived are shown in Figure 4. The selected times of centrifuging were either 30 or 40 min. For a given curve these times were, of course, the same. Each plotted point in Figure 4 is the mean regain from two separate samples, and the lines are least-squares solutions. As a rule, three different speeds were used, three being sufficient both to determine a straight line and to guard against possible serious departures from linearity. All three runs were made without interruption, other than to remove samples, weigh them, and replace them with new ones. Temperature effects were minimized by making the high-speed run first, following with the medium- and low-speed runs. The rotor temperature is highest after the high-speed run, and successively diminishes after the others. Some temperature observations after high-, medium-, and low-speed runs, selected at random, are: high, 33.6°C; medium, 32.5°C; low, 30.7°C; and high, 33.0°C; medium, 31.8°C; low, 30.0°C. The room temperatures were about 27°C. The same procedure was followed during the extensive test of the S^2-R relationship shown in Figure 3. In that test, runs of different durations were also made in succession during a day. The run of longest duration was made first.

Structural Effects

For the reasons already stated, all intercepts in Table II must be considered to be too high numeri-

cally to correspond to the moisture regains at maximum swelling capacities. This is especially apparent from the intercepts listed for the fibers and yarns of glass (items 21 to 24), in which the true swelling capacities and hence the regains are zero. There is no obvious relationship between intercept and glass fiber fineness; rather, the correlation is between intercept and fiber organization. The intercept is largest for the highly organized glass yarn; it is smaller in the bonded mat, with its partly parallelized fibers; and it is smallest in the unorganized wool and Fiber A.

This suggested that the intercepts for the other fibers might be reduced by unravelling the cloths or by untwisting the cords and the yarns. Further intercept reduction might occur if the fiber arrangement were still further disorganized, as by cutting to fine states of division. Untwisting would reduce the number of fiber-to-fiber cylindrical elements of contact. After cutting, the fiber arrangement would be much more random, and a large fraction of the cylindrical elements of contact would be reduced to mere points of contact where the fibers cross. If the water retained after centrifuging, over and above the regain corresponding to the swelling capacity, is held by capillarity, then unravelling, untwisting, or cutting should diminish it unless the effects are compensated by larger available volumes.

In most cases, as may be seen in Figure 5, unravelling and untwisting led to larger regain values and larger intercepts. With three of the rayons the expected decrease occurred on cutting. But in all cottons and in Fiber G the effect of cutting was the opposite of that expected. Although these experiments with disorganized fiber structures did not lead to the desired goal—reduction of excess retained water—the results are presented for their possible general interest and because they illustrate the great variety of results that may be obtained when centrifuging a given kind of swollen fiber in various structural forms or states of division.

Orientation Effects

Substantial reduction in the moisture regain values was obtained with oriented fiber structures, such as cords, yarns, and rovings. A similar reduction in moisture retention brought about by orienting the structural axis parallel to the centrifugal field was recently reported by Preston, Nimkar, and Gundavda [4] in their work on glass fibers. The arrangement of the samples in the centrifuge has been described and is illustrated in Figure 2. Three typical curves are shown in Figure 6; for comparison, S^2-R curves obtained with the high-speed angle centrifuge are shown for unoriented samples. Since the retentions were obtained with different centrifuges having different effective radii, the regains are plotted against mean accelerations, rather than against the proportional squares of the speeds. The retentions after centrifuging at the two highest accelerations were always nearly the same; their means are therefore entered in Table II. Duplicate samples were

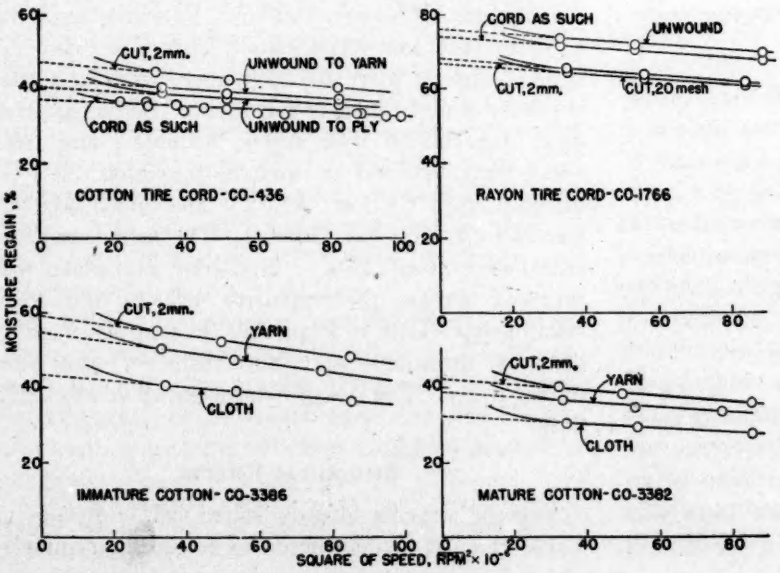

FIG. 5. *Effect of structural form of textile on moisture regain after centrifuging.*

used so that each entry is the mean for four separate determinations. The standard errors are also entered in Table II; since they are based on only four determinations, they have slight quantitative significance, but they indicate qualitatively the reproducibility of the retentions from sample to sample. Because of the near equality of the retentions after the two highest speeds, the intercept procedure was not followed. The regains for oriented samples in Table II are the means of those actually observed.

Moisture Gradients in Oriented Samples

Another, and final, reduction in moisture regain was attained by cutting the oriented samples after centrifuging and determining the regain on that portion of the sample nearest the centrifuge rotor axis. Usually the samples were cut into four approximately equal lengths, but sometimes into only three lengths. In the first trials, the centrifuge was stopped quickly with the brake, and the samples were cut as quickly as possible to minimize moisture equalization. In the final experiments (with cotton cord and yarn and rayon cord (items 4, 5, and 14)), the moistures were fixed by freezing so that no moisture equalization could occur before cutting. The samples were centrifuged for the usual half-hour at room temperature. Then, without stopping, a shallow wire-screen tray containing dry ice was placed in the centrifuge housing immediately above the rotating system. More dry ice was fed by hand through a hole at the bottom of the housing. Centrifuging was continued until the samples were frozen. The time necessary for this was determined in a preliminary experiment. The speed reduction that occurred on adding dry ice was, in part, compensated by increasing the voltage. Within the limits of error of the moisture determinations, they were the same as after the first experiments without freezing.

Only the moisture regain values of the nearest fourths or thirds of the oriented samples are entered in Table II. However, moisture regain data for all sample portions were obtained, giving data for moisture gradients. The gradients for three materials are shown in Figure 7. Linearity of the relationship was assumed, and least-squares lines were drawn.

Since the cutting had to be done quickly, even cutting of the frozen samples, the cut lengths were only approximately equal. Because of loops over the supporting stirrups, equal lengths would have been difficult to obtain with more leisurely cutting. The abscissas in Figure 7 are therefore not lengths, but proportional dry weights which are known from the moisture analyses. The total dry weight of a sample (sum of the four parts) is expressed as unity on the scale of abscissas. The fractional weight (near end/total sample) after dividing by 2 is the abscissa of the center of mass of the near-end length. The abscissas for the succeeding lengths are derived in the same way, keeping in mind that their half-fractional

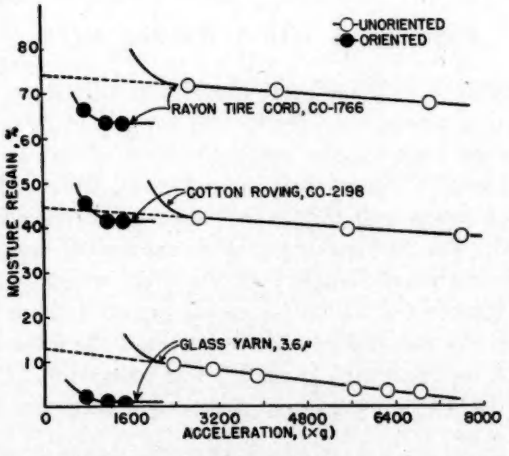

FIG. 6. *Effect of orientation of fibrous axes in the centrifugal field on moisture regain.*

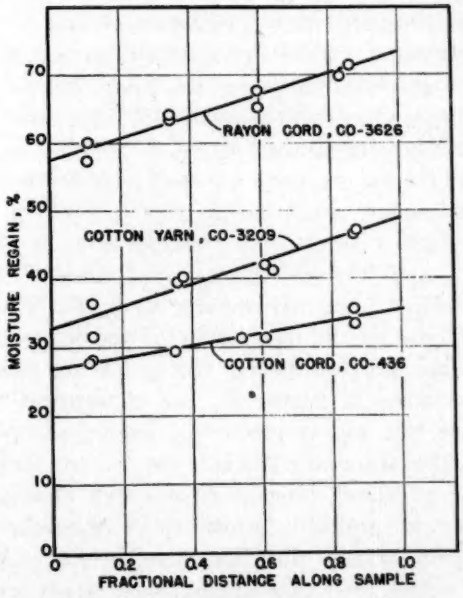

FIG. 7. *Moisture gradients in oriented samples in direction away from centrifuge rotor axis. Samples were frozen during centrifuging.*

weights must be added to the whole fractional weights of all preceding lengths.

The moisture gradient so determined was considerably larger than expected. By extrapolation of the lines in Figure 7, the moisture differences between the sample ends, in percent of dry weight, are as follows: cotton cord, 8.5%; cotton yarn, 16.0%; rayon cord, 15.5%. The extreme near-end and far-end accelerations for centrifuge speed 3,100 r.p.m. were calculated as $G = 1{,}010$ g and $G = 1{,}950$ g, respectively. One would expect that an accumulation of water at the far end of a sample would be thrown off because the acceleration is larger there. Actually, it is known from the nearly identical regain values in oriented samples after centrifuging at the two highest accelerations shown in Figure 6 that the retentions are nearly independent thereof.

A possible explanation of these moisture gradients follows from a consideration of the effect of tension on swelling. According to Skau [7], the effect of tension on a yarn is to decrease the percentage swelling of the fibers and the yarn. Also, Nickerson [2] has shown that a yarn under stress exhibits a lower desorption regain—8.19% for a yarn under a dead-weight load of 60% of its breaking strength, as compared to 8.78% for the unstressed yarn, both yarns being equilibrated at 21°C and 65% relative humidity. In the present experiments on oriented samples, there was a tension gradient along the specimen ranging from zero at the far end to maximum values at the end nearest the center of rotation. According to this reasoning, maximum moisture loss should take place from that portion of the skein nearest the center of rotation.

Thus far the emphasis has been on the removal of external water, which has no part in swelling, since the problem of measuring swelling is to be able to draw a line between internal and external water. Nevertheless, one may inquire as to the effect of centrifuging on the distribution of the water within the fibers, and the bearing, if any, on the gradients such as those in Figure 7. An experiment to investigate this was conducted as before, except that the samples were only partially swollen by conditioning for a limited time in a saturated atmosphere. The internal gradients proved to be relatively small and in the reverse direction—that is, the moisture regain values, after centrifuging, were larger towards the rotor axis. After the half-hour of centrifuging at mean $G = 1{,}650$ g, the following average moisture regains were found in the three cut lengths from duplicate samples of each material: cotton tire cord: near, 13.3%; middle, 12.5%; far, 11.3%; cotton yarn: near, 13.1%; middle, 12.5%; far, 12.1%. In view of the previous discussion of the gradients existing in the fully swollen samples, this last result appears to be anomalous. In any case, the internal gradients are small and can be expected to have little bearing on the gradients shown in Figure 7.

A possible explanation of this reversal in the direction of the moisture gradients in partially swollen samples has been suggested by Skau [8]. As with the fully swollen samples, an attempt was made to fix the moisture distribution by freezing the samples prior to stopping the centrifuge. As discussed before, a tray of dry ice was placed in the centrifuge housing above the rotor, and centrifuging continued until the samples were frozen. It is to be remembered that the oriented samples were centrifuged inside a glass sheath, which was insulated from the outer metal tube by a cork at the near end and an annular air space at the far end. Under such conditions, the cooling of the samples takes place fairly slowly. Thus, the outer metal tube is very cold relative to the sample. Water vapor distills from the relatively warm sample, and is removed by condensing on the cold inside wall of the tube. Further, it would be expected that the evaporation would be greatest at the far end, nearest the open end of the glass sheath. The over-all loss of moisture that occurred during this process tends to bear out this suggestion. The regain for the cord decreased from a value of 14.2% prior to centrifuging to an average value of 12.4%; the regain for the yarn decreased from 14.9% to 12.6%.

Experiments with a Wetting Agent

Except with glass yarn, negative results were obtained in attempts to reduce the amount of retained water by lowering the surface tension of the water. The wetting agent used was Aerosol OT.* The concentration was 0.2%, and the measured surface tension was 29 dynes/cm. With unoriented samples in the high-speed angle centrifuge, the moisture regain intercept of 73.8% for rayon tire cord (item 13, Table II) was reduced to 71.4%; and the intercept 12.8% for glass yarn (item 21) was reduced to 3.8%. But the slight increase of the 44.5% intercept for

* The mention of trade products does not imply their endorsement by the Department of Agriculture over similar products not mentioned.

cotton roving (item 11) to 45.7% seems to represent the general effect of adding a wetting agent to the water. In later experiments with oriented samples centrifuged at $G = 1{,}480$ g, the comparative percentage retentions between samples swollen in distilled water and those swollen in 0.5% Aerosol solution were: cotton tire cord, 31.8% and 33.3%; cotton yarn, 43.3% and 48.0%; cotton roving, 41.6% and 43.7%; and rayon tire cord, 63.5% and 64.6%. The generally slightly larger retentions observed with Aerosol solution probably follow from more thorough wetting of the fibers and contact-angle diminution. However, in this series of experiments the retentions were, in the main, quite definitely independent of surface tension.

A similar, but successful, effort to reduce the retentions by surface tension lowering is that of Preston and Nimkar [3]. With a wetting agent the surface tension was reduced to, among other fractions, one of about one-half—*i.e.*, 36 dynes/cm., instead of 73 dynes/cm. (see Table III in [3]). Their studies were made on viscose rayon, Fortisan, and glass. These authors stated, justifiably on the basis of their data, that the effect of surface tension lowering is most marked in viscose rayon, which was their coarsest fiber in respect to fiber diameter. On the basis of results given in Table II, it is believed that the retentions, in excess of those corresponding to the swelling capacities, and the effectiveness of all schemes designed to reduce these excess retentions, such as orientation, moisture determination on the near ends of cut oriented samples, and surface tension lowering, are determined largely by fiber coarseness in the sense of surface roughness. The data in Table II which support this belief are: First, the intercept values themselves show this effect of surface roughness—for example, the mature cotton cloth (item 1) as compared with the immature (item 2), the mature cotton yarn (item 9) as compared with the immature (item 10), and the serrated rayons (items 13, 15, and 16) as compared with the unserrated and smooth rayon Fiber G (item 17). Second, the influence of surface roughness on the effectiveness of orientation in reducing the excess retention may be noted by comparing moisture regain values—for the mature cotton yarn (item 9) 64% of the excess retention is removed by orientation, whereas for the immature yarn (item 10) only 42% of the excess is removed; for the smooth-surface rayon Fiber G (item 17) 40% of the excess is removed as compared to only 17% for the serrated rayon (item 15); for the glass yarn of smooth fibers (item 21) 90% of the excess retention is removed.

The data of Preston and Nimkar (Table III in [3]) support this view since, as this laboratory's fiber photomicrographs show, the order of decreasing fiber surface roughness is viscose rayon, Fortisan, and glass. The argument for this view is presented briefly in Table III. But first let us examine the relation between excess retention, after centrifuging, and surface tension.

Consider a minute liquid aggregate of any geometrical form whatsoever which is held in place against centrifugal action by forces of a capillary nature. Let p = perimeter, the length of the solid-liquid line of contact; v = aggregate volume; γ = surface tension; β = contact angle; d = liquid density; and α = centrifugal acceleration.

The perimeter is proportional to some length, l, so we can write $p = K_p l$; the force F_1 which resists

TABLE III. EFFECT OF SURFACE TENSION LOWERING (BASED ON PRESTON AND NIMKAR [3])

Line	Property	Retentions and derived quantities (% of dry weight) Viscose rayon (5 den./fil.)	Fortisan (1 den./fil.)	Fortisan (0.4 den./fil.)	Fortisan (0.1 den./fil.)	Glass (0.6 den./fil.)
1	Observed retention, $\gamma = 73$*	103	48	55	63	13.5
2	Observed retention, $\gamma = 36$*	92	42	47	56	8
3	Observed difference	11	6	8	7	5.5
4	Moisture regain†	40	30	30	30	0
5	Observed excess, $\gamma = 73$‡	63	18	25	33	13.5
6	Observed excess, $\gamma = 36$**	52	12	17	26	8
7	Theoretical difference††	40	11.5	16	21	8.7
8	Obs. diff./theor. diff.§	0.28	0.52	0.50	0.33	0.63

* γ = surface tension (dynes/cm.).
† From desiccation rate technique.
‡ Line 1 minus line 4.
** Line 2 minus line 4.
†† Line 5 times 0.64.
§ Line 3 divided by line 7.

removal of the aggregate by the centrifuge is therefore

$$F_1 = K_p l\gamma \cos\beta. \quad (1)$$

The volume of the aggregate is proportional to the cube of the same length, l, so that we can write $v = K_v l^3$, $m = K_v l^3 d$, and, for the centrifugal force F_2,

$$F_2 = K_v l^3 \alpha d. \quad (2)$$

At the aggregate's equilibrium size $F_2 = F_1$, so that

$$K_v l^3 \alpha d = K_p l\gamma \cos\beta, \quad (3)$$

from which

$$l = \left(\frac{K_p}{K_v}\right)^{\frac{1}{2}}\left(\frac{\gamma \cos\beta}{\alpha d}\right)^{\frac{1}{2}}. \quad (4)$$

But $v = K_v l^3$, so that the volume of the aggregate is

$$v = K_v \left(\frac{K_p}{K_v}\right)^{\frac{3}{2}}\left(\frac{\gamma \cos\beta}{\alpha d}\right)^{\frac{3}{2}} = (K_p)^{\frac{3}{2}}(K_v)^{-\frac{1}{2}}\left(\frac{\gamma \cos\beta}{\alpha d}\right)^{\frac{3}{2}}. \quad (5)$$

Putting $(K_p)^{\frac{3}{2}}(K_v)^{-\frac{1}{2}} = K$, we have, finally,

$$v = K\left(\frac{\gamma \cos\beta}{\alpha d}\right)^{\frac{3}{2}}. \quad (6)$$

The volume, or the mass, of an aggregate is proportional to the $\frac{3}{2}$ power of the surface tension times the contact-angle cosine factor. Preston and coworkers [4] derived a somewhat different expression for the relative mass of water retained by a given fiber after centrifuging. The other relation expressed by equation (6)—*i.e.*, that the aggregate volume, or mass, is inversely proportional to the $\frac{3}{2}$ power of the acceleration—will be used later. Changing from pure water to dilute wetting agent solution does not appreciably affect the density, d. Since the fibers are completely wetted by both pure water and wetting agent solution, $\beta = 0$ in both cases and $\cos\beta = 1$. The numerical value of K in equation (6) is a geometrical shape factor only. For individual aggregates, K must take on a wide range of values because the aggregates have a large variety of shapes. Its average value for a sample is determined by fiber surface characteristics and fiber arrangement. In general, in changing from pure water to wetting agent solution, K changes also because the aggregates become smaller and have smaller volume-perimeter relations.

It is now possible to pursue the argument by means of Table III. The data in lines 1, 2, and 3 are taken directly from Table III of the Preston and Nimkar paper [3]. Line 4 of Table III contains the maximum moisture regain values as determined by the desiccation rate technique described in Part I (page 254). The values on line 4 are taken from Table I in Part I; the Fortisan value from item 17; the rayon value from the average of items 12, 13 and 14. Glass, of course, is considered to have no swelling capacity. Line 5 contains the Preston and Nimkar excess retentions over and above the maximum moisture regain values when the surface tension was 73 dynes/cm. When the surface tension was reduced to 36 dynes/cm., the new average aggregate volume, or the proportional mass, should have been, by equation (6), to the pure water mass as

$$(\tfrac{1}{2})^{\frac{3}{2}} = \frac{1}{2.8} = 0.36,$$

and the fractional difference in retention should have been observed to be

$$1.00 - 0.36 = 0.64.$$

This is the factor that was used to compute from line 5 the theoretical retention differences (line 7) that should have been observed on changing from pure water to wetting agent solution. The observed differences (line 3) are smaller in all cases, and markedly so in the case of the roughest fiber, viscose rayon. The ratios of observed difference to theoretical difference (line 8) increase in the order of fiber surface smoothness, and thus support the previous deductions as to the effect of fiber surface roughness.

A further conclusion can be drawn from the data in Table III if consideration is given to the changes that must have occurred in the volume-perimeter relations of the liquid aggregates. In considering these changes it must be remembered that the volume of a given aggregate decreases more rapidly than the perimeter line of liquid-solid contact.

Apparently, from line 8, Table III, the volume-perimeter relation decreases the most with the glass since only 37% (100% − 63%) of the liquid was left. Apparently, also, the relation decreased the least with the viscose rayon since 72% (100% − 28%) of the liquid remained. Yet the more complete removal of liquid occurred with the glass. This contradiction is removed at once if it is recognized that rough fibers provide more places for aggregates to lodge. As the amount of water diminishes, it becomes scattered among all of the available lodging places as aggregates of small volume-perimeter rela-

tions. The effect of fiber roughness is thus, in a sense, to disperse the liquid. Rough fibers retain more excess liquid after centrifuging than the smooth fibers because there are more aggregates which have reached the limiting volumes expressed by equation (6).

For Fortisan (line 8, Table III) the ratio of observed to theoretical differences is seen to decrease in the order of fiber fineness. This should be true, since the finer the fiber the more fiber-to-fiber contacts there are, and these contacts provide additional places for liquids to lodge.

An additional kind of lodging place for liquids which must be mentioned is the pockets and troughs which are formed in fibers of strongly indentured sections, such as in immature cotton, or of serrated sections, such as in most rayons. Especially in most unoriented samples, a large fraction of these troughs are closed in the direction away from the centrifuge axis, and trapped liquid would not be removed by centrifuging. All of the immature cottons have shown strikingly high total retentions and marked effects of orientation as compared to the mature cottons.

Let us compute what the Preston and Nimkar difference of 11% with viscose rayon (line 3, Table III) would have been had they used accelerations over three times as large. Their acceleration was $G = 1{,}000$ g. The minimum acceleration, when using the high-speed angle centrifuge and the intercept procedure with unoriented samples, was $G = 3{,}200$ g. Equation (6) may be used for this computation; the equation states that the retention is inversely proportional to the $\frac{3}{2}$ power of the acceleration.

With pure water the excess retention was $103\% - 40\% = 63\%$ (line 5, Table III). With an acceleration of $G = 3{,}200$ g this would have been

$$63\left(\frac{1000}{3200}\right)^{\frac{3}{2}} = 63\left(\frac{1}{1.79}\right)^{3} = 63/5.7 = 11.0\%.$$

With wetting agent solution of half the surface tension, the Preston and Nimkar excess retention was $92\% - 40\% = 52\%$ (line 6, Table III). At $G = 3{,}200$ g this would have been, similarly, $52/5.7 = 9.1\%$. The difference, $11.0\% - 9.1\% = 1.9\%$, borders on experimental uncertainty even if, as is assumed in this calculation, all of the excess liquid is undispersed and subject to centrifugal action.

With oriented samples we likewise could obtain no certain effects when changing from pure water to wetting agent solution even though the acceleration was as low as $G = 1{,}480$ g. But it should be kept in mind that the effect of orientation, in itself, is to clear the sample of a considerable portion of the excess liquid that is held when the sample is not oriented. A smaller retention is left to be affected by surface tension lowering.

The Empirical S^2-R Curves and the Inverse Three-Halves Power Law

Figures 3, 4, 5, and 6 consist of S^2-R curves which illustrate various aspects of the present study. Let us now see how they correspond to the inverse $\frac{3}{2}$ power law with respect to acceleration expressed in equation (6),

$$v = K\left(\frac{\gamma \cos \beta}{\alpha d}\right)^{\frac{3}{2}}.$$

Since the mass of water retained is proportional to the volume, and since all other quantities in equation (6) except the acceleration, α, remain the same, we may write

$$m = C\left(\frac{1}{\alpha}\right)^{\frac{3}{2}}, \tag{7}$$

where C is a new constant. To this must be added two constants representing portions of the retained water that are only negligibly affected by the centrifuge. These constants are: (1) the regain corresponding to the swelling capacity itself, m_s, and (2) the water that has been trapped and dispersed over the surface of the fibers in such a fine state of division that the water aggregates are practically unaffected by the centrifuge because of small volume-perimeter relations. Call this trapped and dispersed water m_t. We then have

$$m = C\left(\frac{1}{\alpha}\right)^{\frac{3}{2}} + (m_s + m_t). \tag{8}$$

In doing this it is assumed that the effect of increasing the centrifugal acceleration is only to remove more and more water from the regions of fiber-to-fiber contact. It has been shown experimentally that practically all excess liquid is removed from smooth fibers, such as rayon, Fiber G, nylon, and glass, by centrifuging at high accelerations.

Equation (8) is plotted in Figure 8, with $C = 1$, an acceleration range from zero to 10, and a range for the water content from zero to 3, a third of which consists of the two constant terms, m_s plus m_t.

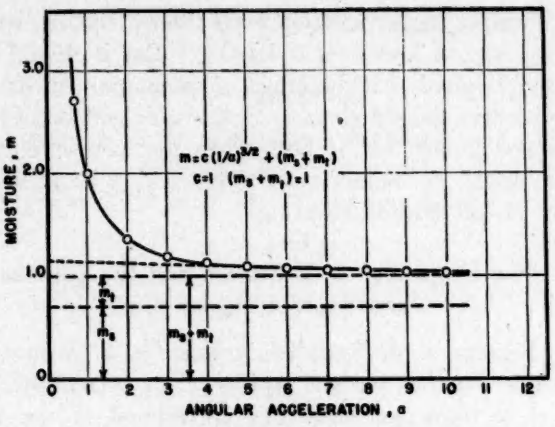

FIG. 8. *The centrifuge equation relating mass of retained moisture to angular acceleration.*

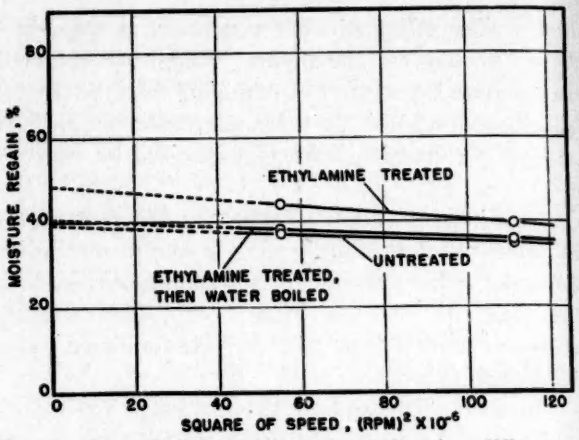

FIG. 9. *Use of the centrifuge for indicating differences in water-holding capacity due to chemical treatment.*

The curve has all the characteristics of the curves in Figures 3, 4, 5, and 6. The value of m decreases very rapidly at first as the acceleration is increased. The rapid fall is followed by a segment so slightly concave upwards that it may be closely approximated by a straight line. The term m approaches a constant value asymptotically. If the term m_t were zero, the asymptote would be the regain corresponding to the swelling capacity, m_s. The term m_t may be small and negligible with certain kinds of fibers. Generally it is large and may even be of the order of magnitude of the regain itself at maximum swelling capacity.

The Measurement of Swelling Capacity Differences

It has been emphasized that, in general, not all nonswelling water is removed by the centrifuge. Therefore, absolute swelling capacities cannot be derived from the moisture regain values obtained with the centrifuge, although close approximations can be obtained if, as we believe, the fibers are smooth and especially if the samples are oriented to facilitate water removal.

Inability to obtain absolute values does not, however, preclude the determination of differences in water-holding capacity brought about by chemical treatments. On chemical treatment the external surface characteristics of the fibers should remain the same except for such changes as are due to the swelling itself. Among such differences are: closer approach to cross-section circularity if the treatment causes increased swelling, and further departure from circularity if the treatment diminishes the swelling capacity.

One instance of practical application is provided by cotton that is "decrystallized" with anhydrous ethylamine [6]. The cut cotton was treated with anhydrous ethylamine for 4 hrs. in an ice-cooled bath and was then squeezed. It was extracted with chloroform and dried in air. A portion of this treated sample was boiled in water for 2 hrs., a process which causes partial recrystallization. These two portions and an untreated control were then swollen, without boiling, in distilled water overnight. They were centrifuged for ½ hr. The data obtained were handled by the intercept procedure. Figure 9 gives the results. The percent regain values at the intercept are as follows: untreated, 40%; ethylamine "decrystallized," 49%; ethylamine "decrystallized" followed by partial recrystallization in water, 41%. The effect of ethylamine treatment was to cause a greater water retention, which is consistent with the increase of amorphous cellulose. Subsequent boiling in water reduced the water-holding capacity, but not quite to its original value before treatment.

A second instance of the practical application of the centrifuge as a means of studying water-holding capacity following chemical treatment of textiles is given in Figure 10. The figure shows the higher water-holding capacity brought about by mercerizing cotton; it also shows the marked decrease in both unmercerized and mercerized material due to subsequent formaldehyde treatment [1].

Great caution must be exercised if the centrifuge is used for indicating capacity differences other than those introduced by chemical treatments. Results for the mature and immature cotton yarns (items 9 and 10, Table II) illustrate this necessity, although they represent, perhaps, extreme cases. The intercepts are 39.2% and 55.1%, indicating a moisture regain difference of about 16%. With oriented sam-

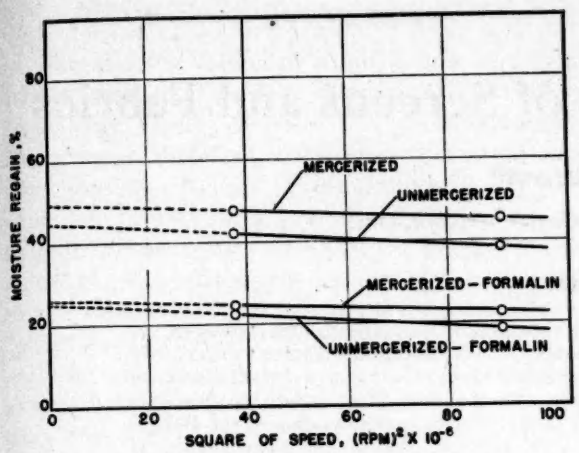

FIG. 10. *Use of the centrifuge for measuring changes in water-holding capacity due to chemical treatment.*

ples, the regains were 29.3% and 43.6%, but the difference was still about 14%. By the desiccation rate technique the moisture regains were 23.6% and 28.0%, so that the true regain difference appears to be between 4% and 5%, that for the immature cotton being the larger. The need for caution was further exemplified by the results for the rayon studied. According to the centrifuge data in Table II, the moisture regain of Fiber G (items 17 and 18) is much smaller than that of the other rayons (items 13 to 16). According to the desiccation rate data, the rayons do not differ greatly among themselves.

Summary and Conclusions

In order to carry out studies of the swelling capacity of textile fibers in water, a sensitive, yet simple and rapid technique was required. At first the centrifuge technique seemed to meet these requirements. Consequently, the centrifuge technique was subjected to a rather extensive study. In this technique the moisture regain in fibers after swelling and centrifuging is taken as proportional to the swelling capacity. The absolute swelling capacity is obtained from the regain after dividing by the specific volume of the fiber. The complication of dealing with the two variables of time and centrifuge speed was circumvented by noting that the nearly straight line obtained by plotting the moisture regains against the squares of the speeds gave the same intercepts on the regain axis for any selected standard centrifuging time of 20 min. or more, provided the minimum acceleration was above 3,200 g. Time of centrifuging was thus eliminated as a working variable.

The intercepts on the regain axis, while highly reproducible, could not be converted to the true swelling capacities. This was shown by the retention of an appreciable percentage of water in samples of glass fibers. It was found that the excess moisture retentions were reduced in samples supported so that the axes of the yarns and cords lay along the direction of the centrifugal force. Further reduction occurred on cutting these "oriented" samples after centrifuging and determining the moisture regains of the cut lengths nearest the centrifuge axis. In spite of many variations of the technique, it was not found possible to obtain, in general, the true swelling capacities of fibers. On the other hand, the centrifuge technique appears to be very suitable for detecting and measuring differences in water-holding capacity brought about by chemical treatment, etc.

A theoretical representation of the experimentally observed speed squared-moisture regain curves was obtained from simple capillary consideration. The equation states that the retention equals a constant times the reciprocal of the acceleration to the three-halves power plus two additive constants. The first of these additive constants is the regain corresponding to the swelling capacity; the second is water that has become finely dispersed and lodged upon the fiber surface. The latter constant has been shown experimentally to be dependent upon fiber surface roughness of microscopic dimensions.

Acknowledgment

The authors gratefully acknowledge the suggestions offered and the aid given by Dr. C. M. Conrad, who had general supervision over these studies.

Literature Cited

1. Goldthwait, C. F., TEXTILE RESEARCH JOURNAL **21**, 55 (1951).
2. Nickerson, R. F., *Ind. Eng. Chem.* **34**, 1149 (1942).
3. Preston, J. M., and Nimkar, M. V., *J. Textile Inst.* **40**, P674 (1949).
4. Preston, J. M., Nimkar, M. V., and Gundavda, S. P., *J. Textile Inst.* **42**, T79 (1951).
5. Rollins, M. L., Fort, H. H., and Skau, D. B., "Cellulose-Water Relations: A Selected Bibliography with Special Reference to Swelling of Cotton and to Its Utilization in Water-Resistant Fabrics," Washington, D. C., U. S. Department of Agriculture, Library List No. 44, 1949. (Contains 523 abstracted titles, including over 80 on moisture and swelling measurements in particular.)
6. Segal, L., Nelson, M. L., and Conrad, C. M., *J. Phys. Colloid Chem.* **55**, 325 (1951).
7. Skau, E. L., TEXTILE RESEARCH JOURNAL **16**, 556 (1946).
8. Skau, E. L., private communication.

(Manuscript received August 31, 1951.)

Aerodynamic Properties of Screens and Fabrics

S. F. Hoerner*

Wright Air Development Center, Dayton, Ohio

Abstract

General rules for the pressure loss of flow across wire screens and simple fabrics are devired herein from the available test data. At *higher* Reynolds numbers the results obtained agree satisfactorily with the Borda-Carnot theory, which considers the dynamic losses to be due to a sudden expansion of the cross section behind the openings of an obstacle. On the other hand, at *very low* Reynolds numbers the pressure loss seems to be proportional to the velocity, corresponding to the Hagen-Poiseuille kind of flow. In the intermediate range of the Reynolds number the loss coefficient is found by statistical analysis to be a function of this number and the solidity ratio of the material.

Aerodynamic Parameters

Several terms are generally known to describe the aerodynamic properties of screens, wire mesh, fabrics, and similar materials Throughout this report the following terms are used: "permeability," the degree by which the material is pervious to, or penetrable by, the air; "porosity," the ratio of the projected geometrical area of the openings across the material to the total area of the material; "solidity," the complement of the porosity—that is, the ratio of the projected area of the solid parts of the material to the total area of the material.

The following notation is used in this report:

$S_\square$	total area of the material
$S_\bullet$	projected solid area of the material
S_{op}	open area of the material
φ	solidity ratio of the material $= S_\bullet/S_\square$
d	diameter of the cylindrical elements of which the screen or fabric is composed
μ	viscosity of the air
ρ	density of the air
ν	kinematic viscosity $= \mu/\rho$
w	velocity ahead of the material
q	dynamic pressure of the flow $= 0.5\rho w^2$
Δp	pressure differential across the material
x	subscript, indicating the average "maximum" velocity within the openings of the material

The loss of pressure which a flow encounters upon passing through a pervious sheet of material is found by means of tests conducted in a closed channel (duct) or in a testing machine. This loss is suitably indicated by the coefficient

$$\zeta = \frac{p_{\text{ahead}} - p_{\text{behind}}}{0.5\rho w^2} = \frac{\Delta p}{q}, \qquad (1)$$

where the denominator indicates the dynamic pressure corresponding to the average velocity of the flow along the duct. In terms of conventional aerodynamics, the pressure loss is the equivalent of a drag force created by the flow on the elements of the obstacle. Therefore, a drag coefficient, defined by equation (7), is used later in this paper to describe the pressure differential.

The pressure loss depends upon the Reynolds number. This number, indicating the ratio of the dynamic to the viscous forces of the flow, can be based on various characteristic velocities and lengths. Throughout this paper the characteristic number, R_x, shall be considered:

$$R_x = \frac{w_x d}{\nu} = \frac{w}{S_{op}/S_\square}\frac{d}{\nu}, \qquad (2)$$

where w_x denotes the average "maximum" velocity (that is, the velocity across the narrowest cross section) through the openings of the respective pervious material:

$$\frac{w_x}{w} = \frac{S_\square}{S_{op}} = \frac{1}{1-\varphi}, \qquad (3)$$

if considering incompressible flow. The characteristics in compressible fluids depend upon the Mach number, $M = w/a$, where a = speed of sound.

* Present address: Gibbs & Cox, Inc., New York City.

Reynolds Number Range

The simplest model of a fabric is a wire-mesh screen (Figure 1). The dimensions of such a screen are clearly defined and are measurable. Many tests, therefore, have been conducted with such screens. Recent investigations [6, 8] indicate that fabrics show practically the same aerodynamic properties as screens if the dimensions are identical. Generally the pressure differential due to the flow of air through a pervious material is caused by viscous forces (friction between the air particles and the surface or skin of the elements) as well as by dynamic forces (separation of the flow from the rear of the elements and corresponding pressure losses). Usually, however, the flow of air through fabrics is considered to be similar to the purely viscous flow through narrow tubes [7]. The law of Hagen and Poiseuille [1(*a*)] was accordingly employed to classify the permeability of fabrics:

$$\Delta p \sim \frac{l}{S_{op}} w_x \mu. \qquad (4)$$

However, the proportion $\Delta p \sim w_x$ is applicable only for the fully developed flow through tubes, the length, l, of which is several or many times their diameter. Equation (4) may therefore properly be used to describe the flow at *low* velocities through a *thick* material with *narrow* pores, correspondingly resulting in a very low Reynolds number. On the other hand, the length of a nozzle opening, as illustrated in Figure 1, is only equal to the wire or yarn diameter, d. Accordingly, Figure 7 does not show a linear relationship between Δp and w. It is only at extremely low velocities that such a law (equation (4)) may be expected to hold true, as indicated in the graph by the line through the origin. Hence, a different approach to the problem of permeability seems to be advisable, starting at the other end of the Reynolds number scale—that is, with the dynamic forces.

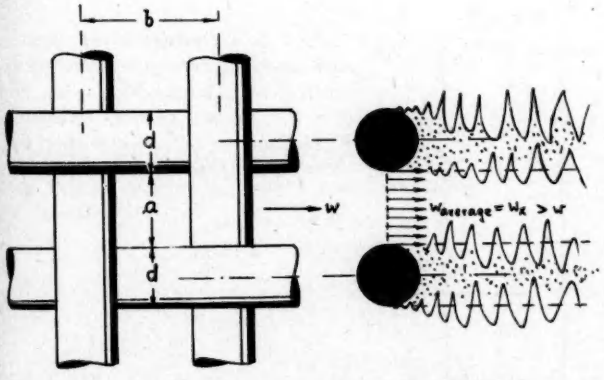

FIG. 1. *Geometry and flow pattern of screens and simple fabrics.*

Dynamic Losses

At sufficiently high Reynolds numbers, the flow passes the forehalf of the cylindrical elements (Figure 1) up to their maximum thickness without major losses. The average velocity is increased from w to w_x. Downstream from the narrowest point of the opening, the flow separates from the surface of the cylinders. Subdivided into many little jets, it discharges into the space behind the screen. This discharge, or, geometrically considered, the sudden expansion of the cross-sectional area, results in a loss of momentum, as derived by Borda and Carnot [1(*b*)]:

$$\zeta = \frac{\Delta p}{q} = \left(\frac{S_\bullet / S_\square}{1 - \frac{S_\bullet}{S_\square}} \right)^2 = \left(\frac{\varphi}{1 - \varphi} \right)^2. \qquad (5)$$

As shown in Figure 2, reasonable agreement between this theory and available experimental data is found at Reynolds numbers above $R_x = 10^3$ and for solidity ratios greater than $\varphi \approx 0.5$. Below the latter limit, the flow pattern past the cylindrical elements of screens or fabrics becomes more and more similar to that in free flow. An equation covering this kind of flow is plotted in Figure 2 for a basic drag coefficient of 1. Such low solidity ratios,

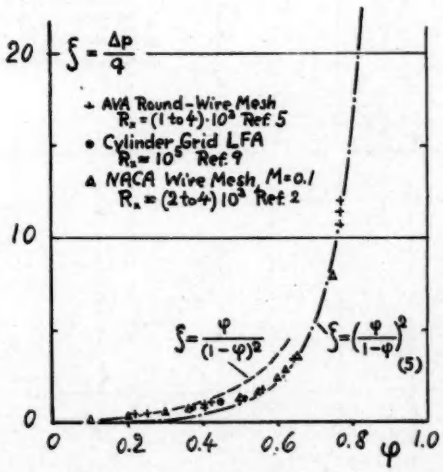

FIG. 2. *Dependence of pressure-loss coefficient of screens and fabrics upon solidity ratio.*

however, do not seem to be of much practical interest so far as fabrics are concerned.

Equation (5) applied for a solidity ratio $\varphi = 0.5$ is plotted in Figure 3 against Reynolds numbers between $R_x = 10^4$ and 10^5. At still higher Reynolds numbers, between 10^5 and 10^6, a critical drop of the pressure-loss coefficient may be expected—a drop which is analogous to that known for spheres and cylinders in free flow. In this case, the flow is no longer detached from the rear of the cylindrical elements. No experimental data are available, however, in this range; and it is not likely that these high Reynolds numbers will ever be encountered during the practical application of screens or fabrics.

Friction Losses

The application of fabrics in the field of parachutes involves Reynolds numbers which are below the purely dynamic range. Additional viscous or friction losses must therefore be considered. In the following paragraphs an attempt is made to derive these losses from basic skin-friction principles.

Considering the cylindrical elements of screens or fabrics at low Reynolds numbers, their drag (or pressure loss) is assumed to be proportional to the "wetted" surface area, the average dynamic pressure of the air flow prevailing through the openings, and the proper skin-friction drag coefficient [1(*c*)]. Since the wetted-area ratio is approximately

$$\frac{S_{\text{wet}}}{S_\square} \sim \frac{S_\bullet}{S_\square} = \varphi, \tag{6}$$

it is suitable to present the pressure loss in the form of a drag coefficient similar to those employed in conventional free-flow aerodynamics:

$$C_{Dx\bullet} = \frac{D}{q_x S_\bullet} = \frac{\Delta p}{q_x \varphi}, \tag{7}$$

where $q_x = 0.5\rho w_x^2$ denotes the average dynamic pressure of the flow through the narrowest cross section of the openings, and $D = S_\square \Delta p$ is the drag force. Introducing the pressure-loss coefficient, according to equation (1):

$$C_{Dx\bullet} = \frac{q/q_x}{\varphi}\zeta = \frac{(1-\varphi)^2}{\varphi}\zeta, \tag{8}$$

where $(1 - \varphi)$ indicates the porosity of the material. As can be found in engineering handbooks [1(*c*)], the viscous skin-friction drag coefficient of a plane wetted surface is

$$C_{f\,\text{viscous}} = \frac{D_{\text{viscous}}}{qS_{\text{wet}}} = \frac{5.33}{R_l}, \tag{9}$$

where R_l denotes the Reynolds number based on

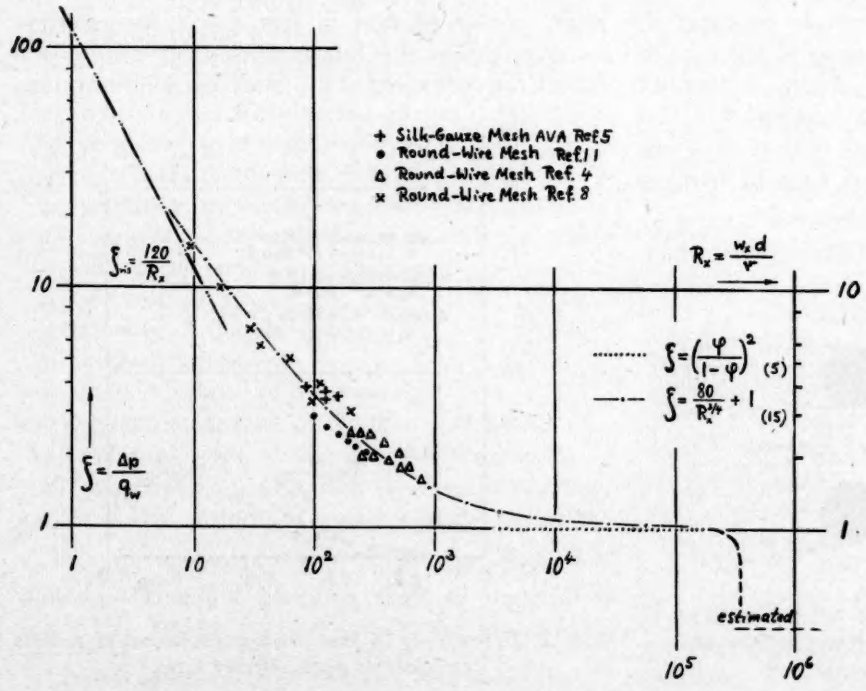

FIG. 3. *Dependence of pressure-loss coefficient of screens and fabrics with a solidity ratio of* $\varphi \approx 0.5$ *upon Reynolds number,* R_x (*equation (2)*), *according to theory and from experiments.*

the length, l, of the surface. Consequently,

$$C_{Dx\text{•viscous}} \sim C_{f\ \text{viscous}} \sim 1/R_x. \tag{10}$$

The constant required is found by extrapolating the experimental data plotted in Figure 4 to the range around $R_x = 1$:

$$C_{Dx\text{•viscous}} \approx 60/R_x. \tag{11}$$

This function, covering Reynolds numbers below $R_x \approx 10$, corresponds to the Hagen-Poiseuille law (equation (4)). Although this range of Reynolds number is not directly of interest so far as, for instance, parachute materials are concerned, it should be mentioned that the circular cylinder in free flow does not really obey a drag law corresponding to those of Poiseuille or Stokes. Lamb's theory (mentioned in [12]) predicts a slope of the drag-coefficient curve which is less negative than that shown in Figure 4, at Reynolds numbers below $R_x \approx 10$. Experiments [12] indicate, however, that the theoretical prediction is verified only if the flow space around the tested wires is extremely large. In the case of screens this is by no means the case. It is therefore assumed that the air flow through these screens adjusts itself, more or less, to the Poiseuille law, which means that their drag or loss coefficient varies with $1/R_x$.

The coefficient of dynamic loss (equation (1)) can also be converted into a drag coefficient:

$$C_{Dx\text{•dynamic}} = \varphi, \tag{12}$$

which is plotted in Figure 4 against Reynolds numbers around $R_x = 10^4$. Between this range of Reynolds number and $R_x \approx 1$ there is a wide region of transition in which the skin-friction drag coefficient approaches the laminar coefficient [1(c)]:

$$C_{f\ \text{laminar}} = \frac{1.33}{\sqrt{R_l}}. \tag{13}$$

The flow pattern changes here from the viscous type (without any flow separation) to that characterized by laminar flow separation. Expressing the experimental points, it was approximately found

$$C_{Dx\text{•friction}} \approx \frac{40}{R_x^{\frac{3}{4}}}. \tag{14}$$

The sum of equations (12) and (14) gives the total drag coefficient, as plotted in Figure 4. Usually, the solidity of fabrics is high (above 90%). The limiting curve for $\varphi \to 1$ gives, therefore, roughly the drag of fabrics as a unique function of the Reynolds number, R_x.

Permeability as a Function of Solidity

Combining equations (8), (12), and (14), the pressure-loss coefficient is

$$\zeta = \frac{\varphi}{(1-\varphi)^2}\left(\frac{40}{R_x^{\frac{3}{4}}} + \varphi\right). \tag{15}$$

This equation holds true between $R_x \approx 1$ (for all solidity ratios) and $R_x \approx 10^3$ (for solidity ratios $\varphi > 0.5$). According to Figure 5, the experimental points with $R_x = 10^2$ are well expressed by equation (15) beyond $\varphi \approx 0.5$. At lower solidity ratios, the conditions of free flow prevail. For $R_x = 10^3$, equation (15) gives values which are but slightly higher than those obtained from equation (5).

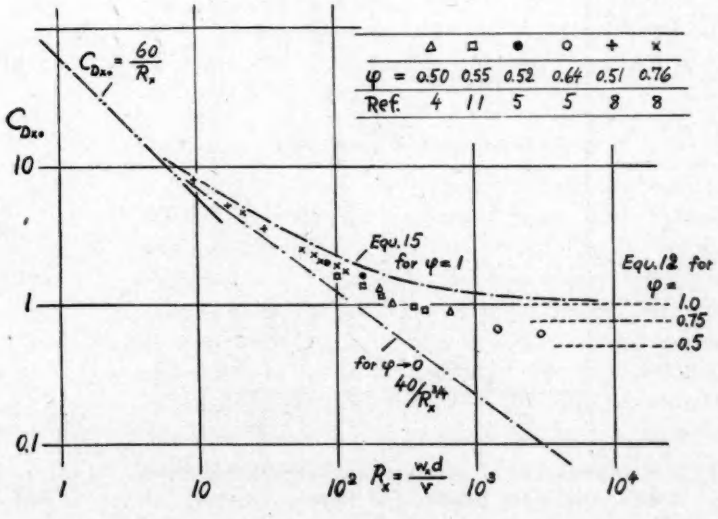

FIG. 4. *Drag coefficients of various screens and fabrics, according to theory and from experiments.*

At solidities $\varphi \to 1$, the pressure-loss coefficient is $\zeta \to \infty$. It therefore seems to be more convenient in this case to use the reversed parameter

$$1/\zeta = q/\Delta p. \qquad (16)$$

The experimental points plotted in Figure 6 show good agreement down to porosities $(1 - \varphi)$ close to zero $(\varphi \to 1)$. A number of fabrics included in the graph fit into the pattern if assuming an average Reynolds number $R_x \approx 2 \cdot 10^2$. The experiments [6, 8] were conducted on conventional fabric-testing machines. These machines draw air from the open space around the machine through the fabric to be tested. In doing this, an additional pressure differential, having a magnitude of $\Delta p = q$, is necessarily created in front of the material, due to the acceleration of the air from rest to w. This amount is of no practical importance, so far as highly solid fabrics are concerned, up to $w_{ASTM} \approx 400$. On the other hand, a material with $w_{ASTM} = 1{,}000$, which is equivalent to $\zeta = 8$, shows an inaccuracy of $\frac{1}{8} \approx 12\%$. The results obtained from such a testing machine can be corrected by subtracting $\Delta\zeta = 1$ from the measured ζ value; see equation (18). All of the experimental points in Figure 6, as far as applicable, are corrected according to this method.

Knowing the correlation between ζ and φ, or between $(1/\zeta)$ and $(1 - \varphi)$, it should be possible to estimate the geometric porosity of any material by measuring the aerodynamic permeability. Parachutes are an example where the discussed characteristics of fabrics are of practical interest. Considering a man-carrying parachute during steady descent, the load of the canopy corresponds to a pressure differential of the order of $\frac{1}{3}$ in. of water, which is near the origin of the graph in Figure 7. The maximum velocity within the openings of the material, corresponding to this pressure, is of the order of $w_x = 30$ ft./sec. Assuming a yarn diameter of the order of 0.01 in., the resulting Reynolds number is around $R_x = 200$. According to Figure 4, this is a region where about half of the pressure differential is due to dynamic losses and the other half is caused by friction within the openings. The permeability of such cloth corresponds to $w_{ASTM} \approx 150$ ft./min.; $\zeta = 300$ to 400; $q/\Delta p \approx 0.3\%$. The corresponding porosity $(1-\varphi)$ of the material is between 5% and 8%, as found from Figure 6. This example gives a general idea where practical cases are located in the various graphs. Of course, considering the opening phase

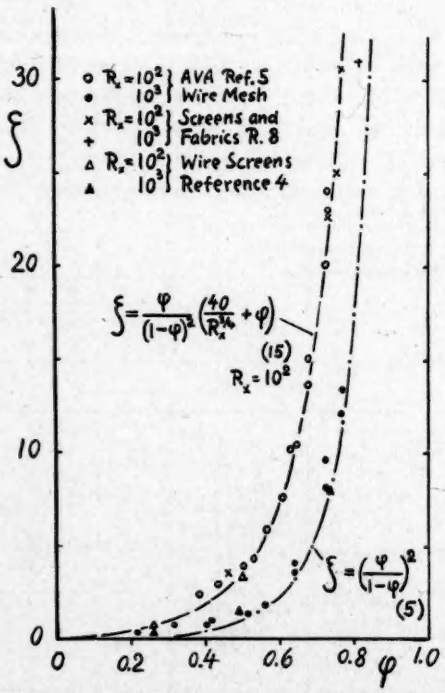

FIG. 5. *Dependence of pressure-loss coefficient of round-wire screens upon solidity and Reynolds number.*

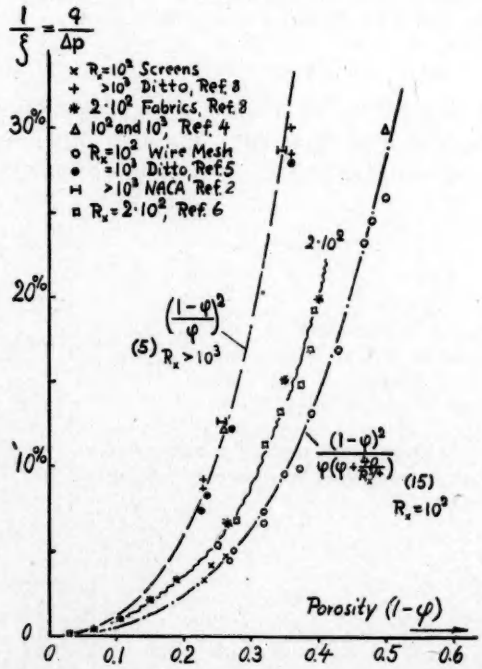

FIG. 6. *Dependence of the nondimensional permeability factor of screens and fabrics upon porosity ratio.*

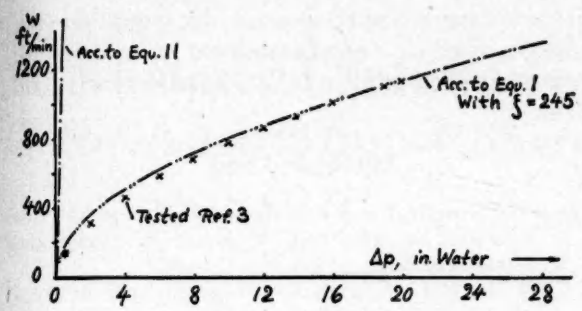

FIG. 7. *Dependence of the permeability,* w, *of a parachute material (with 2 × 47 threads per inch) upon the applied pressure differential,* Δp.

of a parachute, load and pressure differential are temporarily much higher than in the case mentioned here.

Method of Testing Materials

The permeability of fabrics is usually determined in a testing machine by measuring the air flow which passes through the material under a standard pressure differential. According to the American Society for Testing Materials the permeability is thus indicated by the average velocity

$$w_{\text{ASTM}} = \frac{Q(\text{ft.}^3/\text{min.})}{S\square(\text{ft.}^2)}, \tag{17}$$

given in ft./min. at a pressure differential equivalent to 0.5 in. of water. This velocity can easily be converted into a pressure-loss coefficient:

$$\zeta = \frac{8 \cdot 10^6}{w^2_{\text{ASTM}}} - 1, \tag{18}$$

which is correct only for the condition defined by $\Delta p = 0.5$ in. of water. In Great Britain the standard testing pressure is 10 in., and in Germany 16 mm. of water. The resulting permeability values are by no means nondimensional, and they are not comparable.

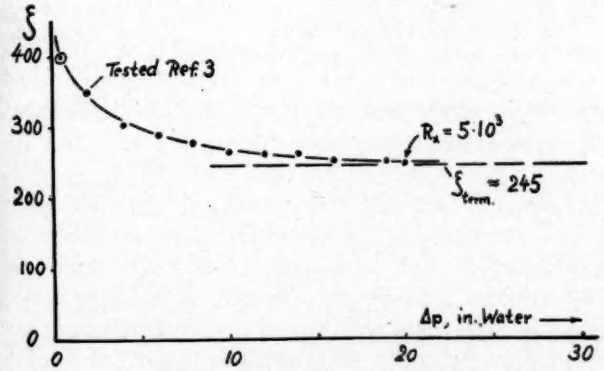

FIG. 8. *The loss coefficient,* ζ, *of the fabric used in Figure 7.*

As illustrated in Figure 7, the velocity, w, across an average parachute fabric varies approximately as the square root of the pressure differential, Δp. The viscous function (corresponding to equation (11)), which is also plotted in the graph, gives only the zero tangent of the permeability curve, at pressure values that are far below the range in which one is usually interested. The experimental points are relatively close to the theoretical curve corresponding to the constant terminal ζ value (at high Reynolds numbers). It thus seems reasonable to indicate the permeability of fabrics by the dimensionless pressure-loss coefficient, ζ. According to Figure 8, this coefficient decreases with the pressure differential, approaching a terminal value. ζ values at different pressure values vary in magnitude, but by no means as much as the velocity does if tested at different Δp values. If, for instance, $\Delta p = 10$ in. of water is used as a standard, the ζ value in Figure 8 is found to be close to the terminal level.

The reverse of the pressure-loss coefficient (equation (16), Figure 6) can be considered a permeability measure. This parameter indicates the dynamic pressure, q, of the flow passing through the material which is necessary to create the prevailing pressure differential, Δp:

$$\frac{100}{\zeta} = \left(\frac{q}{\Delta p}\right)^{\%} = \frac{w^2_{\text{ASTM}}}{80{,}000 - w^2_{\text{ASTM}}}. \tag{19}$$

This equation is only correct for conditions at $\Delta p = 0.5$ in. of water. An A.S.T.M. permeability of $w = 200$ ft./min., for example, yields a $q/\Delta p$ value of 0.5%.

Influence of Compressibility

Thus far, the aerodynamic characteristics of fabrics and similar materials have been treated without considering the compressibility of the air. According to Adler [2], the loss coefficient, ζ, increases steadily with the Mach number, $M = w/$(velocity of sound), up to a critical condition. Here the speed of sound is attained within the openings of the material, and there is no economical means to increase the rate of flow much further. Adler [2] gives this limit by

$$M_{\text{crit}} \approx 0.58(1 - \varphi), \tag{20}$$

which is valid for $\varphi > 0.6$ or 0.7, which covers most of the conventional fabrics. As an example, the critical speed for the cloth of Figures 7 and 8, with a porosity $(1 - \varphi) \approx 6\%$, is given by $M \approx 0.035$; $w_{crit} \approx 38$ ft./sec., or 2,300 ft./min. The material is theoretically bound to encounter this limiting status at a Δp corresponding to some 100 in. of water. The pressure-loss coefficient is increased to roughly twice the basic amount upon reaching M_{crit}. The critical condition of this material is consequently to be expected around $\Delta p = 200$ in. of water (provided that the material would withstand such a pressure). Assuming a parachute with an opening shock corresponding to 20 g, the pressure differential of the canopy material is of the order of $\Delta p = 30$ in. of water, which seems to be far from the expected critical limit. Other technical cases may exist, however, where the compressibility does affect the aerodynamics of fabrics.

Summary

The reader should be reminded that, due to the partly statistical methods of analyzing the available experimental data, some of the present conclusions are tentative and many are only approximate.

Contrary to previous treatments of the subject, the flow through screens, fabrics, and similar materials is considered in this paper chiefly from the dynamic (not the viscous) side of aerodynamics. Accounting for the dynamic losses behind the elements of the material, this part of the pressure loss across the material is readily derived (Figure 2).

The additional frictional losses of the flow across the material are found from a statistical analysis of the available experimental data. According to Figures 3, 5, and 6, it is possible to predict the pressure-loss coefficient as a function of geometrical solidity and the proper Reynolds number.

To the present author, the conventional method of measuring and quoting the permeability of fabrics is without much satisfying foundation. The pressure-loss coefficient (equation (1)) seems to be a better measure, and the reverse of it (equation (16)) could be used as a nondimensional parameter indicating the permeability of fabrics and other materials.

Literature Cited

1. (*a*) Theoretical and experimental data on the flow through nozzles can be found in engineering handbooks.
   (*b*) The Borda-Carnot loss of pressure can be found in the literature on diffusers.
   (*c*) Drag coefficients can be found in handbooks, such as Hoerner, "Aerodynamic Drag," 1951.
2. Adler, Variation with Mach Number of Static and Total Pressure Through Various Screens, *Natl. Advisory Comm. Aeronaut. Wartime Rept.* L-23 (1946).
3. Battles, Porosity Characteristics of Parachute Materials, *U. S. A. F. Air Materiel Command Tech. Rept.* 5665 (1948).
4. Eckert and Pflueger, Tests Concerning the Pressure Loss of Various Round-Wire Screens, *Luftfahrt-Forsch.* p. 142 (1941); *Trans. Natl. Advisory Comm. Aeronautics, Tech. Memo.*
5. Flachsbarth, "Drag of Various Screens," Vol. IV, Goettingen, Germany, Ergebnisse Aerodynamische Versuchsanstalt, 1932.
6. Longnecker, Air Flow Through Woven Materials, M.S. Thesis, Lowell Textile Institute, Lowell, Mass., June 1950.
7. Rainard, Air Permeability of Fabrics, TEXTILE RESEARCH JOURNAL **17**, 167 (1947).
8. Robertson, Air Porosity of Open-Weave Fabrics, TEXTILE RESEARCH JOURNAL **20**, 838 (1950).
9. Scholkemeier, Drag Tests on Various Dive-Brake Grids, German Rept. LFA Brunswick (Apr. 10, 1945) (available on loan from Central Air Documents Office, Wright Field, Dayton, Ohio).
10. Schubauer, Spangenberg, and Klebanoff, Aerodynamic Characteristics of Damping Screens, *Natl. Advisory Comm. Aeronaut. Tech. Note* 2001 (1950). (Generally, this source gives ζ values which are lower than from any other reference.)
11. Simmons and Cowdrey, Measurements of the Aerodynamic Forces Acting on Porous Screens, *Aeronaut. Research Comm.* (*England*) RM 2276 (1945).
12. White, *Proc. Roy. Soc.* (*London*), p. 472 (1946).

(*Manuscript received August 10, 1951.*)

A Numerical Solution of the Differential Equation for Adsorption-Controlled Diffusion in a Solid

Hiroshi Fujita*

Department of Fisheries, Faculty of Agriculture, Kyoto University, Maizuru, Japan

Introduction

The mathematical theory of the diffusion process in which an adsorbate diffuses into a porous solid and is adsorbed on the internal surface is of considerable significance in connection with investigations of such phenomena as the dyeing of fibers and the water uptake by high polymeric substances. The dyeing process has thus far been analyzed chiefly by applying the usual simple diffusion theory without taking the controlling effect of dye adsorption into consideration. However, it is probable that in some cases such a treatment of the problem leads to an unsatisfactory representation of given experimental facts, since, as would be expected from the term "dyeing," the diffusion of dye in a fiber should be more or less controlled by the internal adsorption. Few papers have appeared in the literature dealing with the mathematics of the adsorption-controlled diffusion, and many interesting and important problems still remain unresolved in the field of research on this subject.

In connection with the dyeing of fibers in a finite dye bath, Crank *et al.* [1, 2, 3] and Wilson [11] made a very important and excellent contribution to this subject with a detailed investigation of a case in which the rate of dye adsorption on the interior surface in a cylindrical fiber was defined by an isotherm of the Freundlich type. One of their mathematical solutions has been verified experimentally by Lindberg [5] on the sorption of HCl by a wool fiber. A general case of the process of diffusion with adsorption has recently been studied independently by Reese and Eyring [6] and by Katz, Kubu, and Wakelin [4] in relation to the chemical reaction occurring in a high polymer. They used an irreversible bimolecular kinetics for the adsorption process, and obtained approximate solutions with the assumption that diffusion proceeds more rapidly than adsorption. It is questionable, however, if their solutions are applicable to a more general case in which the rate of diffusion is of comparable order with that of adsorption. In order to check this point we must employ a system of nonlinear partial differential equations consisting of a material continuity equation and the kinetic relation mentioned above. The mathematical difficulty resulting from this set of equations has not as yet been resolved either analytically or numerically.

In the present paper an attempt is made to evaluate a numerical solution of this problem without making any particular assumptions such as were used by Reese and Eyring and by Katz *et al.*

Basic Equations

Regarding the dyeing of a fiber it would be desirable, from the practical point of view, to solve the case of a cylindrically shaped solid; however, since the procedure of calculating successive values of the desired solution is somewhat involved and tedious, we shall confine our interest here to the case of a flat plate. Accordingly, our solution is certainly of less practical interest, but it may be of some use in the sense that it provides a more correct form of the solution of the given problem than that which may be obtained with any particular assumptions such as were used by Katz *et al.*

Consider a homogeneous porous solid of plate-like shape immersed in a solution whose concentration is kept at a constant value, C_o, for the entire run. Adsorbate diffuses into the solid through its porous spaces and is adsorbed on the internal surface area. If the flat surface of the plate is large enough to justify the assumption that the flow of solution in the solid is unidimensional in the direction of its thickness, and if the diffusion coefficient of the adsorbate in the fluid phase of the void space

* Associate Professor of Applied Physics.

in the solid is assumed to be constant, the equation for material continuity has the form

$$\frac{\partial C}{\partial t} = D\frac{\partial^2 C}{\partial x^2} - \frac{1}{\alpha}\frac{\partial n}{\partial t}, \quad (1)$$

where C is the adsorbate concentration in the liquid phase, n is the amount of adsorbate taken up on the interior surface area per unit apparent volume of the solid, α is the porosity of the solid (assumed to be constant), D is the diffusion coefficient, x is the space coordinate (as shown in Figure 1), and t is the time. The boundaries of the plate are represented by $x = \pm X$.

Next, in accordance with the Katz-Kubu-Wakelin treatment [4], we assume for the rate of adsorption of diffusing material the following bimolecular kinetics:

$$\frac{\partial n}{\partial t} = kC(N - n), \quad (2)$$

where k is the rate constant and N is the saturation value of n.

Equations (1) and (2) constitute a system of partial differential equations determining C and n as functions of space, x, and time, t, and are the fundamental relations of the present study. Because of its nonlinearity, it is very difficult to solve this set of equations by means of the known procedures in mathematical analysis, and, in fact, this analytical difficulty appears to be insuperable at present. In the Katz-Kubu-Wakelin treatment, as cited in the Introduction, the term $\frac{1}{\alpha}\frac{\partial n}{\partial t}$ in the right-hand side of equation (1) is neglected in comparison with the term $D\frac{\partial^2 C}{\partial x^2}$. This neglect is physically equivalent to assuming that diffusion is rapid but of finite duration in comparison with the rate of adsorption. Thus, in this approximation, equation (1) is substituted by

$$\frac{\partial C}{\partial t} = D\frac{\partial^2 C}{\partial x^2}, \quad (3)$$

which is a familiar diffusion equation the analytic solution of which may be obtained readily by referring to textbooks on heat conduction theory. Substitution of such a solution into equation (2) and integration of the resultant equation give immediately the solution of n. This is the outline of the Katz-Kubu-Wakelin method of solution of the problem. In a later part of the present paper (p. 284) an application of this method to the case

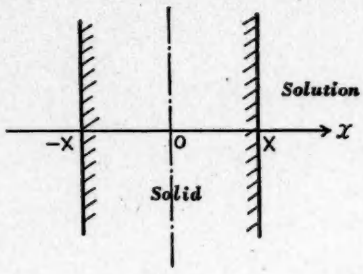

FIG. 1

under consideration is made, and the solution obtained is compared with our numerical solution in order to test the validity of the approximation involved in this method.

The initial and boundary conditions which allow a unique determination of the solutions for C and n are taken here as follows. The initial condition is that the solid contains no adsorbate at the beginning—namely,

$$C(x, 0) = 0, n(x, 0) = 0 \quad (-X < x < X). \quad (4)$$

The boundary condition* is as follows:

$$C(X, t) = C(-X, t) = \gamma C_o \quad (t > 0), \quad (5)$$

where γ is a partition function for the distribution of the adsorbate between the two phases at the boundaries of the plate.

Numerical Solution

In order to carry out the numerical integration of the given set of equations under conditions (4) and (5), it is convenient to introduce the following nondimensional variables:

$$\frac{x}{X} = z, \frac{tD}{X^2} = \tau; \frac{C}{C_o\gamma} = \varphi,$$

$$1 - \frac{n}{N} = \psi; \frac{\gamma k C_o X^2}{D} = \epsilon, \frac{N}{C_o\gamma\alpha} = \beta.$$

Then, equations (1), (2), (4), and (5) reduce to dimensionless forms as follows:

$$\frac{\partial \varphi}{\partial \tau} = \frac{\partial^2 \varphi}{\partial z^2} + \beta\frac{\partial \psi}{\partial \tau}, \quad (6)$$

$$\frac{\partial \psi}{\partial \tau} = -\epsilon\varphi\psi; \quad (7)$$

$$\varphi(z, 0) = 0, \psi(z, 0) = 1 \quad (-1 < z < 1), \quad (8)$$

$$\varphi(1, \tau) = \varphi(-1, \tau) = 0 \quad (\tau > 0). \quad (9)$$

* The author wishes to thank Dr. S. M. Katz for his invaluable suggestion regarding this condition.

Equation (3) is written as follows:

$$\frac{\partial \varphi}{\partial \tau} = \frac{\partial^2 \varphi}{\partial z^2}. \tag{10}$$

It will be seen at once that the essential parameters of the problem are ϵ and β, the physical meanings of which are evident enough to require no particular explanations.

At present, a considerable number of ways in which any partial differential equation of the diffusion type may be replaced by a finite difference equation are known, but in the present study use is made of Takahashi's method [7] for equation (6) since this is sufficiently accurate for our purposes and is familiar to Japanese researchers.

According to Takahashi's method, equation (6) may be replaced approximately by the finite difference equation of the form

$$\varphi(z, \tau + \lambda) = \frac{1}{2s}\int_{-s}^{s} \varphi(z + \xi, \tau)d\xi + \beta\lambda \frac{\partial \psi}{\partial \tau}, \tag{11}$$

where s is the length of the small and equal subdivisions of the given range of z, $-1 < z < 1$, and λ is a small quantity defined by

$$\lambda = \frac{s^2}{6}. \tag{12}$$

The accuracy of the above replacement has been investigated in detail by Watanabe [10], who has shown that this replacement introduces an error of the order of s^6. Therefore, if the magnitude of s is moderately small, equation (11) will give a solution that is sufficiently accurate for practical purposes.

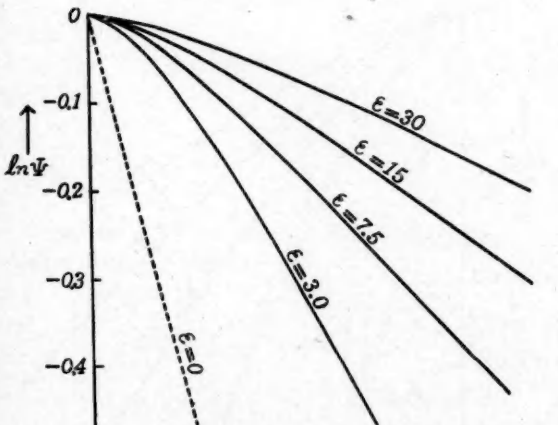

FIG. 2. *Relation between ln Ψ and* kC_0t *obtained by the numerical solution.*

Combining equation (11) with equation (7) gives

$$\varphi(z, \tau + \lambda) = \frac{1}{2s}\int_{-s}^{s} \varphi(z + \xi, \tau)d\xi - \beta\epsilon\lambda\varphi(z, \tau)\cdot\psi(z, \tau), \tag{13}$$

which, if the integral is evaluated by means of Simpson's one-third rule, becomes

$$\varphi(z, \tau + \lambda) = \tfrac{1}{6}[\varphi(z + s, \tau) + 4\varphi(z, \tau) + \varphi(z - s, \tau)] - \beta\epsilon\lambda\varphi(z, \tau)\cdot\psi(z, \tau). \tag{14}$$

Next, replacing the differentiation with respect to τ in equation (7) by the usual difference formula, there results

$$\psi(z, \tau + \lambda) = \psi(z, \tau)[1 - \epsilon\lambda\varphi(z, \tau)]. \tag{15}$$

This equation involves an error of the order of λ^2 or s^4, so that it is less accurate in comparison with equation (14), although equation (14) is itself less accurate than equation (13) by an order of s since Simpson's one-third rule has introduced an error of the order of s^5 in equation (14).

At the boundaries of the plate, $z = \pm 1$, by virtue of equation (9), equation (7) takes the form:

$$\frac{\partial \psi}{\partial \tau} = -\epsilon\psi,$$

which can be integrated to give

$$\psi = \exp(-\epsilon\tau). \tag{16}$$

Hence, recourse to equation (15) is unnecessary in calculating the boundary values of ψ.

In the Katz-Kubu-Wakelin approximation, which is discussed in the following section, the parameter β does not appear in the mathematical treatment of the problem; only the parameter ϵ is essential to their solution. Therefore, for our purpose, which is to examine the validity of the approximation involved in the Katz-Kubu-Wakelin method by the numerical solution of the difference equations derived above, it is preferable to carry out the numerical integration in a scheme in which ϵ is varied and β is fixed. Thus, a number of numerical solutions subjected to the conditions that $\beta = 1.0$ and $\epsilon = 0$, 3.0, 7.5, 15, and 30 have been computed by taking the value of 0.2 for s. This value of s is that usually adopted in applying Takahashi's method to practical problems, but it may be somewhat too large to obtain a considerably precise

result. A discussion on this subject will be made in a separate publication by the present author.

In order to compare the numerical solutions thus obtained with the corresponding approximate solutions determined by the Katz-Kubu-Wakelin method, it is convenient to give the results in a plot in which ln Ψ is represented as a function of $kC_o t$, where Ψ is defined as

$$\Psi = \int_o^1 \psi dz,$$

and $\gamma = 1$. The assumption that $\gamma = 1$ is physically equivalent to the condition that no film resistance to material transfer exists at the interface between the solid and the solution. Figure 2 shows our numerical results in the form of such a plot. Here, the dotted line corresponding to $\epsilon = 0$ is a representation of $\ln \Psi = -kC_o t$, which can be obtained without recourse to the finite difference method described above.

Approximate Solution Based on the Katz-Kubu-Wakelin Treatment

In the Katz-Kubu-Wakelin treatment of the present problem, equation (10) must first be solved for the conditions (8) and (9). This is a standard problem in the theory of heat conduction, and the desired solution may be obtained readily as follows:

$$\varphi = 1 - 2\sum_{n=0}^{\infty} \frac{(-1)^n}{\alpha_n} e^{-\alpha_n^2 \tau} \cos \alpha_n z, \qquad (17)$$

where

$$\alpha_n = \frac{(2n+1)\pi}{2}.$$

Substituting this solution into equation (7) and integrating, there results

$$\psi = \exp\left[-\epsilon\tau + 2\epsilon \sum_{n=0}^{\infty} \frac{(-1)^n}{\alpha_n^3} \times (1 - e^{-\alpha_n^2 \tau}) \cdot \cos \alpha_n z\right], \qquad (18)$$

whence it follows that

$$\Psi = e^{-\epsilon\tau} \int_o^1 \times \exp\left[2\epsilon \sum_{n=0}^{\infty} \frac{(-1)^n}{\alpha_n^3} (1 - e^{-\alpha_n^2 \tau}) \cdot \cos \alpha_n z\right] dz, \qquad (19)$$

which may be written as

$$\ln \Psi = -\epsilon\tau + \ln G, \qquad (20)$$

where

$$G = \int_o^1 \times \exp\left[2\epsilon \sum_{n=0}^{\infty} \frac{(-1)^n}{\alpha_n^3} (1 - e^{-\alpha_n^2 \tau}) \cdot \cos \alpha_n z\right] dz. \qquad (21)$$

From equations (20) and (21) the plot of ln Ψ as a function of $kC_o t$ can be computed for any value of ϵ, assuming, as before, that $\gamma = 1$. It should be noted that, as has been mentioned previously, the parameter β is not introduced in the solutions for φ and ψ.

It is seen that for large values of τ the computation of G is made without any special difficulty, whereas, for relatively small values of τ less than, for example, 0.1, it involves a considerable amount of labor because of the slow convergence of the infinite series in equation (21). To avoid this difficulty it is convenient to transform the infinite series to an alternative form which admits of rapid and accurate evaluation at the small values of τ mentioned above.

To obtain the necessary form we put

$$J \equiv \sum_{n=0}^{\infty} \frac{2(-1)^n}{(2n+1)\pi} \times \exp\left(-\frac{(2n+1)^2\pi^2}{4}\tau\right) \cdot \cos\left(\frac{(2n+1)\pi}{2} z\right),$$

$$q \equiv \exp(-\pi^2\tau), \quad \xi \equiv \frac{z}{2}.$$

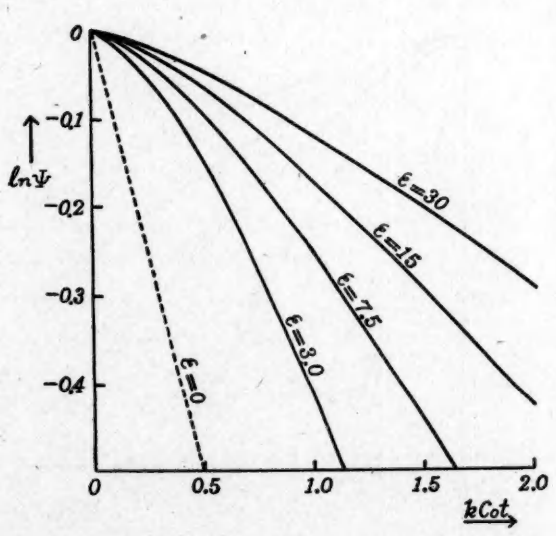

FIG. 3. *Relation between ln Ψ and $kC_o t$ obtained by the approximate solution.*

J thus defined is then written in the form

$$J = \sum_{n=0}^{\infty} \frac{2(-1)^n}{(2n+1)\pi} \cdot q^{(n+\frac{1}{2})^2} \cdot \cos(2n+1)\pi\xi. \quad (22)$$

Making use of the definition formula of $\vartheta_1(\xi, q)$, one of the *theta* functions whose parameter is q, as in [8]:

$$\vartheta_1(\xi, q) = 2 \sum_{n=0}^{\infty} (-1)^n q^{(n+\frac{1}{2})^2} \sin(2n+1)\pi\xi,$$

equation (22) may be written as

$$J = \int_{z/2}^{\frac{1}{2}} \vartheta_1(\xi, q) d\xi. \quad (23)$$

When the value of τ is very small the value of q is very near unity; in such a case, therefore, the q-expansion formula for $\vartheta_1(\xi, q)$ is evidently of no use for computation of it because of the slow convergence of the series. However, with the aid of Jacobi's imaginary transformations [9] the ϑ functions can be transformed to different series forms which converge more quickly as q approaches unity. Making use of one of these transformations, $\vartheta_1(\xi, q)$ is put in the form

$$\vartheta_1(\xi, q) = \frac{2}{\sqrt{\pi\tau}} e^{-\frac{\xi^2}{\tau}} \sum_{n=0}^{\infty} (-1)^n \times \exp\left(-\frac{(2n+1)^2}{4\tau}\right) \cdot \sinh\frac{(2n+1)\xi}{\tau}. \quad (24)$$

It will be seen that the series in this form is certainly suitable for the requirement noted above. In fact, if we are interested only in such an interval as $0 < \tau < 0.1$, and if we recall that z is limited in the range where $-1 < z < 1$, equation (24) may be simplified further, within an accuracy of the order of e^{-10}, to

$$\vartheta_1(\xi, q) = \frac{1}{\sqrt{\pi\tau}} \left[e^{-\frac{1}{\tau}\left(\frac{1}{2}-\xi\right)^2} - e^{-\frac{1}{\tau}\left(\frac{1}{2}+\xi\right)^2} \right]. \quad (25)$$

On inserting this expression into equation (23) and integrating, we obtain

$$J = \frac{1}{2}\left[\Phi\left(\frac{1-z}{2\sqrt{\tau}}\right) + \Phi\left(\frac{1+z}{2\sqrt{\tau}}\right) - \Phi\left(\frac{1}{\sqrt{\tau}}\right) \right], \quad (26)$$

where $\Phi(\mu)$ is the error function, defined as

$$\Phi(\mu) = \frac{2}{\sqrt{\pi}} \int_o^{\mu} e^{-\mu^2} d\mu.$$

In this way, so far as the interval of τ is concerned, the form of G may be replaced with sufficient accuracy by the following:

$$G = \int_o^1 \exp\left\{ \epsilon \int_o^{\tau} \left[\Phi\left(\frac{1-z}{2\sqrt{\tau}}\right) + \Phi\left(\frac{1+z}{2\sqrt{\tau}}\right) - \Phi\left(\frac{1}{\sqrt{\tau}}\right) \right] d\tau \right\} dz. \quad (27)$$

Here, the integral with respect to τ can be evaluated exactly in terms of known functions to give

$$\tau \left[\Phi(\theta)(1+2\theta^2) + \Phi(\theta')(1+2\theta'^2) - \Phi(\theta'')(1+2\theta''^2) - 2(\theta^2 + \theta'^2 - \theta''^2) + \frac{2}{\sqrt{\pi}} (\theta e^{-\theta^2} + \theta' e^{-\theta'^2} - \theta'' e^{-\theta''^2}) \right], \quad (28)$$

where

$$\theta = \frac{1-z}{2\sqrt{\tau}}, \quad \theta' = \frac{1+z}{2\sqrt{\tau}}, \quad \theta'' = \frac{1}{\sqrt{\tau}}.$$

The form thus derived, although it is somewhat involved, is free from the difficulty of convergence of the infinite series.

By the proper use of equations (20), (21), (27), and (28) the numerical calculation was carried out for the same cases of ϵ as were considered in the previous section concerning the numerical integration of the finite difference equations; the results obtained are plotted in Figure 3 as the relation between $\ln \Psi$ and $kC_o t$.

Discussion

It is now possible to compare our numerical solutions with the corresponding approximate

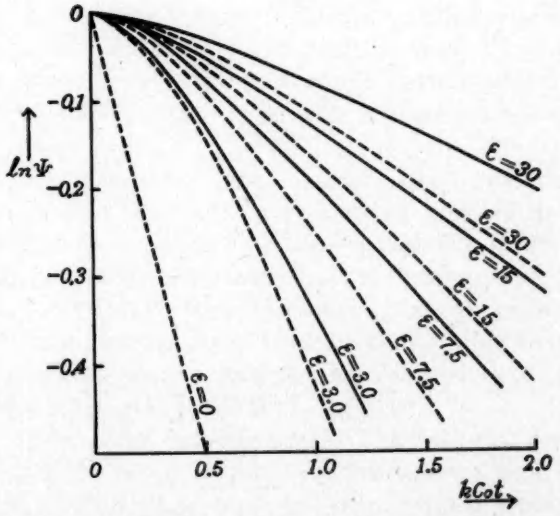

FIG. 4. *Comparison of the numerical and the approximate solutions with respect to the plot of ln Ψ against* $kC_o t$. ——, *numerical solution;* – – –, *approximate solution.*

solutions with regard to the plot of ln Ψ and $kC_s t$. For this purpose the plots shown in Figures 2 and 3 are presented together in Figure 4. Comparison of these two families of curves indicates the degree of accuracy or the validity of the approximate solution for ψ determined by using the Katz-Kubu-Wakelin method of solution. It appears that the approximate solution becomes useless even for practical purposes with increasing values of ϵ and time. However, it is considered that, since our numerical solutions were evaluated with a rather specified condition that $\beta = 1$* and with a relatively large magnitude of the space increment—that is, $s = 0.2$—there may be some doubt about this conclusion. Indeed, this statement is true to some extent, as will be illustrated in a subsequent paper in which a numerical integration similar to that made in the present paper will be repeated by taking a smaller value of s to improve the accuracy of the present solutions. However, even with this improvement the only change introduced in Figure 4 is a slight approach of the solid curves to the corresponding dotted curves; thus, it may be inferred that the estimation of the degree of accuracy of the Katz-Kubu-Wakelin method as might be made roughly from Figure 4 would not be far from the truth.

* As is easily understood from the analysis developed above, the approximate solution by the Katz-Kubu-Wakelin treatment reduces to the exact solution of the problem in the limit when $\beta \to 0$. Therefore, it may be considered that the deviations of the approximate solutions from the corresponding exact ones shown in Figure 4 are essentially due to the finiteness of β.

Acknowledgment

The author wishes to express his sincere thanks to Professor Neal R. Amundson of the University of Minnesota and to Dr. Sidney M. Katz of E. I. du Pont de Nemours & Company for their kind assistance. Acknowledgment is also due to Mr. Akira Kishimoto of our department for his help in making the numerical computations.

Literature Cited

1. Crank, J., *Phil. Mag.* **39**, 140 (1948).
2. Crank, J., *Phil. Mag.* **39**, 362 (1948).
3. Crank, J., and Godson, S. M., *Phil. Mag.* **38**, 794 (1947).
4. Katz, S. M., Kubu, E. T., and Wakelin, J. H., TEXTILE RESEARCH JOURNAL **20**, 754 (1950).
5. Lindberg, J., TEXTILE RESEARCH JOURNAL **20**, 381 (1950).
6. Reese, C. E., and Eyring, H., TEXTILE RESEARCH JOURNAL **20**, 743 (1950).
7. Takahashi, Y., *J. Meteorol. Soc. Japan* **19**, 321 (1941).
8. Tomotika, S., "Theory of Elliptic Functions," Tokyo, Kawade Book Co., 1942, p. 131.
9. Tomotika, S., "Theory of Elliptic Functions," Tokyo, Kawade Book Co., 1942, p. 170.
10. Watanabe, N., *Misc. Repts. Faculty Eng. Kyushu Univ.* **21**, 43 (1949).
11. Wilson, A. H., *Phil. Mag.* **39**, 48 (1948).

(Manuscript received January 28, 1952.)

Letters to the Editor

Short communications in the form of Letters to the Editor are intended to provide prompt publication of significant new research results and to permit an exchange of views on papers previously published in the Journal. These communications are not submitted to formal review as are research papers, and the editors do not assume any share of the author's responsibility for the information given or the opinions expressed. When work previously published in the Journal is the subject of critical comment, the authors of the original paper are given an opportunity to submit a reply, which will be published concurrently when possible.

The Use of Density Gradient Columns for the Determination of Specific Gravity

American Enka Corporation
Research Department
Enka, North Carolina
January 31, 1952

To the Editor
Textile Research Journal

Dear Sir:

Over the past 15 years there have appeared a number of references to the use of "density gradient columns" for the determination of specific gravity of a variety of substances, including textile fibers. *Inter alia,* see Hermans and Vermaas; Boyer, Spencer, and Wiley; Tessler, Woodberry, and Mark (*J. Polymer Sci.* **1**, 156, 249, 437 (1946)); Preston and Nimkar (*J. Textile Inst.* **41**, T446 (1950)); and Stock and Scofield (Textile Research Journal **21**, 521 (1951)). These authors attribute first use of such a column to K. Linderstrom-Lang (*Nature* **139**, 713 (1937)).

Your historically-minded readers may be interested in a similar, but much earlier, application of this principle, antedating Dr. Linderstrom-Lang's note by almost 300 years. The reference is found in Galileo's great work *Dialogues Concerning Two New Sciences,* first published at Leyden, Holland, in 1638 by the Elzevier Press (which press, it may be noted, continues to this day to publish outstanding scientific works). Two of the three participants in the *Dialogues* are Salviati, who speaks for Galileo himself, and Sagredo, an eager and intelligent follower. On pages 69 and 70 of the Crew and de Salvio translation (Northwestern University Press, Chicago, 1939), we find the following paragraphs:

"Sagredo. By means of another device I was able to deceive some friends to whom I had boasted that I could make up a ball of wax that would be in equilibrium in water. In the bottom of a vessel I placed some salt water and upon this some fresh water; then I showed them that the ball stopped in the middle of the water, and that, when pushed to the bottom or lifted to the top, would not remain in either of these places but would return to the middle.

"Salviati. This experiment is not without usefulness. For when physicians are testing the various qualities of waters, especially their specific gravities, they employ a ball of this kind so adjusted that, in certain water, it will neither rise nor fall. Then in testing another water, differing ever so slightly in specific gravity, the ball will sink if this water be lighter and rise if it be heavier. . . . I wish to add that this notable difference in specific gravity can be produced not only by solution of some heavier substance, but also by merely heating or cooling; and so sensitive is water to this process that by simply adding four drops of another water which is slightly warmer or cooler . . . one can cause the ball to sink or rise."

Thus, not only did the "Tuscan Artist" anticipate in principle Dr. Linderstrom-Lang's very useful and interesting invention; he also anticipated another modern sensitive technique for determining the specific gravity of a body by changing the temperature of the suspending liquid until the body neither sinks nor floats (see, for example, Randall and Longtin, *Anal. Chem.* **11**, 44 (1939)).

Truly, as the Preacher wrote, "The thing that hath been is that which shall be; and that which is done is that which shall be done: and there is no new thing under the sun."

Charles H. Lindsley

The Low-Angle Scattering of X-Rays by Conifer Tracheids

COMMONWEALTH SCIENTIFIC AND INDUSTRIAL RESEARCH ORGANIZATION,
DIVISION OF FOREST PRODUCTS
South Melbourne, Australia
February 4, 1952

To the Editor
TEXTILE RESEARCH JOURNAL

Dear Sir:

Following the theoretical work of Kratky [7], the low-angle scattering of a number of textile fibers has been studied in a series of investigations by Heyn [3, 4], in which it was demonstrated that the low-angle diagram provides a means of determining the micellar angle—*i.e.*, the angle between the mean direction of micellar orientation and the major cell axis—as well as the average distance separating the micelles. In view of this work it is of interest that the low-angle scattering diagram of wood presents certain features not present in those of other fibers studied by Heyn, and provides further information concerning the submicroscopic organization of the walls of the component cells.

In the present study, the "low"- and "wide"-angle diffraction diagrams of wood specimens taken from successive growth rings of a cross section of a stem of *Pinus taeda* L. were examined. Similar results were obtained with *Pinus radiata* D.Don. This material is particularly suitable for study of the influence of changes in the submicroscopic cell wall organization upon the x-ray diagram because in successive growth rings from the stem center the average length of the tracheids increases [15] and, as shown by Preston [9, 12], the micellar angle, θ, for the layer *S2* (Figure 5) decreases. It is also probable that a similar change in micellar angle with cell length also occurs in layer *S1* [14]. In the primary wall, *P* (Figure 5), the micellar orientation is constant irrespective of the tracheid length [11, 13].

The specimens, taken from selected growth rings, were examined with the x-ray beam oriented with respect to the specimen in the following directions (see Figure 1): (*a*) perpendicular to the cell length and perpendicular to the tangential walls of the cells; (*b*) perpendicular to the cell length and perpendicular to the radial walls of the cells; (*c*) perpendicular to the cell length and in a direction diagonal with respect to the radial and tangential walls.

In Figure 2 (*a–c, f–h*), both the wide-angle and the low-angle diagrams are shown for the second growth ring in the three directions (*a*), (*b*), and (*c*), respectively, of Figure 1. The wide-angle and low-angle diagrams for a specimen from ring 11 for the direction (*a*) (Figure 1) is shown in Figures 2(*e*) and 2(*j*), respectively. The diagrams for the directions (*b*) and (*c*) are not reproduced in Figure 2 because they were essentially similar to that for direction (*a*). In Figure 3(*a–e*), the low-angle diagrams for specimens from growth rings 2, 4, 7, 9, and 11, with the beam oriented in direction (*c*) (Figure 1), are shown.

In his survey of the low-angle scattering of a variety of native cellulose fibers, Heyn [3] observed two types of diagrams (shown diagrammatically in Figure 4). From fibers with a large micellar angle a "cross type" of diagram was obtained (Figure 4(*a*)), whereas in fibers with a small micellar angle a pronounced equatorial streak was observed (Figure 4(*b*)). Intermediate types of diagrams were observed in other fibers.

In the series of specimens taken from successive growth rings of *Pinus taeda,* the wood from the second growth ring gave a scattering diagram in which the equatorial cross observed by Heyn in other fibers is apparent (Figure 3(*a*)). In the wood from the fourth growth ring the two arms of the cross are seen to be nearer the equator (Figure 3(*b*)); this becomes progressively more apparent through subsequent rings until in the eleventh growth ring the two

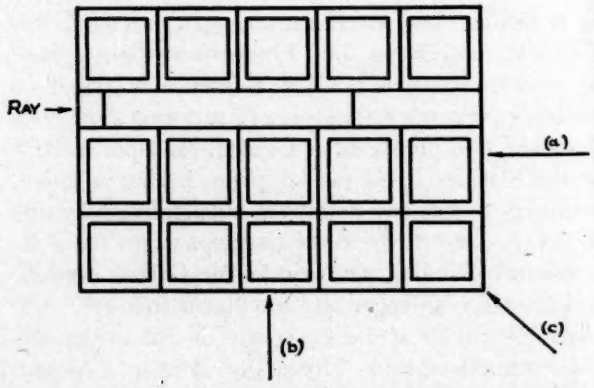

FIG. 1. *Diagrammatic representation of a transverse section of wood from a conifer stem, showing the orientation of the x-ray beam with respect to the specimen. A number of tracheids are shown in transverse section.*

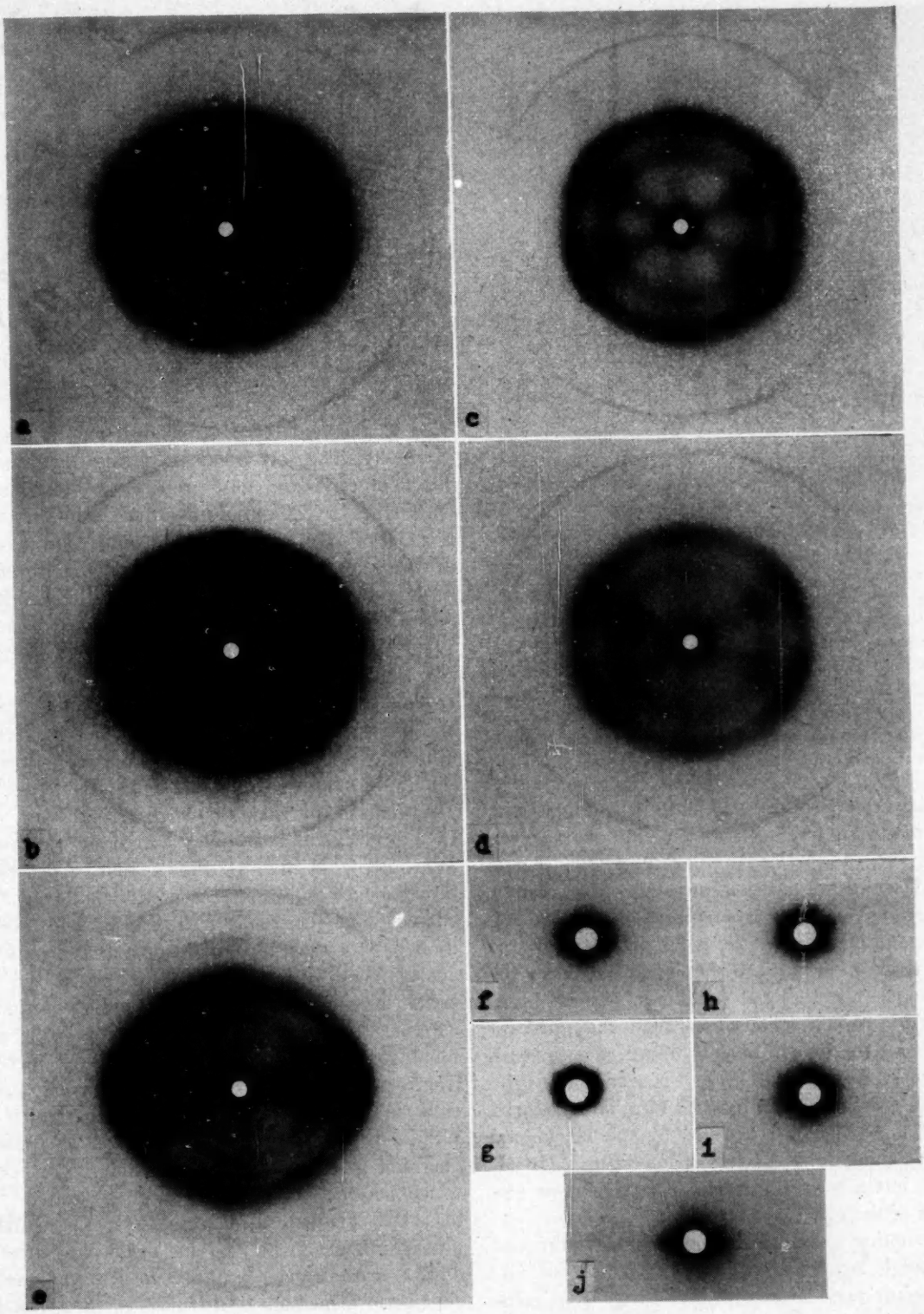

FIG. 2. *X-ray diffraction diagrams of wood from* Pinus taeda. *For wide-angle diagrams* (a–e), *specimen-film distance = 4.0 cm.; for low-angle diagrams* (f–j), *specimen-film distance = 10.22 cm. NiK$_\alpha$ radiation.*

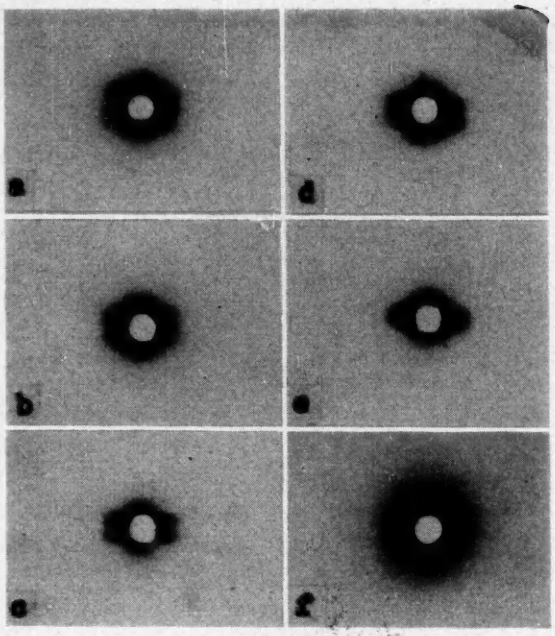

FIG. 3. a–e—*Low-angle x-ray diagrams of wood from different growth rings of* Pinus taeda. *Specimen-film distance = 10.22 cm. NiK_α radiation.* a—*Ring 2; average tracheid length, 2.4 mm.* b—*Ring 4; average tracheid length, 3.2 mm.* c—*Ring 7; average tracheid length, 3.8 mm.* d—*Ring 9; average tracheid length, 4.2 mm.* e—*Ring 11; average tracheid length, 4.4 mm.* f—*Low-angle x-ray diagram of a block of conifer cambium* (Larix *sp.*).

equatorial arms have merged to form a single equatorial streak (Figure 3(*c–e*)). In addition, however, the diagrams of wood showed features, apparent in Figure 3, which are not present in low-angle scattering diagrams of the fibers studied by Heyn [3]. Thus, in the diagram of the wood from the second growth ring, in addition to the equatorial cross discussed above, a meridional streak was present (Figure 3(*a*)). When followed through the series of diagrams for the fourth, seventh, ninth, and eleventh growth rings (Figure 3(*b–e*)), it is seen that, as the equatorial cross gradually fuses to form an equatorial streak, this change is paralleled by the meridional streak becoming progressively more diffuse. In all cases the intensity of the meridional streak was less than that of the equatorial streak.

In attempting an interpretation of these features of the low-angle scattering diagrams of wood, the following points may be considered: First, from combined optical and wide-angle x-ray studies of conifer tracheids, it has been established [16] that the middle layer, *S2* (Figure 5), makes the major contribution to the x-ray diagram, and can be considered to give

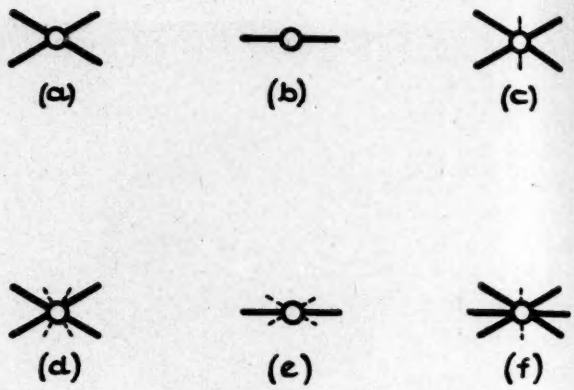

FIG. 4. *Types of low-angle scattering diagrams observed in native cellulose fibers.*

rise to the equatorial streaks shown in Figure 3. Secondly, the low-angle scattering diagram of a block of cambium cells, prepared as described previously [11, 13], is only a diffuse halo surrounding the central spot (Figure 3(*f*)). This is in agreement with earlier x-ray diffraction studies of cambium at wide angles [11, 13]. It is therefore concluded that the meridional streaks (Figure 3) arise from the outer and inner layers of the secondary wall (*S1* and *S3*, Figure 5).

This interpretation is supported by the fact that the intensity of the meridional streaks as compared with the equatorial streaks is greater in low-angle diagrams of early wood, in which the layer *S2* is thin, than in late wood, in which *S2* is thicker. Also, in a previous optical investigation by Preston and Wardrop [14] it was shown that a decrease in birefringence in transverse section of layer *S1* occurred with increasing cell length, and this was thought to reflect a decrease in micellar angle. By analogy with the changes occurring in the equatorial streaks with changing micellar orientation (Figure 3), the increasing diffuseness of the meridional streak in diagrams from cells of increasing length might be interpreted as shown diagrammatically in Figure 4 (*c*, *d*, and *e*), in which it is supposed that the single meridional streak present in diagrams from short cells is resolved into two streaks which become progressively more separated. That these two streaks are not resolved in the actual diagrams (Figure 3) may be due to masking effects by diffuse scattering by nonoriented cell wall constituents, or to dispersion of the micelles about the direction of orientation, for which there is some evidence from optical [16] and electron-microscopic studies [5]. In general, however, the changes in the low-angle scattering diagram are consistent with the

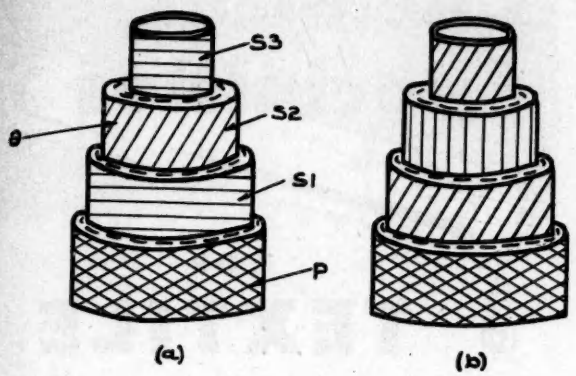

FIG. 5. *Diagrammatic representation of the cell wall organization of conifer tracheids [6, 16]:* (a) *in a short cell,* (b) *in a long cell.*

change in cell wall organization with cell length shown in Figure 5. Photometric examination of the diagrams gave the same value of the maximum scattering angle for both the meridional and equatorial streaks, corresponding to an average intermicellar distance of 56 Å., as calculated from the Bragg equation. This is unexpected, in view of Lange's conclusion [8] on the basis of light absorption measurements that there is relatively less cellulose in the outer part of the secondary cell wall.

Finally, comparing the wide-angle diagrams of wood from ring 2 with the beam oriented in the directions (*a*), (*b*), and (*c*) of Figure 1, it can be seen (Figure 2 (*b* and *c*)) that in the case with the beam perpendicular to the wood rays (direction (*b*), Figure 1) an equatorial arc is present, which is absent from both of the other diagrams. In the corresponding low-angle diagram an equatorial streak is present (Figure 2 (*g*), Figure 4 (*f*)). Regarding the wide-angle diagram (Figure 2 (*b*)), it is claimed by Berkley and Woodyard [2] that such a diagram indicates the presence of transversely and longitudinally oriented micelles, as well as helically oriented micelles of intermediate orientation. However, since the micellar organization of the cell wall in each layer is continuous, and since there is no optical or microscopic evidence to indicate the presence of three such directions of orientation in the secondary wall of conifer tracheids, this interpretation is improbable. Since the equatorial arc is present only in the one diagram (direction (*b*), Figure 1), it must arise either from some feature of the geometry of the specimen when in this orientation, or from some morphological feature of the radial walls. Since the radial walls are extremely pitted, it was possible that these structures gave rise to the equatorial arc, but this latter possibility can be rejected since there is no feature of the fine structure of the pits to account for it. Another possibility, however, considered by Bailey and Berkley [1] and by Preston [10] does appear to offer an explanation—*viz.*, that an equatorial arc can arise from those walls the plane of which is parallel to the x-ray beam. In the specimens studied, in late wood the tangential walls were approximately twice the length of the radial walls (perpendicular to the cell length), and this may account for the prominence of the arc when the beam was oriented in the direction (*b*) with respect to the specimen. Occasionally [2] such an equatorial arc has been observed when the beam is oriented in the direction (*a*), although not in the present study. This interpretation appears to be confirmed by the observation that the equatorial arc shown in Figure 2 (*b*) and the low-angle equatorial streak (Figure 2 (*g*)) disappeared on crushing the specimen (Figure 2 (*d* and *i*)) so that in effect the tangential walls were eliminated. Further, there was no difference observed in the diffraction diagrams of specimens with cells of circular cross section, such as compression wood, irrespective of the orientation of the specimen with respect to the x-ray beam.

Literature Cited

1. Bailey, I. W., and Berkley, E. E., *Am. J. Botany* **29**, 231 (1942).
2. Berkley, E. E., and Woodyard, O. C., TEXTILE RESEARCH JOURNAL **18**, 519–25 (1948).
3. Heyn, A. N. J., TEXTILE RESEARCH JOURNAL **19**, 163–72 (1949).
4. Heyn, A. N. J., *J. Am. Chem. Soc.* **72**, 2284–5 (1950).
5. Hodge, A. J., and Wardrop, A. B., *Australian J. Sci. Research* **B3**, 165–269 (1950).
6. Kerr, T., and Bailey, I. W., *J. Arnold Arboretum (Harvard Univ.)* **15**, 327–49 (1934).
7. Kratky, O., and Porod, G., *J. Colloid Sci.* **4**, 35–70 (1949).
8. Lange, P. W., *Svensk Papperstidn.* **53**, 749–66 (1950).
9. Preston, R. D., *Phil. Trans.* **B224**, 131–74 (1934).
10. Preston, R. D., *Proc. Roy. Soc. (London)* **B133**, 327–48 (1946).
11. Preston, R. D., *Proc. Roy. Soc. (London)* **B134**, 202–18 (1947).
12. Preston, R. D., *Biochim. et Biophys. Acta* **2**, 376–83 (1948).
13. Preston, R. D., and Wardrop, A. B., *Biochim. et Biophys. Acta* **3**, 549–59 (1949).
14. Preston, R. D., and Wardrop, A. B., *Biochim. et Biophys. Acta* **3**, 585–92 (1949).
15. Sanio, K., *Jahrb. wiss. Botan.* **8**, 401–20 (1872).
16. Wardrop, A. B., and Preston, R. D., *Nature* **160**, 911–12 (1947); *J. Exp. Botany* **2**, 20 (1951).

A. B. WARDROP

1952 GORDON RESEARCH CONFERENCES

Textile Conference

July 14–18, 1952

Colby Junior College, New London, New Hampshire

W. J. Hamburger, *Chairman*
J. Edward Lynn, *Vice-Chairman*

Monday, July 14

Morning—"New Polymers for the Formation and Modification of Textile Fibers," by Herman F. Mark, Polytechnic Institute of Brooklyn

Evening—"Influence of Some Colloid Chemical and Physical Factors on Textile Performance of Synthetic Fibers, Especially of the Acrylonitrile Type," by Bruno R. Roberts, Chemstrand Corporation

Tuesday, July 15

Morning—"Response of Fiber Assemblages to Compression as Influenced by Certain Fiber Properties," by Kenneth L. Hertel, University of Tennessee

Evening—"Transmission and Attenuation of Energy in High Polymers," by A. G. H. Dietz, Massachusetts Institute of Technology

Wednesday, July 16

Morning—"The Relationship Between the Chemical Structure and the Mechanical Behavior of Wool," by Richard O. Steele, Textile Research Institute

Evening—"The Relationship Between the Chemical Structure and the Mechanical Behavior of Synthetic Fibers," by Turner Alfrey, Jr., Dow Chemical Company

Thursday, July 17

Morning—"Action on Wool of Certain Low Molecular Weight Reagents," by Harold P. Lundgren, Western Regional Research Laboratories, United States Department of Agriculture

Evening—"Effects of Chemical Treatments on the Mechanical Behavior of Human Hair," by Henry M. Morgan, Fabric Research Laboratories

Friday, July 18

Morning—"The Effects of Various Fabric Types on Body Comfort as Measured by Physiological Responses of Human Subjects," by Orville C. Wetmore, E. I. du Pont de Nemours & Company

FOR

TEXTILE

PROCESSING

LUPOMIN*
A series of cationic nitrogen compounds for softening and finishing textiles.

BENSAPOL*
Liquid detergent derived from Monopole Oil for wool scouring.

ORATOL L-48*
A neutralized sulphonated ester of a higher alkanolamide for increased scouring efficiency.

SULPHONATED OILS
A wide range of types available in numerous concentrations, grades and degrees of sulphonation.

SULPHONATED RED OIL S-I-L
A water-soluble oil (sulphonated Oleic Acid) with good detergent and emulsification properties. 50% and 85%.

MONOPOLE OIL*
Double sulphonated castor oil for bleaching, dyeing, finishing and as a dispersant for dye solutions.

PARNOL NO. 85
An anionic dodecyl-benzene sulphonate with exceptional wetting properties and high detergent characteristics.

LOMAR PW*
A condensation product of alkyl aryl sulphonates used as dispersing agents for insoluble pigments.

SUPERCLEAR*
Product of natural vegetable gums with complete solubility and outstanding penetrating properties for fine printing.

WETSIT CONC.*
A liquid wetting agent of the alkyl aryl type with rapid wetting and penetrating properties.

HYDROZIN
A clear-dissolving, soluble Zinc Formaldehyde Sulphoxylate, for discharge printing and stripping.

GUMS
A wide range of gums including Arabic, Tragacanth, Karaya, Irish Moss, etc. In both liquid and powder form.

*Reg. Trademark

Write for our Chemicals & Specialties Catalog.

JACQUES WOLF & CO.
Chemicals
PASSAIC, N. J.